Assessing oncolytic viral therapy and its barriers: a mathematical approach

by

Sana Jahedi

MSc. in Mathematics, Shahid Beheshti University, Tehran, Iran, 2012
Bachelor of Arts, Alzahra university, 2009

A THESIS SUBMITTED IN PARTIAL FULFILLMENT OF THE REQUIREMENTS FOR THE DEGREE OF

Doctor of Philosophy

In the Graduate Academic Unit of Department of Mathematics and Statistics

Supervisor(s): James Watmough, PhD, Dept. of Math & Stat,
Lin Wang, PhD, Dept. of Math & Stat.

Examining Board: Edward Wilson-Ewing, PhD, Dept. of Math & Stat,
Branimir Ćaćić, PhD, Dept. of Math & Stat,
Aurora Nedelcu, PhD, Dept. of Biology.

External Examiner: Morgan Craig, PhD,
Département de mathématiques et de statistique,
Université de Montréal.

This thesis is accepted by the
Dean of Graduate Studies

UNIVERSITY OF NEW BRUNSWICK

April 22,2022

Abstract

Oncolytic viral therapy is a targeted therapy in which natural or genetically modified viruses are used specifically to target cancer cells and not harm healthy cells. Despite some promising results in in vitro and in vivo studies of oncolytic viruses, many questions about treatment regimens and outcomes remain unanswered. Mathematical modelling can be helpful to shed light on understanding cancer cell dynamics and treatment outcomes.

Firstly, we propose a set of ordinary differential equations that describes the interactions between cancer cells and free virus during oncolytic viral therapy. Then, using stability and sensitivity analyses, we seek to understand possible treatment outcomes. Then, by identifying thresholds for infection-related parameters such as the virulence level of the virus, the viral time scale and the infection transmission rate, we identify the type of virus that can lead to optimal treatment outcome.

Some research suggests that a virus-specific immune response, such as one that becomes activated to prevent infection spread, may burden the success of oncolytic viral therapy. Extending our model, we propose models which include interactions between cancer cells, viruses, and antibody molecules/cytotoxic T cells during oncolytic viral therapy. We identify conditions under which each of the mentioned immune responses can be established by focusing on infection-related parameters. Our result shows virus-specific immune responses are not always detrimental: they

can also be neutral or beneficial. Then by focusing on the virulence level of the free virus, we identify the extent to which the effect of a virus-specific immune response is detrimental and beneficial and show how the negative effect can be reduced or how beneficial results can be enhanced.

Due to properties such as self-renewal and long-lasting quiescence, cancer stem cells are responsible for tumour recurrence and the failure of many conventional therapies. Here, we assess the efficacy of targeting cancer stem cells with oncolytic viruses. We show that targeting cancer stem cells does not always enhance the treatment efficacy, and optimal stem cell specificity depends on the rate of mitosis of infected cells. When infected cells are mitotic, the optimal result is obtained by perfect stem cell targeting.

Dedication

Atama və anama, sənsiz bu səyahət mümkün deyildi

Preface

All the chapters of this thesis except for chapter 1, which is a general motivation, and chapter 5, which is a summary of the results will be submitted for publication in peer-reviewed journals with the scope of mathematical modelling.

Chapter 2 is available on biorxiv through https://doi.org/10.1101/2021.07.19.452846.
Fighting cancer with oncolytic viral therapy: Finding threshold parameters for success. S. Jahedi, L. Wang, J. Watmough.

Contributions of authors:
SJ developed and analyzed the mathematical model; contributed to writing
LW and JW advised the project and contributed to writing.

Chapter 3 will be submitted to a peer-review journal with the scope of mathematical oncology.
Effect of antiviral immune response on oncolytic viral therapy: burden or enhancer?
S. Jahedi, L. Wang, J. Watmough.

Contributions of authors:
SJ developed and analyzed mathematical models; contributed to writing.
LW and JW advised the project and contributed to writing.

Chapter 4 will be submitted for publication.

Targeting cancer stem cells with oncolytic viral therapy: a mathematical approach.

Sana Jahedi, Kamran Kaveh, James. Watmough,

Contributions of authors:

SJ developed and analyzed mathematical models; contributed to writing.

KK developed the model, advised and contributed to writing.

JW advised and contributed to writing.

Acknowledgements

I want to take this opportunity to thank all the people who have had a major role in completing this thesis, without whom definitely, I would not be able to complete this chapter of my life, specifically my supervisors, Professor James Watmough and Professor Lin Wang.

James, you are a wonderful scientist, very intelligent and down to earth. I was very fortunate that you accepted to be my supervisor. You have a great personality. You are always positive and a source of motivation. You encouraged me to choose the subject that I like to work, then shed light on my path by introducing me the key resources and teaching me the key concepts. You allowed me to collaborate with other researchers and be involved in the projects that were not related to my thesis. I appreciate all your recommendations about modelling and coding, without them none of the projects could be done. I deeply appreciate your patience and support.

Lin, you are an amazing teacher, very respectful, patient, supportive and motivational. I have learned a lot from you during the last three years and I learned coding from you. I wish I could have taken more courses with you, the dynamical system course that I had with you, was one of the most beneficial courses that I have ever had during my entire studies and I deeply appreciate that. About the projects, you had an amazing role as an advisor and always tackle the key points, without you, neither of them would be as good as they are now.

I want to express my sincere appreciation to Dr. Kamran Kaveh, who has also advised me on all my projects related to my thesis. Thank you for all the long lectures and discussions on the biological and modelling aspects of the projects. Kamran, you are a wonderful professor. I got interested in the oncolytic viral therapy subject after I met you in the 2018 CMS meeting, which was a key incident in my life.

Finally, in the chaos of my life, there was a small decision that made a huge difference in my life. The decision to go to Aarms summer school in 2019 made me meet Professor James Yorke. Jim, you completely changed my life. You made me follow my instinct and go after all the questions that sounded crazy to others. You are not only a great scientist and coach, but you are also an amazing friend who believes in supporting his students. I am so proud to be your student, and hopefully, I will treat my students in future the same way that you treat me. Thank you for all the long discussions and meetings we have had. You are a day booster that brings a lot of joy into my life.

I would like to thank the examining committee Dr. Morgan Criage, Dr. Branimir Ćaćić, Dr. Aurora Nedelcu, Dr. Edward Wilson-Ewing. I am grateful for your constructive criticism, and for the time you spent analyzing this thesis. Your reports helped me to improve my thesis.

I want to manifest my deepest appreciation to my parents, siblings, and partner. Thank you for your love, support, faith, and companionship; all of you are amazing, and I am so lucky to have you.

I would like to thank all my friends Shohreh Rahmati, Ali Beykzadeh, Yavar Abdolmaleki, Robert Santacruz, Marco de Cesare, Juping Ji, Ali Gharouni, Doyeon Kim, Vedshruti Bundhoo, Lorry Jane Binayat, Donna and Alan McFadden. Thank you all for the wonderful memories that you have created for me. Your presence made my experience at UNB more enjoyable.

I appreciate all the faculty and staff members who have helped me throughout recent years; Dr. Sanjeeve Seahra, Ms. Mahin Salmani, Dr. Nicholas Touikan, Dr. Patrick Reynolds and Ms. Cindy Thomas.

Table of Contents

List of Tables

List of Figures

Chapter 1

Introduction

Cancer was the leading cause of death in Canada from 2015 to 2019 [34] and currently is the leading cause of death worldwide: according to World Health Organization (WHO), nearly 10 million people died of cancer in 2020 [111]. Hence, research on cancer causes, prevention, and treatment is vital. In 2000, Hanahan and Weinberg [38] classified the six core hallmarks of cancer as (1) self-sufficiency in growth signals, (2) evading apoptosis, (3) limitless replicative capability, (4) insensitivity to growth suppressor signals, (5) sustained angiogenesis, and (6) metastasis and invading the tissue. Genetic mutations can occur in a cell that cause it to mimic a response to growth signals, start to proliferate, overcome programmed cell death, divide indefinitely, and form a tumour. Cancer cells may also detach from the tumour and migrate to other sites of the host body through blood vessels and cause metastasis. The hallmarks of cancer are recently being updated, and eight more characteristics were added to the previous list, including reprogramming cellular metabolism, avoiding immune destruction, genomic instability, tumour promoting inflammation, unlocking phenotypic plasticity, senescent cells, nonmutational epigenetic reprogramming, and polymorphic microbiomes [37, 39].

Currently, there are different therapies used for treating cancer patients, ranging from conventional therapies to targeted therapies. Conventional therapies used for cancer treatment are surgery, chemotherapy, and radiation therapy. Cancer treatment may completely eradicate the tumour and cure cancer, shrink the tumour, or slow tumour growth and prevent cancer progress. Most cancer treatments affect the process that cancer cells go through to divide and proliferate. In conventional therapy, the drug used is not specific to cancerous cells. Hence, conventional therapy is cytotoxic to all the cells, meaning that while killing cancer cells, it can also damage some of the normal cells. Hence, a patient during conventional therapy may suffer from severe side effects [14, 17]. Targeted therapy, in contrast, is a type of treatment in which drugs are used to identify and specifically target and kill cancer cells and leave healthy cells unharmed. In this thesis, the therapy that we will study and analyze is oncolytic viral therapy. Oncolytic viral therapy is a targeted therapy in which a natural or genetically modified virus is used to selectively target and kill cancer cells without harming healthy cells. The idea of using viruses as a cancer treatment was formed when doctors noticed that some cancer patients experienced a short period of remission after a viral infection [55]. Some oncolytic viruses only enter cancer cells because of an antigen expression only found on the surface of cancer cells [87]. Others only target cells with specific signalling pathways which are only active in cancer cells. For example, a reovirus is a natural oncolytic virus that targets cells with overexpressed protein epidermal growth factor receptor (EGFR); this protein activates the Ras signalling pathway [16]. Oncorine, a genetically modified adenovirus (H101), is the world's first oncolytic virus that was approved to be used clinically in cancer treatment: it was approved in 2005 by China's Food and Drug Administration for treatment of head and neck cancer [80]. Many more potential oncolytic viruses are currently undergoing clinical trials: such as stomatitis virus [30], type 1 herpes simplex virus [32], Zika virus [101].

Oncolytic viruses have four different functions [35]: oncolysis, carrying transgene expression, blocking angiogenesis, and antitumor immunity. Oncolysis is the process in which an oncolytic virus infects cancer cells, replicates in them, and eventually kills them. A transgene is a type of gene that can be transformed with engineering techniques. Oncolytic viruses can be equipped with certain genes, such as tumour suppressor genes, to enhance their oncolytic effects [41]. Oncolytic viruses can be armed with angiogenesis inhibitors to block angiogenesis [104]. Oncolytic viruses can also be armed with some cytokines or chemokines to activate antitumor (tumour-specific) immune responses [12,21,35,47,92]. This thesis only focuses on the oncolysis functionality of oncolytic viruses and the barriers to the success of oncolytic viral therapy.

To date, clinical trials conducted using various oncolytic viruses have shown that these agents are less toxic to patients than conventional therapies [9, 70], which makes this therapy popular. However, the therapeutic success of oncolytic viruses is limited [24, 124], and the complete eradication of a tumour has rarely been achieved when an oncolytic virus has been used as a single agent [31, 40]. These clinical reports motivate us to investigate the possible outcomes of oncolytic viral therapy. Which factors play a crucial role in deriving a particular treatment outcome? What is the optimal treatment outcome, and when is it obtained? This thesis applies computational and analytical mathematical approaches to understand the dynamics of tumour cells during oncolytic viral therapy and determine treatment outcomes.

The reproduction of new viruses during the infection process in a host cell follows the viral replication cycle (see Figure 1.1 for a schematic representation of the viral replication cycle). The viral replication cycle may vary between different species, but generally includes six stages: attachment, penetration, disassembly (uncoating), replication, assembly, and release [2, 23, 71, 94]. First, a virus attaches itself to the receptor on the host cell's membrane. Second, the virus penetrates the host cell

membrane. Third, the virus capsid is disassembled, and the viral genome is released in the intracellular area of the host cell. Fourth, the viral genome manipulates the host cell machinery and causes it to produce the viral genome. Fifth, the viral proteins and the newly replicated genome assemble into new virions. Finally, new virions are released from the host cell either by lysing the host cell (bursting the host cell membrane) or by apoptosis (meaning, they wait till infected cells die). If a virus lyses the host cell, then its replication cycle is referred to as a lytic cycle. Oncolytic viruses are viruses that follow a lytic cycle. For the success of oncolytic viral therapy, each part of this cycle must be completed successfully.

When a virus enters a host body, the immune system activates various cells, molecules and proteins to prevent infection of host cells. This type of immune response is called a virus-specific immune response since it is specific to the pathogen presented. Studies related to oncolytic viruses mention two different types of immune responses: virus-specific and tumour-specific. As we mentioned before, virus-specific immune responses get activated to inhibit infection, and tumour-specific responses are the body's response to the presence of a tumour. Various immune cells are activated to kill tumour cells and interrupt the tumour growth progress. Some oncolytic viruses can trigger exhausted tumour-specific immune responses to become activated again. Here, we only focus on virus-specific immune responses and their role in inhibiting infection. Different types of virus-specific immune responses can block different stages of the viral replication cycle. For example, specific antibody molecules (Ab) can prevent attachment, and they can remove a virus from the body before it encounters the target cell [81]. Interferons (IFNs) are a large group of proteins produced by a host cell to interfere with virus replication. Iversen et al. [43] showed that Natural Killer (NK) cells could activate IFN-β expression in infected cells, which interferes with the production of virions. A Cytotoxic T lymphocyte (CTL) is a type of white blood cell that can kill infected cells. Hence, per the preceding discussion, a virus-specific

immune response can be a barrier to the success of oncolytic viral therapy. Here, using mathematical approaches, we establish when a virus-specific immune response could hinder treatment success. In addition, we also discuss how to overcome this barrier.

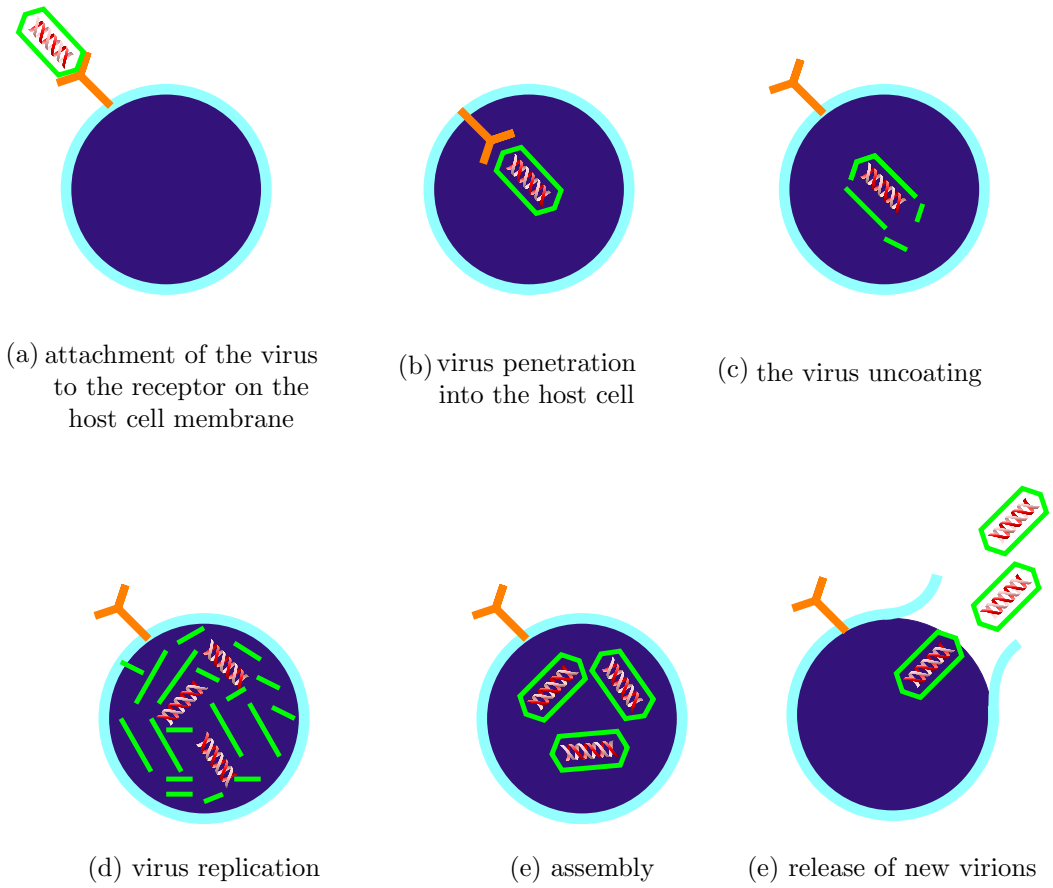

Figure 1.1: **A schematic representation of viral replication cycle**.

Intratumoral heterogeneity is known to be a major cause of tumour recurrence and the failure of many conventional therapies [76,78,102]. The phenotypic heterogeneity inside a tumour is both morphological and functional. One of the most important features of epigenetic heterogeneity inside a tumour is that only a small subpopulation of cells, known as cancer-initiating cells, can initiate a tumour clone. Cancer-initiating cells are also known as cancer stem cells. Cancer initiating cells can self-renew and

differentiate via symmetric and asymmetric proliferation events. The process of stem cell division into two identical daughter stem cells, or into one stem cell and one differentiated cell, is called self-renewal. Whereas stem cell differentiation is the process of division into two identical differentiated cells. A stem cell hierarchy starts from a stem cell which gives birth via self-renewal to progenitor cells with stem-like properties. Progenitor cells then self-renew or differentiate. Division of progenitor cells finally terminates when they divide into fully differentiated cells which are mature cells that cannot divide [15]. Most conventional therapies kill the differentiated cells and fail in targeting cancer stem cells. The phenotypic heterogeneity of tumours has a significant impact on the effectiveness of treatment strategies. Tumour initiating cells have some common properties, such as long-lasting quiescence, high levels of multi-drug resistance expression, and high DNA repair capability [89, 90, 106], which cause conventional therapies like chemotherapy [123] and radiotherapy [97] to fail in eradicating cancer stem cells. It seems therapies that are not affected by the common properties of cancer-initiating cells lead to more effective results. Oncolytic viruses enter tumour cells through infection, and hence target proliferating and quiescent stem cells [18]. On the other hand, most of these properties are common to both cancer-initiating cells and intact normal stem cells. Using tumour specific promoters, oncolytic viruses can be engineered to only target cancer cells and not replicate in healthy normal cells. The complete eradication of cancer stem cells is observed in some in vitro studies of targeting cancer stem cells with oncolytic viruses [8, 29]. However, the complete eradication of cancer stem cells is not reported in most in vivo models of targeting cancer stem cells with oncolytic viruses [6, 8]. In this thesis, we use mathematical modelling to analyze the efficiency of targeting cancer stem cells with oncolytic viruses.

In this thesis we develop and analyze a mathematical model for the population dynamics of cancer cells and their interactions with free virus and immune system

during oncolytic viral therapy. We thus use mathematical analyses and numerical simulations to explain tumour cell dynamics and identify treatment outcomes. In addition, we use bifurcation and sensitivity analyses, which in their simplest form involve keeping some parameters constant while changing the rest to determine how sensitive the predicted outcomes are to changes in parameters. All the models introduced in this thesis consist of ordinary differential equations. Hence our work seeks to explore the temporal aspects of oncolytic viral therapy. We use dynamical system theory combined with numerical simulations as tools to describe our results.

Now, we review some of the mathematical models in the literature that our main models are based upon. The interaction between cancer cells, an oncolytic virus and the immune system is quite complex. For example intratumoral heterogeneity, the type of immune response that will be established and the stage of the viral replication cycle that it will interfere with are some of complexities that are involved in the modelling of interactions between cancer cells, the free virus, and the immune system during oncolytic viral therapy. To understand how virus-specific immune responses affect the outcomes of oncolytic viral therapy, and to understand general outcomes of oncolytic viral therapy, first we disregard any interaction with the immune response including both virus-specific and tumour-specific immune responses. We also assume the oncolytic virus administrated targets all cancer cells equally and does not have a preference in targeting cancer stem cells over differentiated cells. So firstly we review some classic mathematical models that describe interaction between uninfected cancer cells, X, infected cancer cells, Y, and the free virus, V, during oncolytic viral therapy.

Wodarz and Komarova [118] proposed Model (1.1) to study the interaction between uninfected cancer cells and infected cancer cells during oncolytic viral therapy. In Model (1.1) $\bar{r}$ and $\bar{s}$ are the per capita mitosis rates of uninfected and infected cancer cells at zero density, respectively. K is the maximal tumour size due to nutrient

limitations. The death rates of uninfected and infected cancer cells are denoted by $\bar{d}$ and $\bar{d}'$, respectively. Lastly, β is the horizontal transmission rate. The authors showed that there is an optimal value for the death rate of infected cells at which the tumour reaches a minimum size. Hence, this work shows the importance of death rate of infected cancer cells on the treatment outcome.

$$\dot{X} = \bar{r}X(1 - \frac{X+Y}{K}) - \bar{d}X - \beta XY, \tag{1.1a}$$

$$\dot{Y} = \bar{s}Y(1 - \frac{X+Y}{K}) - \bar{d}'Y + \beta XY. \tag{1.1b}$$

Later on, Komarova and Wodarz [60] introduced a more general set of ordinary differential equations, Model (1.2) for describing cancer cell dynamics during oncolytic viral therapy. They used different types of infection spread term and as a proof of concept showed that viruses with higher horizontal transmission rate result in lower tumour size. Hence, this work shows the importance of the horizontal infection transmission rate in the treatment outcome. In addition, they also claim that if the viral spread rate is high enough, in the case of fast spread, then tumour eradication is possible.

$$\dot{X} = xF(x,y) - \beta G(x,y)y, \tag{1.2a}$$

$$\dot{Y} = \beta G(x,y)y - \bar{d}'y. \tag{1.2b}$$

In both Models (1.1) and (1.2) authors assume that the turnover of free virus is fast enough to maintain a quasi-steady state. Therefore, the density of the free virus is proportional to the density of the infected cells. Hence, no equation for the free virus is indicated. One of the downsides of this is that the interaction of the free virus with the immune system cannot be captured explicitly by a model in which no equation representing virus dynamics is considered. For example, this model cannot

describe the effect of an antibody response that kills the free virus, nor discuss the impact of interferons that block virion production.

Dingli et al. [25] proposed Model (1.3) to describe interactions between cancer cells and free virus during oncolytic viral therapy. They showed that the production rate of free virus, q, has a crucial role in the efficacy of treatment outcomes. As the production rate of free virus increases, more tumour shrinkage is observed under the therapy. In the following model $\bar{m}$ denotes the clearance rate of the virus.

$$\dot{X} = \bar{r}X(1 - \frac{(X+Y)^{\epsilon}}{K^{\epsilon}}) - \beta XV, \tag{1.3a}$$

$$\dot{Y} = \beta XV - \bar{d'}Y, \tag{1.3b}$$

$$\dot{V} = qY - \bar{m}V. \tag{1.3c}$$

In both Models (1.2) and (1.3) it is assumed that viral transmission is only horizontal, but in Model (1.1) it is assumed that viral transmission is both horizontal and vertical. Horizontal transmission occurs explicitly when a free virus penetrates an uninfected cell and makes it infected as shown in Model (1.3), or implicitly when an infected cell encounters an uninfected cell as shown in Models (1.1) and (1.2). Vertical transmission occurs when an infected cell divides and produces infected daughter cells, which is only considered in Model (1.1). The virus can fully invade the tumour only when transmission occurs both horizontally and vertically. We propose Model (2.1) in Chapter 2 to assess oncolytic viral therapy and its outcomes. Similar to Wodarz and Komarova [118] in Model (2.1) we assume infection transmission is both horizontal and vertical. In addition, similar to Dingli et al. [25] in Model (2.1) quasi-steady state assumption is relaxed and an equation representing virus dynamics is considered.

Chapter 2 is devoted to analysis of Model (2.1). In Chapter 2 the following questions

are answered:

1. What is the optimal tumour size under therapy?
2. When is the optimal tumour size obtained?
3. What is the control threshold of therapy?
4. What is the optimal threshold of therapy?
5. How does the virulence level of free virus affect treatment outcomes?
6. What is the optimal virulence level?
7. How does relaxation of the quasi-steady state affect the treatment outcomes? In other words, how does the viral timescale affect the treatments' results?

After understanding the gist of the dynamics of cancer cells, including both infected and uninfected cancer cells, and the dynamics of the free virus during oncolytic viral therapy by using Model (2.1), we extend Model (2.1), to incorporate the effect of a virus-specific immune response on the treatment outcomes. To do this, first, we review some classic models that show the interaction between uninfected cells, infected cells, the virus and a virus-specific immune response.

One of the first models that is introduced to study the effect of a CTL immune response on the viral load is the following Model that was proposed by Nowak and Bangham [85]. They showed that CTL responsiveness is not correlated with viral load in the case of HIV (Human Immunodeficiency Virus). In the following model c denotes the production rate of CTLs per infected cell, p denotes the rate at which a CTL kills infected cells, and m_z is the death rate of CTLs. In the following model λ

denotes the production rate of uninfected target cells.

$$\dot{X} = \lambda - \bar{d}X - \beta XV, \tag{1.4a}$$

$$\dot{Y} = \beta XV - \bar{d}'y - pYZ, \tag{1.4b}$$

$$\dot{V} = qY - \bar{m}V, \tag{1.4c}$$

$$\dot{Z} = cYZ - m_z Z. \tag{1.4d}$$

Komarova and Wodarz [61, chapter 12] proposed the following model to study the effect of a CTL immune response on oncolytic viral therapy. They showed that if in the absence of a CTL immune response a tumour is partially infected, then the establishment of a CTL immune response is only detrimental because tumour size is bigger in the presence of a CTL immune response; however, they do not discuss the extent to which a CTL immune response is harmful.

$$\dot{X} = \bar{r}X(1 - \frac{X+Y}{K}) - \bar{d}X - \beta XY, \tag{1.5a}$$

$$\dot{Y} = \bar{s}Y(1 - \frac{X+Y}{K}) - \bar{d}'Y + \beta XY - pYZ, \tag{1.5b}$$

$$\dot{Z} = cYZ - m_z Z. \tag{1.5c}$$

According to De Boer and Perelson [20], T-cells compete for infected cells. The proliferation rate of T-cells saturates due to competition between T-cells for infected cells. Hence, Eq. (1.5c) can be rewritten as the following, where CTLs are produced at the rate $(cYZ)/(1 + \varepsilon Z)$. When the population of CTLs reaches its abundance,

CTLs proliferation rate converges to cY/ε.

$$\dot{Z} = cY\frac{Z}{1+\varepsilon Z} - m_z Z. \tag{1.6}$$

Using Models (1.4) and (1.5) and Equation (1.6), we extend Model (2.1) and propose Model (3.4) to study the effect of a CTL immune response on the outcomes of oncolytic viral therapy.

As we mentioned before, another way that an immune response can reduce effectiveness of oncolytic viral therapy is by blocking attachment. Proteins on the surface of a virus trigger B-cells to secrete antibodies. Antibodies can attack and neutralize viruses [1]. Wodarz and Nowak [119] proposed the following system of equations to model the effect of antibody immune response on the viral load.

$$\dot{X} = \lambda - \bar{d}X - \beta XV, \tag{1.7a}$$

$$\dot{Y} = \beta XV - \bar{d}'y, \tag{1.7b}$$

$$\dot{V} = qY - \bar{m}V - pVZ, \tag{1.7c}$$

$$\dot{Z} = cV\frac{Z}{1+\varepsilon Z} - m_z Z. \tag{1.7d}$$

Note that since the secretion of antibodies is stimulated by the viruses, the rate of stimulation of antibodies $(cVZ)/(1+\varepsilon Z)$ is proportional to the abundance of the free virus.

In Chapter 3 we use numerical and analytical approaches to address the following questions about the effect of establishment of CTLs and antibodies on oncolytic viral therapy:

1. When is a CTL (or an antibody) immune response established during an on-

colytic viral therapy?

2. Is a CTL (or antibody) immune response a barrier to the success of oncolytic viral therapy?

3. If the answer to the above question is no, when is the establishment of a CTL (or antibody) immune response detrimental and when is it beneficial?

4. To what extent is the establishment of a CTL (or antibody) immune response hostile? Can a negative effect be controlled?

5. How does the virulence level of the free virus affect the establishment of a CTL (or antibody) immune response?

6. How does the establishment of a CTL (or antibody) immune response affect the optimal tumour size or the optimal threshold of the therapy?

7. Does the establishment of a CTL (or antibody) immune response affect the minimum viral transmission rate at which treatment starts to work?

Next, we focus on one of the applications of oncolytic vial therapy which is targeting cancer stem cells with oncolytic viruses. Many studies have investigated the efficacy of targeting cancer stem cells with oncolytic viruses in recent years. As a proof of concept, Eriksson et al. [29] showed that targeting cancer stem cells with oncolytic viruses is promising both in vitro and in vivo: they showed that the infected stem cells could not form a tumour. In vitro studies show that targeting cancer stem cells with oncolytic viruses can lead to tumour eradication [8,29]. However, tumour eradication does not often occur in in vivo studies of targeting cancer stem cells with oncolytic viruses [6, 8]. In Chapter 4 we use analytical and computational tools to investigate when targeting cancer stem cell leads to a better result than random targeting or only targeting differentiated cells. In order to do this, we propose a model that takes phenotypic heterogeneity of cancer cells into account during oncolytic viral therapy,

meaning that cancer stem cells and differentiated cells become infected at different rates through incidence with an infected cell.

Many mathematical models, both stochastic and deterministic, have been proposed in the literature to describe population dynamics with a stem cell hierarchy [49, 52, 64, 99, 103]. The following set of ordinary differential equations which was proposed by Johnston [49], is one of the early models that describes the stem cell division process; in this model, X_0, X_1, and X_2 denote the population density of stem cells, the population density of semi differentiated cells, and the population density of fully differentiated cells, respectively. Semi-differentiated cells similar to stem cells can self-renew and differentiate, but fully differentiated cells cannot divide. The self-renewal rate of stem cells (semi-differentiated cells) is denoted by α_3 (β_3) and the differentiation rate of stem cells (semi-differentiated cells) is denoted by α_2 (β_2). The death rates of stem cells, semi-differentiated cells, and differentiated cells are denoted by α_1, β_1, and γ, respectively.

$$\dot{X}_0 = (\alpha_3 - \alpha_2 - \alpha_1)X_0, \tag{1.8a}$$

$$\dot{X}_1 = (\beta_3 - \beta_2 - \beta_1)X_1 + \alpha_2 X_0, \tag{1.8b}$$

$$\dot{X}_2 = \beta_2 X_1 - \gamma X_2. \tag{1.8c}$$

A stem cell niche is a microenvironment in which only stem-like cells can be found [96]. For example, stem cells of the colonic crypt are believed to be at the bottom of the crypt. Stem cell niches regulate stem cell self-renewal, differentiation and maturation. By considering these feedback control signals, the population of stem cells grows logistically [51]. To our knowledge, there is no mathematical model describing the dynamics of cancer cells during oncolytic viral therapy and taking phenotypic heterogeneity of the tumour into account. By considering Models (1.8) and Model (1.1),

we propose Model (4.2) in Chapter 4 to assess efficacy of targeting cancer stem cells with oncolytic viruses.

In Chapter 4, by analyzing Model (4.2), we address the following questions:

1. Does the administration of an oncolytic virus that selectively targets both stem cells and their progenitors lead to tumour eradication?
2. Which phenotype should preferentially be targeted to optimize the therapy? In other words, does a higher specificity in targeting stem-like cancer cells increase the overall efficacy of oncolytic viral therapy?
3. What is the optimal stem cell specificity?
4. What factors affect the optimal stem cell specificity?
5. How does the infected cells' mitotic (self-renewal and differentiation) rate affect the therapeutic outcome?
6. Does the stem cell fraction increase or decrease following an oncolytic therapy in which stem cells are targeted?

Finally, Chapter 5 summarizes the results of this thesis and discusses the future directions.

Chapter 2

Identifying threshold parameters for success in oncolytic viral therapy

We model interactions between cancer cells and a virus during oncolytic viral therapy. One of our primary goals is to identify parameter regions that yield treatment failure or success. We show that tumour size is reduced under therapy. Our analysis shows there are two thresholds for the horizontal transmission rate: a "control threshold" above which treatment is efficient, and an "optimal threshold" beyond which infection prevalence reaches 100% and the tumour shrinks to its smallest size. Moreover, we show that these thresholds depend on the virulence of a virus. We identify a threshold for the virulence of the virus and show how this threshold depends on the timescale of virus dynamics. Our results suggest that when the timescale of virus dynamics is fast, the administration of a more virulent virus leads to greater tumour size reduction. Conversely, when the viral timescale is slow, a higher virulence can lead to high amplitude oscillations. Furthermore, our numerical observations depict

fast and slow dynamics and suggest the existence of a two-dimensional globally attracting surface that includes the unstable manifold of the interior steady state and a stable limit cycle. All solutions with positive initial conditions rapidly approach this two-dimensional attracting surface, and the trajectories on the attracting surface slowly tend to the limit cycle. Our analysis shows that the optimal virulence of an oncolytic virus depends on the timescale of virus dynamics.

2.1 Introduction

The idea of using viruses as a cancer treatment was formed when doctors noticed that some cancer patients experienced a short period of remission after a viral infection [55]. Oncolytic viruses are natural or modified viruses that specifically target cancerous cells, replicate in them and eventually kill the infected cancer cells via lysis. Oncolytic viruses can also be armed with genes encoding cytokines and chemokines that activate antitumour immune cells [12, 21, 35, 47, 92], but here we only focus on their use as oncolytic agents.

To date, clinical trials conducted using various oncolytic viruses have shown that these agents are less toxic than conventional therapies [9, 70], which makes this therapy popular. However, the therapeutic success of an oncolytic virus is limited [24, 124], and the complete eradication of a tumour has rarely been achieved when an oncolytic virus has been used as a single agent [31, 40]. This motivates us to study interactions between virus and cancer cells during oncolytic viral therapy to identify barriers and find ways to overcome them. Here, we use mathematical modelling to address the following questions. What are the outcomes of oncolytic viral therapy? Under which condition is a specific outcome possible? Can oncolytic viruses be used as a cure or only as a containment method? And how does the virulence of the virus affect the treatment outcomes? Moreover, we examine how to

optimize the efficiency of viral therapy by identifying which parameter regions will lead to the best outcome under treatment.

Several mathematical models of oncolytic virus dynamics have been developed [7,46, 60, 114, 115]. Komarova and Wodarz [61] studied the interactions between infected and uninfected cancer cells under the assumption that the turnover of the virus is fast enough to maintain a quasi-steady state. They showed there is an optimal value for the death rate of infected cells at which the tumour reaches a minimum size. Long-term oscillatory behaviour has not been observed in their model, but in vivo studies of oncolytic viruses have suggested oscillatory behaviour [24]. This encourages us to relax the quasi steady state assumption and consider a three-variable model that can capture important dynamics of oncolytic viral therapy not found in the simpler models.

Similar to many viruses, oncolytic viruses come in two types: enveloped and naked. Some examples of naked oncolytic viruses are adenovirus [120] and reovirus [10]. For examples of enveloped oncolytic viruses we can refer to vesicular stomatitis virus [30], type 1 herpes simplex virus [32], and Zika virus [101]. Enveloped oncolytic viruses can be easier for the host immune cells to remove than naked oncolytic viruses [125]. New virions of enveloped viruses can leave the host cells without lysis, but naked viruses only leave the host cells via lysis. Hence, enveloped oncolytic viruses seem to be less efficient than naked oncolytic viruses. Our model describes the interaction of a naked oncolytic virus with infected and uninfected cancer cells during oncolytic viral therapy.

A virus can affect cell death mechanisms in various ways. One type of death that an infection can induce in a cell is lysis. When a cell becomes infected, the virus makes copies of itself until the infected cell's membrane bursts and new virions are released into the extracellular area. The other type is an active death - known as apoptosis,

during which cells activate programmed cell death mechanisms to induce the death of infected cells. Most viruses are equipped with anti-apoptosis proteins that allow them to complete the viral reproduction cycle before an infected cell dies [53]. However, sometimes an infected cell dies quickly in response to an infection to prevent infection spread: the virions released in this way have not completed the viral reproduction cycle and are not infectious. Our model describes the dynamics of oncolytic viral therapy when viruses can complete the viral reproduction cycle before an infected cell dies.

Here, we are interested in understanding how treatment outcome is influenced by an oncolytic virus capable of both horizontal and vertical infection. Similar to Komarova and Wodarz [61], we consider using a mitotic virus. In other words, there are two pathways for infection transmission: horizontal and vertical transmission. Infection is transmitted horizontally when an uninfected cell encounters free virus and becomes infected. Infection transmission is vertical when an infected cell produces infected daughter cells through mitosis. An infected cell may give birth to two infected daughter cells or one infected cell and one uninfected daughter cell. Here, for simplicity we only discuss the scenario where vertical transmission is perfect, meaning an infected cell only gives birth to infected daughter cells.

For some cancers, larger tumours have an increased risk of metastasis: Koscielny et al. [62] showed that the incidence of metastasis increases as the size of a breast tumour increases; in a study on the survival experience of 1894 patients with invasive breast tumours, Narod [82] showed that an increase in tumour size decreases the 15-year survival rate of patients. Hence, the size to which the tumour shrinks is a crucial factor in identifying how successful a cancer treatment is. A therapy that causes considerable tumour shrinkage may be used as a tumour control method and, in combination with other therapies, may lead to tumour eradication. This inspires us to investigate how a virus should be engineered to shrink the steady-state tumour

size compared to the case that no treatment occurs. Understanding the regions of parameter space in which tumour size is minimized is an essential step towards engineering such an oncolytic virus. As we will show, there exists a threshold for the horizontal transmission rate beyond which the tumour size reaches its minimum.

The negative effect caused by a viral infection on the functionality of host cells, such as a lower cell division rate or a higher mortality rate after infection is called virulence [84]. Here, we consider using an virulent virus. Our goal is to assess how the virulence of a virus affects the final tumour size. Recent studies suggest that extreme levels of viral virulence are not recommended [61]. Here, we show that when the virus becomes more aggressive, the system shows oscillatory behaviour. We derive a threshold for virulence above which a limit cycle exists. Our numerical observations suggest this limit cycle is almost every where globally stable: that is to say, it attracts every solution that starts from a positive point which is not on the stable manifold of the positive steady state.

Capturing fast and slow dynamics is very beneficial to understanding treatment outcomes over the longer term, especially when the fast behaviour is followed immediately by a slow behaviour. For example, when dynamics are fast, and the treatment outcome is followed only for a short time, it may appear as if the treatment is successful in the sense that huge tumour shrinkage is observed on a short timescale, but tumours may appear again over a longer timescale. On the other hand, when the dynamics are too slow, tumour growth may not be noticeable when solutions are only observed for a short time, but in practice, a tumour may get big enough to be a concern again within some years. We show for which parameter region and for which state spaces fast and slow dynamics occur.

2.2 Model

We make the following assumptions to achieve a tractable model that helps us focus on our research questions mentioned in the previous section.

(A1): To model nutrient limitations, we assume the mitosis rates are density dependent, dropping linearly to zero at a maximal tumour size K. We denote the per capita mitosis rates of uninfected and infected cancer cells at zero density by $\bar{r}$ and $\bar{s}$, respectively.

(A2): As we mentioned before, we assume there are two pathways for transmission of infection: β is the horizontal rate of infectivity per virus and $\bar{s}$, the mitosis rate of infected cancer cells, is the vertical transmission rate, see Figure 2.1.

(A3): Furthermore, we assume that vertical transmission is perfect: infected cells never produce uninfected daughter cells.

(A4): Uninfected and infected cancer cells die at rates $\bar{d}$ and $\bar{d}+\bar{a}$ respectively. These rates are assumed to be lower than the per capita mitosis rates $\bar{r}$ and $\bar{s}$, respectively.

(A5): The virus is virulent:

- infection reduces the cell mitosis rate, $\bar{s} < \bar{r}$;
- infection elevates the death rate of cancer cells, $\bar{a} > 0$.

(A6): As we mentioned in the introduction, we assume our model reflects the dynamics of a virus that can complete the viral reproduction cycle before the host infected cell dies. We further assume that no virion can leave the membrane of an infected cell before the infected cell dies. As Figure 2.1 illustrates, the virus makes $\bar{q}$ copies of itself in each infected cell, and the infected cell dies at the rate $\bar{d} + \bar{a}$. Therefore, $(\bar{d} + \bar{a})\bar{q}$ new virions are produced per each dead infected cell.

(A7): Here, in the interest of keeping consistent with earlier models [61, 72, 117] that

our model is based on, we neglect removal of the viruses with infection. The clearance rate of the virus is denoted by $\bar{m}$.

Under the above assumptions we have the following model:

$$\dot{X} = \bar{r}X\left(1 - \frac{X+Y}{K}\right) - \bar{d}X - \beta XV, \tag{2.1a}$$

$$\dot{Y} = \bar{s}Y\left(1 - \frac{X+Y}{K}\right) - \left(\bar{d} + \bar{a}\right)Y + \beta XV, \tag{2.1b}$$

$$\dot{V} = \left(\bar{d} + \bar{a}\right)\bar{q}Y - \bar{m}V, \tag{2.1c}$$

where X, Y, and V denote the population density of uninfected cancer cells, infected cancer cells, and viruses, respectively. The total tumour size is $X + Y$. Figure 2.1 illustrates the viral cycle. First, viral incidence occurs between an uninfected cancer cell X and the free virus V at rate β. Once the free virus penetrates the target cell, the target cells become infected. Then the virus replicates itself till the membrane of the infected cell is disrupted and the new virions are released in to the extracellular space.

As we mentioned in assumption (A6), Model (2.1) demonstrates the dynamics of a naked oncolytic virus. We assume that new virions are released to the extracellular area only after the infected cell dies. Therefore, the rate at which new virions are produced is $(\bar{d}+\bar{a})\bar{q}$. However, when using an enveloped virus, new virions can leave an infected cell without lysis. For Model (2.1) to describe dynamics of an enveloped oncolytic virus, one should replace equation (2.1c) with $\dot{V} = \bar{q}Y - \bar{m}V$, where $\bar{q}$ now denotes the rate at which new virions are produced by each infected cell. This change does not lead to any mathematical difference in the results: since we report the results for the rescaled model, with different rescalings, the same dimensionless model can be obtained for both scenarios. However, if we extend Model (2.1) to

consider interactions with virus-specific immune responses, treatment outcome will depend on the type of administrated oncolytic virus (naked vs. enveloped).

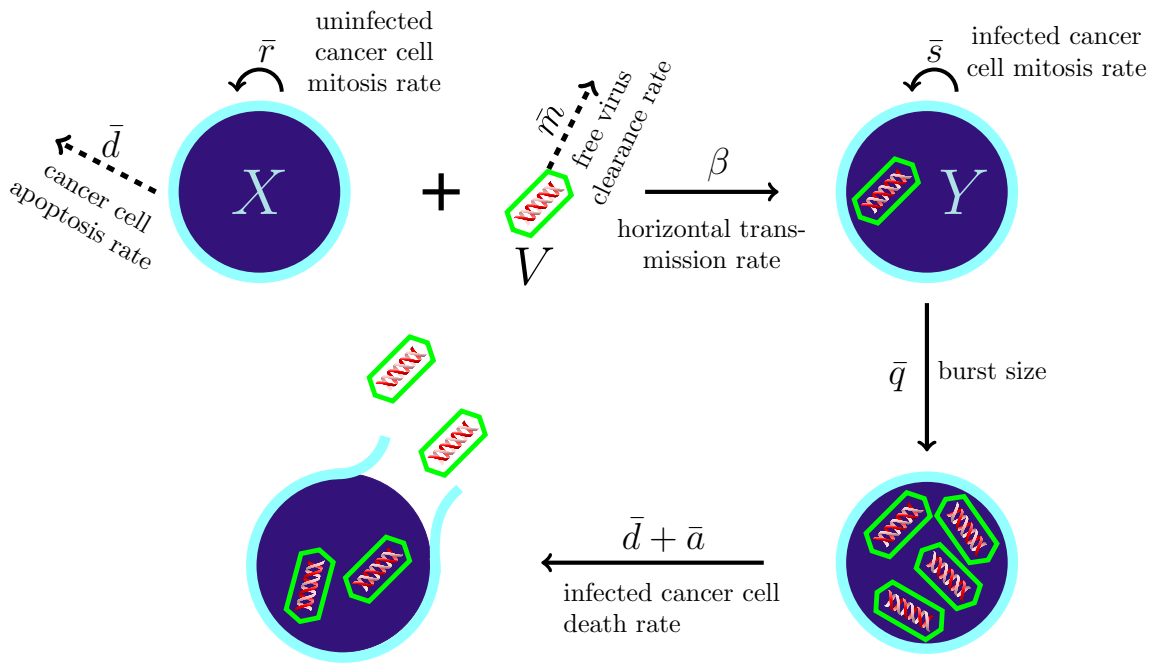

Figure 2.1: **A schematic description of oncolytic viral therapy under Model** (2.1). X, Y, and V denote population densities of uninfected cancer cells, infected cancer cells, and viruses, respectively.

To simplify our analysis, we rescale the parameters and variables of Model (2.1) as follows:

$$
\begin{aligned}
x &= \frac{X}{K}, \qquad y = \frac{Y}{K}, \qquad v = \frac{V\bar{m}}{K\bar{q}(\bar{d}+\bar{a})}, \quad t = \bar{r}\tau, \\
s &= \frac{\bar{s}}{\bar{r}}, \qquad m = \frac{\bar{m}}{\bar{r}}, \qquad b = \frac{\beta K\bar{q}(\bar{d}+\bar{a})}{\bar{r}\bar{m}}, \\
X_U &= 1 - \frac{\bar{d}}{\bar{r}}, \qquad\qquad Y_I = 1 - \frac{\bar{d}+\bar{a}}{\bar{s}}.
\end{aligned}
\tag{2.2}
$$

After applying these rescalings, Model (2.1) turns to the following dimensionless

model. The algebraic calculations are provided in Appendix (section 2.6.1).

$$\dot{x} = x(X_U - (x + y)) - bvx, \tag{2.3a}$$

$$\dot{y} = sy(Y_I - (x + y)) + bvx, \tag{2.3b}$$

$$\dot{v} = m(y - v). \tag{2.3c}$$

Assumptions (A4) and (A5) can be restated in terms of dimensionless parameters as follows.

(H1): $s < 1$ follows from Assumption (A5).

(H2): $X_U > Y_I > 0$ follows from Assumptions (A4) and (A5).

2.3 Analytical results

2.3.1 Invariant sets and steady states

Lemma 2.1. The set

$$\mathcal{W} = \{(x, y, v) : 0 \leq x + y \leq X_U, 0 \leq x, y, v \leq X_U\} \tag{2.4}$$

is a positively invariant and globally attracting set for Model (2.3).

The shaded wedge shape area in Figure 2.2(a) represents $\mathcal{W}$. In the proof of the above lemma we show that each solution of Model (2.3) starting from a nonnegative initial point always remains nonnegative.

Proof. First we show that $\mathcal{W}$ is positively invariant. A solution $(x(t), y(t), v(t))$ of Model (2.3) that starts from an initial point $(0, 0, v(0))$ on the v axis can be written

as

$$(0, 0, v(0)e^{-mt}).$$

Hence, $0 \leq v(t) < v(0) \leq X_U$ for all $t > 0$. Therefore, $(x(t), y(t), v(t)) \in \partial\mathcal{W}$ for all $t > 0$ if $x(0) = y(0) = 0$ and $0 \leq v(0) \leq X_U$.

A solution $(x(t), y(t), v(t))$ of Model (2.3) that starts from an initial point $(x(0), 0, 0)$ in $\mathcal{W}$ on the x axis is of the form

$$\left(\frac{X_U x(0)}{x(0) + (X_U - x(0))e^{-X_U t}}, 0, 0\right).$$

Since $0 < x(0) < X_U$, $0 \leq x(t) \leq X_U$ for all $t > 0$. Hence, $(x(t), y(t), v(t)) \in \partial\mathcal{W}$ for all $t > 0$ if $v(0) = y(0) = 0$ and $0 \leq x(0) \leq X_U$.

A solution $(x(t), y(t), v(t))$ of Model (2.3) that starts from an initial point $(0, y(0), v(0))$ in $\mathcal{W}$ can be written as

$$\left(0, \frac{Y_I y(0)}{y(0) + \big(Y_I - y(0)\big)e^{-sY_I t}}, me^{-mt}\int_0^t y(z)e^{mz}dz + v(0)e^{-mt}\right).$$

Hence, $(x(t), y(t), v(t)) \in \partial\mathcal{W}$ for all $t > 0$ if $x(0) = 0$ and $0 \leq y(0), v(0) \leq X_U$.

Consider a solution $(x(t), y(t), v(t))$ of Model (2.3) that starts from an initial point $(x(0), 0, v(0)) \in \mathcal{W}$. At $t = 0$, $\dot{y} = bx(0)v(0) > 0$. Hence, $(x(t), y(t), v(t)) \in \mathcal{W} \setminus \partial\mathcal{W}$ for $0 < t < t_0$ where $t_0 > 0$. The solution $(x(t), y(t), v(t))$ to leave $\mathcal{W}$ first should cross the boundary of $\mathcal{W}$. If the solution $(x(t), y(t), v(t))$ tends to a point on the x axis or on the y-v plane, then it will remain on the x axis or on the y-v plane, respectively; however, if it tends to a point on any other boundary surfaces of $\mathcal{W}$, it will only be tangent to that boundary and it will turn back into $\mathcal{W}$ again.

Consider a solution $(x(t), y(t), v(t))$ that starts from an initial point $(x(0), y(0), 0)$

in $\mathcal{W}$. At $t = 0$, $\dot{v} = my(0) > 0$. Hence, v is increasing for small values of t. Each solution that starts from a point $(x_0, y_0, 0) \in \mathcal{W}$ where $y_0 > 0$, points inward $\mathcal{W}$ for small $t > 0$ and it will remain in $\mathcal{W}$; it may remain in $\mathcal{W} \setminus \partial\mathcal{W}$ for all $t > 0$, or it will eventually tend to a point on the intersection of boundary of $\mathcal{W}$ with y-v plane.

Every point on the intersection of $\mathcal{W}$ with the surface $v - X_U = 0$ is above of the surface $y - v = 0$, except $(0, X_U, X_U)$. Hence, $\dot{v} < 0$ every where on this boundary except on $(0, X_U, X_U)$. Therefore, v is decreasing along this surface. Consider a solution $(x(t), y(t), v(t))$ starting from an initial point $(x(t), y(t), X_U)$, $(x(t), y(t), v(t)) \in \mathcal{W} \setminus \partial\mathcal{W}$ for small values of $t > 0$; this solution either remains in $\mathcal{W} \setminus \partial\mathcal{W}$ for all $t > 0$, or eventually tends to a point on the boundary of $\mathcal{W}$ on the y-v plane but it will never leave $\mathcal{W}$. The solution starting from $(0, X_U, X_U)$ remains in the boundary of $\mathcal{W}$ on the y-v plane for all $t > 0$.

Where $\mathcal{W}$ meets the surface $x+y-X_U = 0$, $\dot{x}+\dot{y} = sy(Y_I - X_U)$. By inequality (H2), $x+y$ is decreasing when $y \neq 0$. Hence, each solution that starts from an initial point on the intersection of $\mathcal{W}$ with the surface $x + y - X_U = 0$, points inward $\mathcal{W}$ and remains in $\mathcal{W}$.

Next we show that $\mathcal{W}$ is an attracting set and it attracts all the solutions starting in the positive octant (see Figure 2.2). When $x + y \geq X_U$ and $x, y > 0$, by Eqs. (2.3a) and (2.3b) the following inequality holds.

$$\dot{x} + \dot{y} = x(X_U - (x + y)) + sy(Y_I - (x + y)) \leq -sy(X_U - Y_I). \tag{2.5}$$

The above inequality shows that if $x + y \geq X_U$ and $x, y > 0$, then $\dot{x} + \dot{y} < 0$. In other words, the trajectory of each solution $(x(t), y(t), v(t))$ that starts from an initial point (x_0, y_0, v_0) with $x_0 + y_0 \geq X_U$ and $x_0, y_0 > 0$, moves in the direction of decreasing $x+y$, and thus tends inward $\mathcal{W}$ and will remain in $\mathcal{W}$ for all the following times. In other words, there exists $t^* > 0$ such that $(x(t), y(t), v(t)) \in \mathcal{W}$ for all

$t > t^*$.

When $v > y$, $\dot{v} < 0$. Hence v decreases along any trajectory that is above surface $y - v = 0$. Therefore each solution starting from an initial point (x_0, y_0, v_0), for which $x_0 + y_0 < X_U$ and $v_0 > X_U$, tends to a point in $\mathcal{W}$ and will remain in $\mathcal{W}$ for all the following times.

Therefore, for each solution $(x(t), y(t), v(t))$ with an initial point (x_0, y_0, v_0) such that $x_0, y_0, v_0 \geq 0$ and $(x_0, y_0, v_0) \notin \mathcal{W}$, there exists $t_1 > 0$ such that $(x(t), y(t), v(t)) \in \mathcal{W}$ for all $t > t_1$. $\square$

Herein we only study the dynamics of solutions that start from an initial point in $\mathcal{W}$. The shaded plane in the Figure 2.2(b) is the intersection of the surface $y - v = 0$ with $\mathcal{W}$. All steady states of Model (2.3) are on this plane.

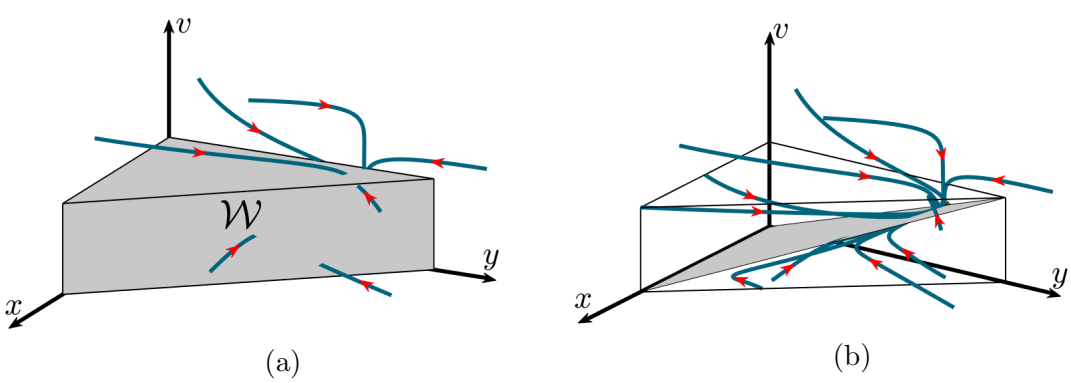

Figure 2.2: $\mathcal{W}$ **is positively invariant and globally attracting.** (a) This panel demonstrates that the trajectory of each solution that starts from a point in the first octant eventually gets attracted to $\mathcal{W}$. (b) This panel is the same as panel (a) but includes the intersection of the surface $y - v = 0$ with $\mathcal{W}$. When a solution starts above the surface $y - v = 0$, it moves in the direction of decreasing v. When a solution starts below the surface $y - v = 0$, it moves in the direction of increasing v.

The tumour size, $x + y$, determines whether the therapy is successful. The following theorem intuitively says that oncolytic viral therapy always reduces the tumour size. In the following theorem $x(t) + y(t)$ is the tumour size at time t under the therapy and $\bar{x}(t)$ is the tumour size without therapy.

Theorem 2.2. *Assume inequalities (H1) and (H2) hold, and under Model* (2.3)*, the virus is introduced at time* $t = 0$*, either directly into cells or into the extracellular environment. Let* $(\bar{x}(t), 0, 0)$ *be the solution of Model* (2.3) *with initial condition* $\big(\bar{x}_0, 0, 0\big)$*, where* $\bar{x}_0 > 0$*, and let* $(x(t), y(t), v(t))$ *be the solution to Model* (2.3) *with initial condition* $\big(x_0, y_0, v_0\big)$*, where* $x_0 > 0$*,* $v_0 > 0$*, and* $y_0 \geq 0$*. If* $x_0 + y_0 = \bar{x}_0$*, then* $x(t) + y(t) < \bar{x}(t)$ *for all* $t > 0$*.*

Proof. According to Eq. (2.3b), for each solution of Model (2.3) that starts with $x_0 > 0$, $v_0 > 0$, and $y_0 = 0$, y is initially increasing ($\dot{y}(0) > 0$). Hence, we conclude that $y(t) > 0$ for all $t > 0$. Now suppose the converse, that there exists a time $t^* > 0$ such that $x(t^*) + y(t^*) \geq \bar{x}(t^*)$, i.e. $\dfrac{x(t^*) + y(t^*)}{\bar{x}(t^*)} \geq 1$.

Define $\rho(t) = \dfrac{x(t) + y(t)}{\bar{x}(t)}, t \geq 0$. Notice that $\rho(t)$ is continuous and differentiable. Now we will show $\rho(t)$ is strictly decreasing on the set of times t for which $\rho(t) \geq 1$. Eqs. (2.3a) and (2.3b) yield

$$\dot{x} + \dot{y} = x\big(X_U - (x + y)\big) + sy\big(Y_I - (x + y)\big).$$

According to inequality (H2), $Y_I < X_U$. Since $y > 0$ for all $t > 0$,

$$\dot{x} + \dot{y} < x\big(X_U - (x + y)\big) + sy\big(X_U - (x + y)\big) = (x + sy)\big(X_U - (x + y)\big).$$

By inequality (H1), $s < 1$, so $x + sy < x + y$. Hence,

$$\dot{x} + \dot{y} < (x + y)\big(X_U - (x + y)\big).$$

Since $x + y \neq 0$,

$$\frac{\dot{x} + \dot{y}}{x + y} < X_U - (x + y).$$

For all $t > 0$ such that $\rho(t) \geq 1$ (i.e. $x(t) + y(t) \geq \bar{x}(t)$),

$$\frac{\dot{x} + \dot{y}}{x + y} < X_U - (x + y)(t) \leq X_U - \bar{x}(t) = \frac{\dot{\bar{x}}}{\bar{x}}.$$

Hence, for all $t > 0$ such that $\rho(t) \geq 1$ (i.e. $x(t) + y(t) \geq \bar{x}(t)$)

$$\frac{\dot{\rho}(t)}{\rho(t)} = \frac{\dot{x} + \dot{y}}{x + y} - \frac{\dot{\bar{x}}}{\bar{x}} < 0.$$

Therefore, $\rho(t)$ is strictly decreasing on the set of all $t > 0$ for which $\rho(t) \geq 1$. But $\rho(t)$ is a continuous function and $\rho(0) = 1$. Therefore, ρ is strictly decreasing on the set of all $t \geq 0$ for which $\rho(t) \geq 1$. Therefore $\rho(0) > \rho(t^*) \geq 1$, contradicting our assumption. □

In the proof of the following theorem, we use a comparison theorem [67], for convenience of the readers, the version of the comparison theorem that we use is provided here.

Theorem 2.3 (Second Comparison Theorem [67])**.** *Let $x(t)$ and $y(t)$ be continuously differentiable functions from $[0, +\infty)$ to $\mathbb{R}$, satisfying*

$$\frac{dx}{dt} \leq \frac{dy}{dt} \qquad \text{for all } t \geq 0, \tag{2.6}$$

and $x(0) \leq y(0)$, then $x(t) \leq y(t)$ for all $t \geq 0$.

Theorem 2.4. *Assume inequalities (H1) and (H2) hold. Under Model* (2.3)

(I) the tumour size under the therapy $x(t) + y(t)$ remains between Y_I and X_U if the initial tumour size is between Y_I and X_U, i.e.,

$$Y_I \leq x(t) + y(t) \leq X_U \text{ for all } t > 0, \tag{2.7}$$

if $Y_I \leq x_0 + y_0 \leq X_U$.

(II) For each solution $(x(t), y(t), v(t))$ *with an initial condition* $\big(x_0, y_0, v_0\big)$*, where* $x_0 > 0, y_0 > 0$ *either there exists* $t^* > 0$ *such that* $Y_I \leq x(t^*) + y(t^*) \leq X_U$*, or* $(x(t), y(t), v(t)) \to (0, Y_I, Y_I)$ *as* $t \to \infty$.

Proof. Part(I): Eqs. (2.3a) and (2.3b) yield the following equation.

$$\dot{x} + \dot{y} = x\big(X_U - (x+y)\big) + sy\big(Y_I - (x+y)\big). \tag{2.8}$$

Since $x, y \geq 0$, $Y_I < X_U$ and $s < 1$, $sy\big(Y_I - (x+y)\big) \leq y\big(X_U - (x+y)\big)$. Therefore, by the above equation

$$\dot{x} + \dot{y} \quad \leq (x+y)(X_U - (x+y)).$$

It now follows from the comparison theorem, if $x_0 + y_0 \leq X_U$, then $x(t) + y(t) \leq X_U$ for all $t \geq 0$.

Similarly, using $s(x+y) \leq x + sy$ from Eq. (2.8)

$$\dot{x} + \dot{y} \geq sx\big(Y_I - (x+y)\big) + sy\big(Y_I - (x+y)\big) = s(x+y)\big(Y_I - (x+y)\big).$$

It now follows from the comparison theorem, if $x_0 + y_0 \geq Y_I$, then $x(t) + y(t) \geq Y_I$ for all $t \geq 0$.

Part(II): Now assume $(x(t), y(t), v(t))$ is a solution starting from initial point $\big(x_0, y_0, v_0\big)$, where $x_0, y_0 > 0$.

As we showed in the proof of Lemma 2.1, $\{(x, y, v) | 0 \leq x + y \leq X_U, x, y, v \geq 0\}$ is a globally attracting set, so a solution starting from a point (x_0, y_0, v_0) with $x_0 + y_0 > X_U$ tends to a point in $\mathcal{W}$. Hence, we only need to show that for each solution $(x(t), y(t), v(t))$ with initial condition $\big(x_0, y_0, v_0\big)$ where $0 < x_0 + y_0 < Y_I$, $x_0, y_0 > 0$

either there exists t^* such that $x(t^*)+y(t^*) \geq Y_I$ or $\lim_{t\to\infty}(x(t), y(t), v(t)) = (0, Y_I, Y_I)$.

Assume $(\hat{x}(t), \hat{y}(t), \hat{v}(t))$ is a solution starting from (x_0, y_0, v_0) such that $x_0, y_0 > 0$, $\hat{x}(t) + \hat{y}(t) < Y_I$ for all $t \geq 0$. We will show $\lim_{t\to\infty}(\hat{x}(t), \hat{y}(t), \hat{v}(t)) = (0, Y_I, Y_I)$. If $x + y < Y_I$ and $x, y > 0$ according to Eq. (2.8), $\dot{x} + \dot{y} > 0$, therefore, $x + y$ increases along the solution $\hat{x}(t) + \hat{y}(t)$ and it is bounded above by Y_I. Hence, $(\hat{x}(t), \hat{y}(t))$ approaches to a point on the plane $x + y = Y_I$ as $t \to \infty$. Let us assume $(\hat{x}(t), \hat{y}(t))$ approaches to (x^*, y^*) such that $x^* > 0$ and $x^* + y^* = Y_I$. By Eq. (2.8), $\dot{x} + \dot{y} > 0$ when $x > 0$. Since $x^* > 0$, $\hat{x} + \hat{y}$ has to leave $x + y = Y_I$ plane in the direction of increasing $x + y$. That is a contradiction, since it means there exists a $t > 0$ such that $\hat{x}(t) + \hat{y}(t) > Y_I$. Hence, $x^* = 0$. Since $x^* + y^* = Y_I$, $y^* = Y_I$. By Eq.(2.3c), when $y = Y_I$, v tends to Y_I. Hence, $(\hat{x}(t), \hat{y}(t), \hat{v}(t)) \to (0, Y_I, Y_I)$ as $t \to \infty$. □

Model (2.3), when inequalities (H1) and (H2) hold, can have four steady states in $\mathcal{W}$, which we will refer to as follows: the tumour eradication steady state, $E_0 = (0, 0, 0)$, the treatment failure steady state, $E_U = (X_U, 0, 0)$, the 100% infection prevalence steady state, $E_I = (0, Y_I, Y_I)$ and the positive steady state, $E_p = (x_p, y_p, v_p)$, where

$$x_p = \frac{s(-Y_I b + X_U - Y_I)}{b(b + 1 - s)}, \tag{2.9a}$$

$$y_p = \frac{X_U b - s(X_U - Y_I)}{b(b + 1 - s)}, \tag{2.9b}$$

$$v_p = y_p. \tag{2.9c}$$

We will also refer to E_p as the positive steady state. The following lemma establishes conditions under which each of the above steady states exists. Here, existence of a steady state means its nonzero components are positive.

Lemma 2.5. Assume inequalities (H1) and (H2) hold. Then E_U and E_I always

exist, and E_p is positive if and only if

$$\frac{s(X_U - Y_I)}{X_U} < b < \frac{X_U - Y_I}{Y_I}. \tag{2.10}$$

Proof. According to inequality (H2), $X_U > 0$ and $Y_I > 0$, thus E_U and E_I always exist.

If $x_p = 0$, then a simple calculation shows $E_p = E_I$. Similarly, if $y_p = 0$, then $E_p = E_U$. However, we are interested in the case where both x_p and y_p are positive. According to inequality (H1), $s < 1$. Thus, $b + 1 - s > 0$. Hence, E_p is positive if and only if both followings are satisfied:

1. $-Y_I b + X_U - Y_I > 0$,
2. $X_U b - s(X_U - Y_I) > 0$.

Equivalently, E_p is positive if and only if $\dfrac{s(X_U - Y_I)}{X_U} < b < \dfrac{X_U - Y_I}{Y_I}$. □

The following lemma summarizes the conditions under which each boundary steady state is locally asymptotically stable.

Lemma 2.6. Assume inequalities (H1) and (H2) hold. Under Model (2.3),

1. E_0 is always unstable,
2. $E_U = (X_U, 0, 0)$ is locally stable if and only if $b < \dfrac{s(X_U - Y_I)}{X_U}$,
3. $E_I = (0, Y_I, Y_I)$ is locally stable if and only if $\dfrac{X_U - Y_I}{Y_I} < b$.

Proof. Part (1): The eigenvalues of the Jacobian of Model (2.3) at E_0 are $-m$, X_U, and sY_I. Since inequality (H2) holds, X_U and Y_I are both positive. Hence, E_0 has two positive eigenvalues. Therefore, it is always unstable.

Part (2): The Jacobian of Model (2.3) at E_U always has a negative eigenvalue, $-X_U$ which is associated with stability to perturbations along the x-axis. The other two

eigenvalues are eigenvalues of the following matrix:

$$A = \begin{bmatrix} s(Y_I - X_U) & bX_U \\ m & -m \end{bmatrix}$$

$\mathrm{tr}A = -m + s(Y_I - X_U)$ and $\det A = -mX_U\left(b - \dfrac{s(X_U - Y_I)}{X_U}\right)$. According to inequality (H2), we have $Y_I < X_U$. Hence, $\mathrm{tr}A$ is always negative. Therefore, the local stability of E_U is determined by the sign of $\det A$. Specifically, E_U is locally stable if and only if $\det A > 0$. Thus, E_U is locally stable if and only if $b < \dfrac{s(X_U - Y_I)}{X_U}$.

Part (3): Jacobian of Model (2.3) at steady state E_I has eigenvalues $\lambda_{I1} = -m$, $\lambda_{I2} = -sY_I$, and $\lambda_{I3} = X_U - Y_I - bY_I$. The first two eigenvalues are negative, so E_I is locally stable if and only if λ_{I3} is negative. In other words, E_I is locally stable if and only if $b > \dfrac{X_U - Y_I}{Y_I}$. □

Our numerical simulations suggest that when a steady state of Model (2.1) is locally stable, it is almost everywhere globally stable, i.e., each solution starting from a positive initial point will tend to that stable steady state. Hence, Theorem 2.4 and Lemma 2.6 together suggest that when $b > \dfrac{s(X_U - Y_I)}{X_U}$ treatment can shrink the tumour and when $b < \dfrac{s(X_U - Y_I)}{X_U}$ treatment fails. According to Lemma 2.6 when $b < \dfrac{s(X_U - Y_I)}{X_U}$, the treatment failure steady state, E_U, is stable. Therefore, when $b < \dfrac{s(X_U - Y_I)}{X_U}$, regardless of initial tumour size, administrating oncolytic virus has no effect, and the tumour grows to the maximum possible tumour size X_U (see Figure 2.3). when $b > \dfrac{s(X_U - Y_I)}{X_U}$ tumour size is eventually smaller than X_U. Therefore, the therapy is effective when $b > \dfrac{s(X_U - Y_I)}{X_U}$. Hence, we define

$$b_c := \frac{s(X_U - Y_I)}{X_U}, \tag{2.11}$$

as the treatment **control threshold** for b.

By Lemma 2.6 when $b > \dfrac{X_U - Y_I}{Y_I}$, the steady state E_I is stable. In this case, our numerical simulations conjecture that tumour size is eventually Y_I. Additionally, by Theorem 2.4, Y_I is the minimal tumour size for a specific virus (fixed set of parameters). Therefore, we define

$$b_o := \frac{X_U - Y_I}{Y_I}, \tag{2.12}$$

treatment **optimal threshold** for b.

Note that by (H1) and (H2), $s < 1$ and $Y_I < X_U$, hence $b_c < b_o$ (see Figure 2.3).

When $b_c < b < b_o$, either E_p is stable or a stable limit cycle exists. For the conditions under which E_p is locally stable see Theorem 2.8 in Section 2.3.2. When E_p is locally stable, our numerical simulation shows it is globally stable for positive initial conditions, meaning it attracts any solution starting from a positive initial point. Hence, When E_p is stable and therapy is started from any positive tumour size, the tumour size under therapy will be eventually the tumour size at E_p, which, by equation (2.9), is

$$T_p = \frac{X_U - sY_I}{b + 1 - s} \tag{2.13}$$

Hence, T_p decreases when all the parameters except b are fixed and the rescaled infectivity rate b increases (see Figure 2.3). Note that T_p does not depend upon m, in other words T_p does not change as m changes.

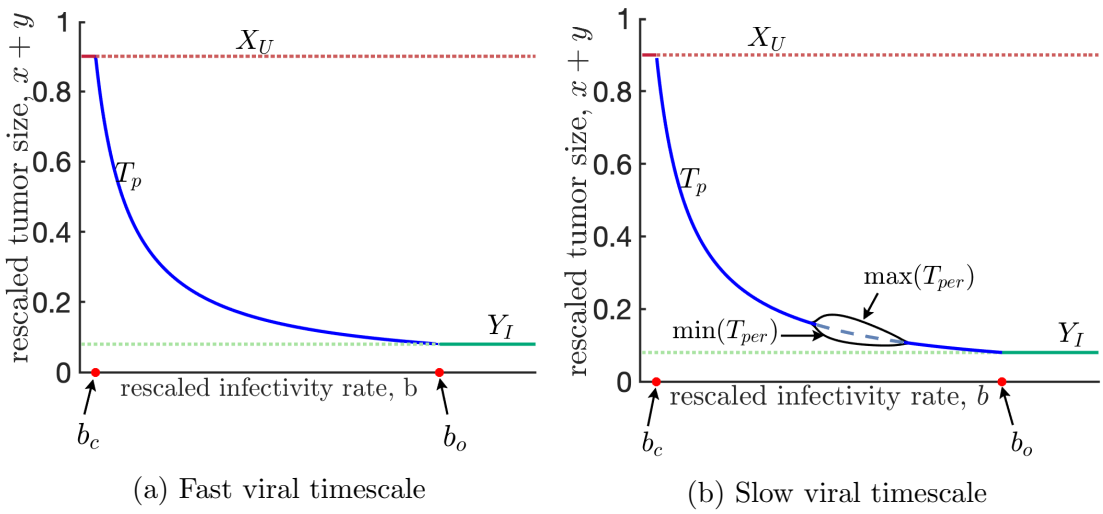

(a) Fast viral timescale

(b) Slow viral timescale

Figure 2.3: **The steady state tumour size decreases as horizontal transmission rate increases.** In this plot, a dashed (solid) curve means that the corresponding steady state is unstable (stable) for the given parameter values. When b is smaller than the control threshold b_c, treatment fails, and the steady state tumour size is X_U. When $b_c < b < b_o$, as b increases T_p decreases. T_p is the steady state tumour size at E_p. When b reaches the optimal threshold, b_o, the minimum tumour size under therapy, Y_I, is obtained. Panel (a) represent a case when viral timescale is fast. In this case E_p is always stable. Panel (b) represents a case when viral timescale is slow. Here, E_p can also be unstable. In this case, when E_p is unstable, a stable limit cycle exists. T_{per} refers to tumour size corresponding to stable limit cycle. This plot shows regardless of viral timescale tumour size under therapy eventually tends to a point between Y_I and X_U. This simulation is conducted under the set of parameters $X_U = 0.9$, $Y_I = 0.08$, $s = 0.5$, and $m = 1$. For the range of parameters chosen here the steady state E_p is stable, see Theorem 2.8.

2.3.2 Emergence of sustained oscillations

Consider the following three-dimensional system of ordinary differential equations

$$\dot{U} = f(U, \mu), \tag{2.14}$$

where $U \in \mathbb{R}^3$ and $\mu \in \mathbb{R}$. A Hopf bifurcation occurs at (U^*, μ^*) if there exists a curve of steady states $(U_{eq}(\mu), \mu) \in \mathbb{R}^{3+1}$ such that $(U_{eq}(\mu^*), \mu^*) = (U^*, \mu^*)$ and $Df\big(U_{eq}(\mu), \mu\big)$ has a pair of complex eigenvalues $\lambda(\mu) = R(\mu) \pm iI(\mu)$, such that

HB(1) $R(\mu^*) = 0$ and $I(\mu^*) \neq 0$,

HB(2) $\dfrac{dR}{d\mu}(\mu^*) \neq 0$,

and the real eigenvalue of $Df\big(U_{eq}(\mu^*), \mu^*\big)$ is negative [63].

To verify the occurrence of a Hopf bifurcation, one should show that the conditions HB(1) and HB(2) are satisfied and this process involves the algebraic calculation of eigenvalues. In 1998, Liu [69] proposed a criterion for the occurrence of Hopf bifurcation without calculation of eigenvalues for a general system of ordinary differential equation of order n. Here, we use this criterion in the proof of Theorem 2.8. Hence, below we restate the criterion "Liu's criterion" for a three-dimensional system of ordinary differential equations and provide a simpler proof for this special case.

Assume $(U_{eq}(\mu), \mu) \in \mathbb{R}^{3+1}$ is a curve of steady states for the system (2.14). Let $Df(U_{eq}(\mu), \mu)$ denote the Jacobian of f with respect to U at $(U_{eq}(\mu), \mu)$. Denote the characteristic polynomial of $Df(U_{eq}(\mu), \mu)$ by P_μ. P is a degree three polynomial in λ therefore, it can be written as $P(\lambda, \mu) = \lambda^3 + P_2(\mu)\lambda^2 + P_1(\mu)\lambda + P_0(\mu)$.

Define the Routh function for the equilibrium $(U_{eq}(\mu), \mu)$ as $H(\mu) := P_2(\mu)P_1(\mu) - P_0(\mu)$ [93].

Lemma 2.7 (**Liu's Criterion).** A Hopf bifurcation occurs at $\mu = \mu^*$ for the system (2.14) if and only if $P_0(\mu^*), P_1(\mu^*) > 0$, and the two following conditions are satisfied.

(i) $H(\mu^*) = 0$,

(ii) $\dfrac{dH}{d\mu}(\mu^*) \neq 0$.

Proof. Assume $P_0(\mu^*), P_1(\mu^*) > 0$ and conditions (i) and (ii) hold, we show that a Hopf bifurcation occurs at $\mu = \mu^*$ for the system (2.14). Since $H(\mu^*) = 0$, $P_2(\mu^*)P_1(\mu^*) = P_0(\mu^*)$. Hence, $P(\lambda, \mu^*) = (\lambda + P_2(\mu^*))(\lambda^2 + P_1(\mu^*))$. Since P has a real simple zero at $\mu = \mu^*$, hence by implicit function theorem P has a real

simple zero $c(\mu)$ in a neighbourhood of μ^*. Since, $P_1(\mu^*) > 0$, $P(\mu^*)$ has a pair of complex zeros in a neighbourhood of $\mu = \mu^*$. Hence, $P = 0$ has a pair of complex root $\lambda_1 = a(\mu) + b(\mu)i$, $\lambda_2 = a(\mu) - b(\mu)i$ and a real simple root $c(\mu)$ in a neighbourhood of $\mu = \mu^*$. Hence, P can be written as

$$P(\lambda, \mu) = \big(\lambda - a + bi\big)\big(\lambda - a - bi\big)\big(\lambda - c\big). \tag{2.15}$$

After simplification we have

$$P(\lambda, \mu) = \lambda^3 - \big(2a + c\big)\lambda^2 + \big(a^2 + 2ca + b^2\big)\lambda - \big(a^2 + b^2\big)c. \tag{2.16}$$

From Eq. (2.16), the Routh function can be written as,
$H = -2a(a^2 + 2ac + b^2 + c^2)$. Therefore,

$$H = -2a\big((a + c)^2 + b^2\big). \tag{2.17}$$

Since $P_0 \neq 0$, H is zero if and only if $a = 0$. Also, Since $P_0 \neq 0$, a and b cannot both be zero simultaneously. Hence, when condition (i) holds, condition HB(1) is satisfied.

Assume that $a(\mu^*) = 0$. We will show $\dfrac{da}{d\mu}(\mu^*) \neq 0$ if and only if $\dfrac{dH}{d\mu}(\mu^*) \neq 0$.

As we showed above $H = -2a\big((a + c)^2 + b^2\big)$, therefore

$$\frac{dH}{d\mu}(\mu^*) = -2\frac{da}{d\mu}(\mu^*)\big((a(\mu^*) + c(\mu^*))^2 + b(\mu^*)^2\big) - 2a(\mu^*)\frac{d}{d\mu}\big((a + c)^2 + b^2\big)(\mu^*).$$

Since $a(\mu^*) = 0$, therefore

$$\frac{dH}{d\mu}(\mu^*) = -2\frac{da}{d\mu}(\mu^*)\big((a + c)^2 + b^2\big).$$

Since $P_0 \neq 0$, then $(a+c)^2 + b^2 \neq 0$, therefore

$$\frac{dH}{d\mu}(\mu^*) = 0 \text{ if and only if } \frac{da}{d\mu}(\mu^*) = 0. \tag{2.18}$$

Hence, when condition (ii) holds, condition HB(2) of occurrence of the Hopf bifurcation is also satisfied. We have now shown (i) and (ii) imply the Conditions HB(1) and HB(2) of the occurrence of a Hopf bifurcation, so by Hopf bifurcation theorem, a Hopf bifurcation occurs when (i) and (ii) hold.

Now assume a Hopf bifurcation occurs at $\mu = \mu^*$ for the system (2.14). We will show that $P_0(\mu^*), P_1(\mu^*) > 0$, and (i) and (ii) hold. Since a Hopf bifurcation occurs at $\mu = \mu^*$, the curve of equilibrium has a pair of complex eigenvalues $a(\mu) \pm b(\mu)i$ and a real negative eigenvalue $c(\mu)$. Hence the characteristic polynomial of the Jacobian matrix at the corresponding equilibrium can be written as Eq. (2.15). Since a Hopf bifurcation occurs at $\mu = \mu^*$, $a(\mu^*) = 0$, $b(\mu^*) \neq 0$ and $c(\mu^*) < 0$. Therefore, $P_0(\mu^*) = -c(\mu^*)b^2(\mu^*) > 0$ and $P_1(\mu^*) = b^2(\mu^*) > 0$. The rest of the proof is similar to the proof of the reverse. □

Notice that Liu's Criterion shows that the real parts of the complex eigenvalues of the steady state U_{eq} change sign when the Routh function H changes sign. Therefore, any Hopf bifurcation curve bifurcating from that the steady state U_{eq} should also cross the surface $H = 0$. Of course H is a function of all the parameters and Hopf bifurcation is a codimension one bifurcation, so one may choose any parameter of interest to check whether a Hopf bifurcation occurs as they pass through the surface $H = 0$.

In the next theorem we investigate the appearance of a limit cycle bifurcating from steady state E_p by calculating the Routh function H and applying Liu's Criterion. In this work, we are interested in all the parameters of Model (2.3) such as b, Y_I, s and m to see what the possible outcomes of the treatment are as each of these

parameters change. Here as we will see in the proof of the next theorem, the Routh function is a function of all those parameters. However, m is of particular interest here since it is a parameter that is neglected (or assumed large) in many models. We are interested in the effect of the timescale of virus dynamics on the outcome of therapy. One may choose a different bifurcation parameter.

Theorem 2.8. *Let* $\dfrac{s(X_U - Y_I)}{X_U} < b < \dfrac{X_U - Y_I}{Y_I}$. *Define,*

$$\Delta := -\Big((x_p+sy_p+bx_p)^2 - x_p(x_p+y_p)b^2\Big) - 2\sqrt{\big(x_p + sy_p + bx_p\big)(x_p + sy_p)(x_p + y_p)x_p b}, \tag{2.19}$$

where x_p *and* y_p *are same as Eq.* (2.9). *Then we have the following results.*

(i) If $\Delta < 0$, *then* E_p *is a stable steady state.*

(ii) If $\Delta > 0$, *then two Hopf bifurcations occur as the parameter* m *changes. We denote these Hopf bifurcation points by* m_1 *and* m_2, *where* $m_1 < m_2$.

(iii) If $\Delta > 0$, *then* E_p *is a stable steady state if and only if* $m \in (0, m_1) \cup (m_2, \infty)$.

Proof. The Jacobian of Model (2.3) at $E_p = (x_p, y_p, v_p)$ is

$$J_p = \begin{bmatrix} -x_p & -x_p & -bx_p \\ (b-s)y_p & -bx_p - sy_p & bx_p \\ 0 & m & -m \end{bmatrix}$$

The characteristic equation for J_p is

$$\begin{aligned} P &= \det(\lambda I - J_p) \\ &= \lambda^3 + \underbrace{(bx_p + sy_p + m + x_p)}_{P_2}\lambda^2 + \underbrace{(b{x_p}^2 + bx_py_p + msy_p + mx_p)}_{P_1}\lambda + \underbrace{mx_py_pb(b+1-s)}_{P_0}. \end{aligned} \tag{2.20}$$

By inequality (H1), $s < 1$. Therefore, P_1, P_2 and P_0 are always positive. The Routh

function H for the above characteristic polynomial is as follows

$$H = P_2P_1 - P_0 = \underbrace{(x_p + sy_p)}_{A} m^2 + \underbrace{\Big((x_p + sy_p + bx_p)^2 - x_p(x_p + y_p)b^2\Big)}_{B} m \tag{2.21}$$
$$+ \underbrace{b\big(x_p + sy_p + bx_p\big)(x_p + y_p)x_p}_{C}.$$

Since $A, C > 0$, $H = 0$ has positive solutions for m if and only if $B < 0$ and $B^2 - 4AC \geq 0$. In other words, H has positive solutions for m if and only if $-B \geq 2\sqrt{AC}$. Notice that $\Delta = -B - 2\sqrt{AC}$. Hence, $H = 0$ has solutions if and only if $\Delta \geq 0$.

When $\Delta < 0$, H is always positive. As we mentioned above P_2, P_1 and P_0 are also positive. Thus, according to the Routh-Hurwitz stability criterion [93], the steady state E_p is locally asymptotically stable. This proves part (i) of the theorem.

When $\Delta > 0$, the quadratic H has two distinct positive roots m_1 and m_2, where $m_1 < m_2$. Of course, $\dfrac{dH}{dm}(m) \neq 0$ for $m = m_1, m_2$. Therefore according to Liu's Criterion, Hopf bifurcations occur as m changes through m_1 and m_2. This proves part (ii) of the theorem.

When $\Delta > 0$, and $m \in (0, m_1) \cup (m_2, \infty)$, then the Routh function is positive and therefore according to the Routh-Hurwitz criterion, E_p is locally asymptotically stable. This proves part (iii). □

Note that when $\Delta = 0$, then the Routh function has a repeated root. Hence, there exists an m^* such that $H(m^*) = 0$, but $\dfrac{\partial H}{\partial m}(m^*) = 0$. Thus, the conditions for the occurrence of Hopf bifurcation with respect to parameter m are not satisfied at $m = m^*$. Therefore, when $\Delta = 0$, for any $m \neq m^*$, E_p is an stable steady state and it is a non-hyperbolic steady state at $m = m^*$. In our numerical simulations, we observed that for $m = m^*$, the steady state E_p is globally stable, and every

solution starting from a positive initial point tends to E_p very slowly, in the way that oscillating solutions are decaying very slowly and tending eventually to E_p.

The above theorem shows for each set of parameters Y_I, b, and s, there are possibly two points m_1 and m_2 at which a Hopf bifurcation occurs. A limit cycle sources from m_1 and sinks in m_2. Based on our numerical simulations (see next section), we conjecture that there is a unique limit cycle for every $m \in (m_1, m_2)$. Our aim is to study the limit cycle through numerical simulations and determine its stability. We will do this by choosing a surface perpendicular to the limit cycles and following the solution as it repeatedly crosses the surface. The following proposition shows that we have a suitable surface $y - v = 0$ to use as the Poincaré section and allows us to set up the return map numerically. This proposition tells that each positive point is either on the stable manifold of E_p or its trajectory crosses $y-v = 0$ surface infinitely many times. There are situations where E_p appears to be globally stable, attracting all the trajectories with positive initial values. Then, trajectories can spiral to E_p, crossing the surface $y - v = 0$ infinitely many times.

Proposition 2.9 (Global dynamics). When $\dfrac{s(X_U - Y_I)}{X_U} < b < \dfrac{X_U - Y_I}{Y_I}$, each trajectory starting from a positive point either crosses the surface $y-v = 0$ infinitely many times or its positive limit set is E_p.

Proof. Let $q(t) = (x^q(t), y^q(t), v^q(t))$ be a solution of Model (2) starting from initial point (x_0^q, y_0^q, v_0^q) such that $x_0^q, y_0^q, v_0^q > 0$ and let ω_q denote the omega limit set of q [112]:

$$\omega_q = \left\{ X \in \mathcal{W} \middle| \exists t_n \geq 0; \lim_{n\to+\infty} t_n = +\infty \text{ and } \lim_{n\to+\infty} q(t_n) = X \right\}.$$

Suppose the trajectory $q(t)$ does not cross the surface $y-v = 0$ in a finite time. Then it remains on one side of the plane $y = v$ for all $t \geq 0$. Here we assume $y^q(t) \geq v^q(t)$ for all $t \geq 0$ (the proof for the case $y^q(t) \leq v^q(t)$ for all $t \geq 0$ is similar).

Let $\mathcal{J} := \{(x, y, v) \in \mathcal{W}; y \geq v\}$. $\mathcal{J}$ is a compact set. Define $L : \mathbb{R}^3 \to R$ such that $L(x, y, v) = v$. L is a continuous function, and the image of a compact set under a continuous function is compact. Hence, $L(\mathcal{J})$ is a compact, and therefore bounded subset of $\mathbb{R}$; since $\{q(t) : t \geq 0\} \subset \mathcal{J}$, $L(q(t))$ is a bounded subset of $\mathbb{R}$. Since, $\dot{L} = \dot{v} = m(y - v)$, $L(q(t))$ is a monotonic (non-decreasing) subset of $\mathbb{R}$ for all $t \geq 0$. Since, $L(q(t))$ is monotonic and bounded, $\lim_{t\to\infty} L(q(t))$ exists. Assume $L_0 = \lim_{t\to\infty} L(q(t))$, hence $\lim_{t\to\infty} v^q(t) = L_0$.

Assume $X(t)$ is a solution of Model (2.3) starting from X_0 such that X_0 is in ω_q. Since an omega limit set is a positively invariant set [112], ω_q is positively invariant. Hence, $X(t) \in \omega_q$ for all $t \geq 0$. For a fixed $t^* > 0$, there exists a sequence $t_n \geq 0$ such that $\lim_{n\to\infty} t_n = \infty$ and $\lim_{n\to\infty} q(t_n) = X(t^*)$. Since L is a continuous function $\lim_{n\to\infty} L(q(t_n)) = L(X(t^*))$, $L(X(t^*)) = L_0$. Therefore, $L(X(t)) = L_0$ for all $t \geq 0$. Hence, $\dot{v} = 0$ on $X(t)$. So, $y = v$ on $X(t)$ so $\dot{y} = 0$. Since $v = y = L_0$ are fixed on $X(t)$, by solving Eq. (2.3b) for $x(t)$, there are two possibilities; either $L_0 = Y_I$, in this case $x = 0$, or $L_0 \neq Y_I$, in this case $x = \dfrac{s(Y_I - L_0)}{b - s}$. Hence, $\dot{x} = 0$ on X. So $X(t)$ is a steady state. Since $b < \dfrac{X_U - Y_I}{Y_I}$, E_I cannot attract solutions with a positive initial condition, we have $L_0 \neq Y_I$. Thus, $\omega_q = \{E_P\}$ and $q(t)$ goes to ω_q which equals E_p.

We have proved that if a trajectory starting from a positive point does not cross surface $y - v$ in a finite time, it will eventually tend to E_p. If that trajectory crosses the surface $y - v = 0$ in a finite time, there are two options: either it crosses the surface $y - v = 0$ in a finite time or eventually tends to E_p. Following the same pattern, we conclude that if a trajectory starting from a positive point does not tend to E_p, it crosses the surface $y - v = 0$ infinitely many times. $\square$

2.4 Results from Numerical Simulations

2.4.1 Global attracting surface

As it is mentioned above in Theorem 2.8, when $\Delta > 0$ and $m_1 < m < m_2$ the steady state E_p is unstable. Our numerical simulations suggest that for each $m \in (m_1, m_2)$, there exists a stable limit cycle (see Figure 2.4). Furthermore, our numerical simulations suggest that when a limit cycle exists, it is almost everywhere globally stable, i.e., each solution starting from a positive initial point that is not located on the stable manifold of the steady state E_p tends to the limit cycle. As an example, in Figure 2.4, the black closed curve is the limit cycle, the point marked by black circle is E_p, and the dotted curve passing through E_p is its stable manifold. Each solution starting from a point on the stable manifold of E_p (the dotted curve in Figure 2.4) tends to E_p. Each solution starting from a positive initial point which is not on the stable manifold of E_p, tends to the limit cycle. The red curves start from a solution outside of the red disk near the stable manifold of E_p. They jump into the interior area of the red disk enclosed by the limit cycle and spiral out from the nearby steady state E_p, and tend to the limit cycle. The green curve oscillations' amplitude gets smaller and spirals in towards the limit cycle. As the figure illustrates, the disk which is traced by the red curve, starting very nearby E_p and bounds to the limit cycle, is the unstable manifold of the steady state E_p. The red disk, together with the steady state E_p and its boundary, the limit cycle, forms a global attracting surface which we denote by G. Each solution with a positive initial condition tends to G.

In Theorem 2.8 we showed that two Hopf bifurcation may occur when parameter m passes through m_1 and m_2. Our simulations suggest that when $m < m_1$ or $m > m_2$ the steady state $E_p = (x_p, y_p, y_p)$ is almost everywhere globally stable, strictly speaking it attracts all the solutions starting from a positive initial point. Therefore, when $m < m_1$ or $m > m_2$, the steady state tumour size is $T_p = x_p + y_p$.

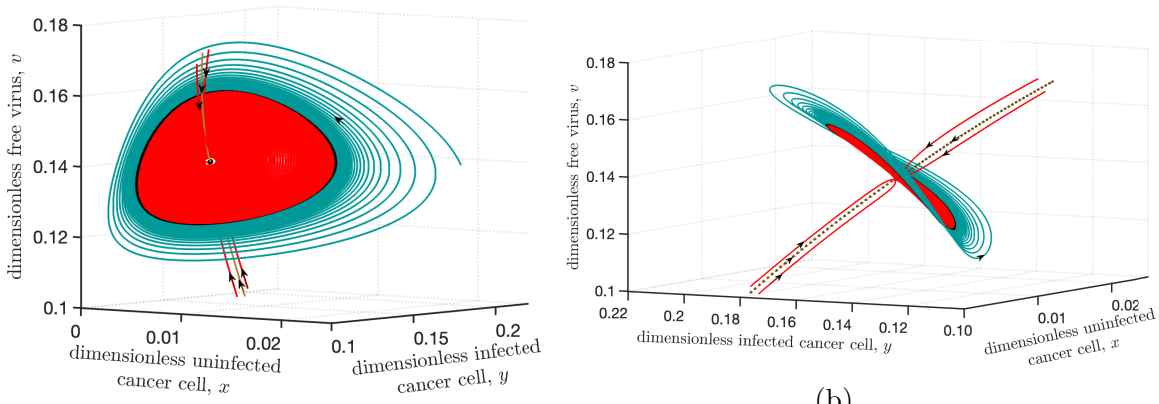

(a) (b)

Figure 2.4: **The global attracting surface (a)** The black curve represents a stable limit cycle, and the point marked by a black circle is E_p. Each solution starting from a positive point (except for the steady state E_p and its one dimensional stable manifold) approaches this limit cycle. The red disk (traced out by the red curves) is the unstable manifold of E_p, and the limit cycle is its boundary. Panel **(b)** is the same figure as panel (a), which has been rotated to show the stable manifold of steady state E_p. The dotted curve shows one dimensional stable manifold of E_p. Every solution starting from a point on the dotted curve is attracted to E_p. The disk centred at steady state E_p with its boundary, the limit cycle, is (numerically) a global attracting surface [112]. This simulation is conducted for $\bar{r} = 1$, $s = 0.5$, $X_U = 0.9$, $Y_I = 0.08$, $m = 0.1$, and $b \sim 5.35$. This b is the mid point of the interval $\left(\frac{s(X_U - Y_I)}{X_U}, \frac{X_U - Y_I}{Y_I}\right)$, on which E_p exists.

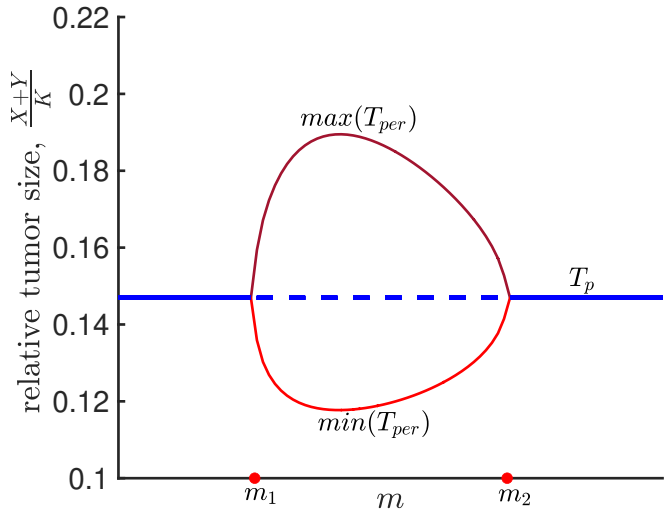

Figure 2.5: **Bifurcation with respect to m:** This plot demonstrates how the oscillation in tumour size changes when variable m changes. As figure describes when m passes through m_1, steady state, $E_p = (x_p, y_p, y_p)$ becomes unstable and a stable limit cycle appears. $T_p = x_p + y_p$, shows the tumour size when E_p is stable, and $\max(T_{per})$ and $\min(T_{per})$ shows the maximum and minimum of tumour size when the limit cycle exists. When m passes through m_2 the stable limit cycle disappears and again E_p becomes stable. This simulation is done for the set of parameters s=0.5, X_U=0.9, Y_I=0.08, and $b \sim 5.35$. This b is the mid point of the interval $\left(\frac{s(X_U-Y_I)}{X_U}, \frac{X_U-Y_I}{Y_I}\right)$, on which E_p is positive.

When $m_1 < m < m_2$, each solution starting from a positive point which is not on the stable manifold of E_p tends to the limit cycle, so in this case the tumour size is oscillating, so it has a maximum, denoted by the upper curve $\max(T_{per})$ and a minimum, denoted by the lower curve $\min(T_{per})$. The Hopf- bifurcation in tumour size with respect to changes in parameter m is illustrated in Figure 2.5. As this figure illustrates, the Hopf bifurcation is global in the sense that as m changes, a continuous path of limit cycles sources from m_1 and sinks in m_2 [74].

2.4.2 Fast-slow dynamics of tumour size

Another interesting result that is observed numerically is that Model (2.1) shows fast and slow behaviour. As we mentioned above, there is a range of parameters for which there is a unique stable limit cycle to which every trajectory starting from a

positive point, except for a single curve (the stable manifold of the steady-state), is attracted. However, not every region of state spaces gets attracted with the same speed. Since the speed of remission is a crucial factor in the therapy, it motivates us to investigate in which regions of state spaces fast and slow behaviour occur.

An example of slow dynamics is shown in Figure 2.6, where two solutions are shown approaching a limit cycle very slowly. Trajectories oscillate with a period of about 57 days. It takes years to get close to the limit cycle. One (green) approaches with decreasing amplitude, and the other (red) approaches with increasing amplitude. The black curve denotes the steady state E_p. This is the steady state that loses its stability at the Hopf bifurcation point when the stable limit cycle is created. The red curve starts with an initial condition near E_p and slowly spirals out to the stable limit cycle. The two yellow circles denote the time interval in which the red trajectory's amplitude grows from 10% of the limit cycle's amplitude to 90%, a period of 8.2 years. In Figure 2.6 we use the parameter values $\bar{r} = 1$, $X_U = 0.9$, $s = 0.5$, $Y_I = 0.08$, $m = 0.1$ and $b \sim 5.35$. This b is the midpoint of the interval $(\frac{s(X_U - Y_I)}{X_U}, \frac{X_U - Y_I}{Y_I})$, on which E_p exists.

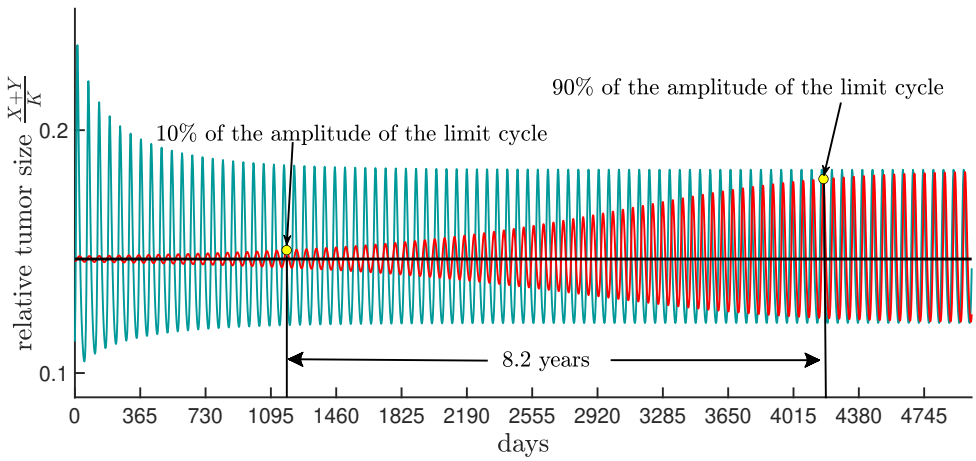

Figure 2.6: **Slow dynamics**. The black curve is the steady state of Model (2.1) that loses its stability and bifurcates in a stable limit cycle when the Hopf bifurcation occurs. As the figure suggests, the red and green curves tend very slowly to the attracting limit cycle. The time between peaks is approximately 57 days. The red curve takes 8.2 years to grow from 10% of the amplitude of the limit cycle to 90%, a very long time for a cancer patient; see the text for the parameter values.

An example of fast dynamics is illustrated in Figure 2.7. Under the set of parameters that this simulation is conducted steady state E_p, which is marked with black circle, has three eigenvalues $e_1 = -0.212$ and $e2, e3 = 0.001 \pm 0.11I$. Therefore, in a neighbourhood of E_p solutions oscillate with the period $\frac{2\pi}{\mathrm{Im}(e_2)} \sim 57$. A thousand random points, marked by yellow circles, are chosen to show fast attraction to the global attracting surface. Each solution that starts from a point marked yellow terminates in a purple point after 57 days. In Figure 2.7 same plot has been provided from two different views to provide a better observation that all the purple points are located on the slow manifold. The slow manifold includes the global attracting surface and extends outside the limit cycle, including the solid green area. Therefore, the slow manifold is the region on the state space that tends very slowly to the limit cycle, as we discussed in Figure 2.6.

In Figure 2.8 we use the Poincaré map defined on the Poincaré surface $y - v = 0$ to observe where the slow manifold is located. The black curve is the limit cycle

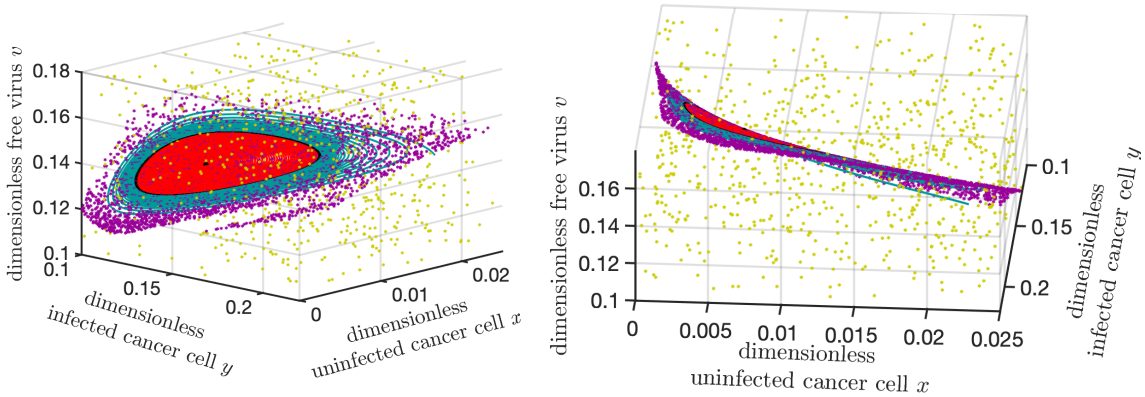

Figure 2.7: **Fast attraction and collapse to the global attracting surface over one period**. The two plots are the same simulation shown in different views. The black closed curve bounding the red disk is an attracting limit cycle, and the black circle near the centre of the red disk is the steady state E_p. In this figure, one thousand random points (yellow dots) are chosen, and the positions of their trajectories after 57 days are shown with purple dots. All the purple dots appear to lie on a 2-dimensional surface that contains the limit cycle, E_p and the unstable manifold of E_p(The global attracting surface is the disk centred at steady state E_p and includes the disk boundary, which is the limit cycle). This shows each trajectory tends quickly to the global attracting surface.

and the black triangle is the steady state E_p. The yellow circle on the limit cycle represents the fixed point $\mathcal{FP}$ of the Poincaré map, which in this case it takes 57 days for the Poincaré map starting from fixed point to return back to it. The rest of the curves are obtained by capturing the orbit of a given point under the Poincaré map. The red curve and the green curves in this figure show slow dynamics. For example for the red curve it takes at least 80 iterations of the Poincaré map for the initial point chosen near to the steady state to tend to $\mathcal{FP}$ and it takes up to 55-57 days between two consecutive points in the orbit, meaning it takes at least 4480 days to approach towards the limit cycle. Starting from any initial condition not located on the green or red curve, second or third point in the orbit under Poincaré map is located either on the red or green curve. The Jacobian of the Poincaré map at $\mathcal{FP}$ has two eigenvalues $e_1 = 7.3295 \cdot 10^{(-6)}$ and $e_2 = 0.8962$. Since $e_2/e_1 = 122280$ means that the fast attraction happens 122280 times faster than the slow dynamics.

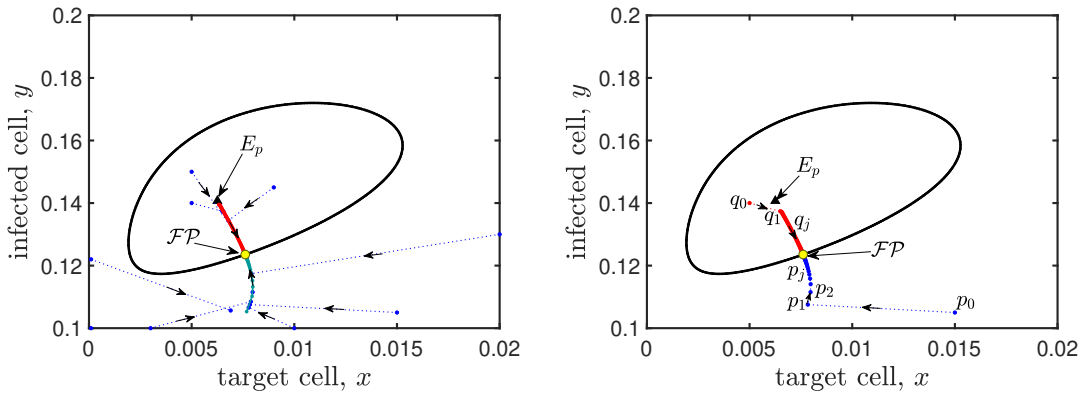

(a) (b)

Figure 2.8: **Capturing fast-slow dynamics using Poincaré map. (a)** This panel illustrates slow attraction to the limit cycle and fast attraction to the slow manifold. Except the black curve which shows the stable limit cycle, every other curve is the positive orbit of a given point under the Poincaré map. Every blue curve starts from an initial point which is not located on the red or the green curves. The second or third point in the positive orbit of each given point which is not located on the red or green curve, is located on the red or green curve. This assures fast attraction to the green and red curve. Each solution starting from an initial point on the green or red curve takes a lot of iterations to reach to the point marked yellow. The yellow point is on the Poincaré section and it returns to itself after one iteration, therefore it is the fixed point of the Poincaré map. The set of all the points on the green and red curve except the fixed point of the Poincaré map, is called the slow manifold for the Poincaré map. Panel **(b)** demonstrates how orbit of a given point under the Poincaré map behaves. To do this, two orbits q_j starting from q_0 and p_j starting from p_0 are shown. Both orbits tend to the fixed point of Poincaré map labelled by $\mathcal{FP}$. The first iteration from p_0 to p_1 takes 55 days. It takes between 56-57 days between every two consecutive points in the orbit of Pj. The time difference between every consecutive point in the sequence q_j changes from 57-60 days and eventually remains 57 days. This simulation is conducted for $\bar{r} = 1$, $s = 0.5$, $X_U = 0.9$, $m = 0.1$ and $b \sim 5.35$. This b is the mid point of the interval $\left(\frac{s(X_U - Y_I)}{X_U}, \frac{X_U - Y_I}{Y_I}\right)$, on which E_P exists.

2.4.3 Dependency of virulence threshold on viral timescale and horizontal transmission rate

Recall parameter $Y_I = 1 - \dfrac{\bar{a} + \bar{d}}{\bar{s}}$. Changes in parameters $\bar{a}$ and $\bar{s}$ lead to changes in Y_I. A more aggressive virus causes a larger increase in the death rate and more decrease in the growth rate of cancer cells after infection, i.e., higher $\bar{a}$ and lower $\bar{s}$. Notice that when $\bar{a}$ increases or $\bar{s}$ decreases, Y_I decreases. Hence, lower values of Y_I mean a more aggressive virus is administrated. Thus, we can use Y_I as an indication of the level of cytotoxicity of the virus. It is important to know how virulent a virus should be engineered to obtain more tumour shrinkage under therapy. Our simulations below suggest that identifying the optimal range for virulence of virus depends on both the viral timescale and infection horizontal transmission rate.

Figure 2.9 is a heat map of the maximum tumour size with respect to parameters b and Y_I in two scenarios: (a) fast viral timescale, $m = 1$, and (b) slow viral timescale, $m = 0.1$. As we mentioned before, regardless of viral timescale when parameters b and Y_I are chosen such that $b < b_c$, treatment fails. Recall that $b_c = \frac{s(X_U - Y_I)}{X_U}$ is the treatment control threshold. Additionally, our numerical simulations recommend that when parameters b and Y_I are chosen such that $b > b_o$, where $b_o = \frac{X_U - Y_I}{Y_I}$ is the treatment optimal threshold, the steady state E_I is globally stable, attracting all the solutions starting from a positive initial point; in this case tumour size is eventually Y_I. Hence, as it is illustrated in Figure 2.9, when parameters b and Y_I are chosen such that $b > b_o$, for a fixed b value, by decreasing Y_I, tumour size decreases, regardless of viral timescale.

Theorem 2.8 shows that the viral timescale affects the outcome of therapy when parameters Y_I and b are chosen such that $\frac{s(X_U - Y_I)}{X_U} < b < \frac{X_U - Y_I}{Y_I}$, this area is the area between the solid and dotted curves in Figure 2.9. As Figure 2.9a illustrates, when the viral timescale is fast, the best range for parameters b and Y_I is the area between

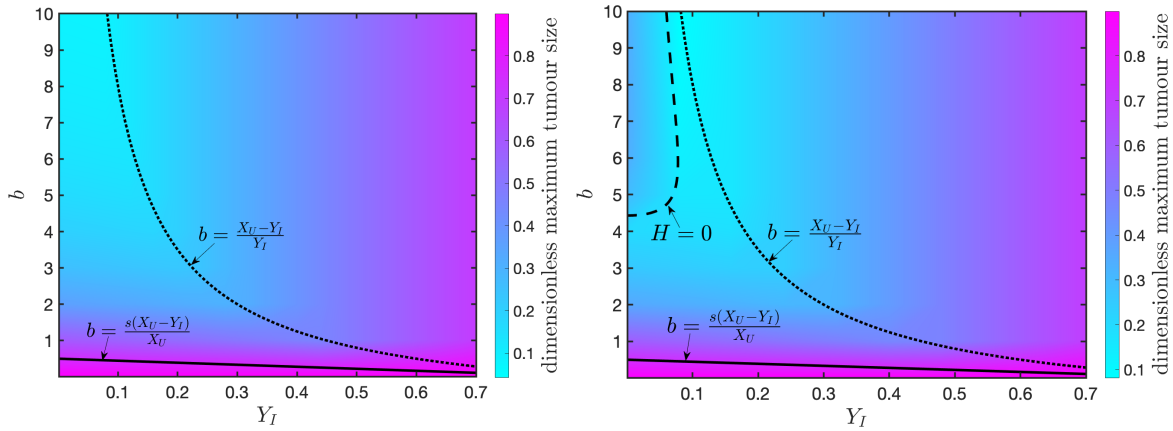

(a) fast viral timescale

(b) slow viral timescale

Figure 2.9: **Changes in the maximum tumour size with respect to b and Y_I.** This figure represents how tumour size changes when parameters b and Y_I change. Parameter values are $s = 0.5$, $X_U = 0.9$, and $m = 1$ in plot (a), and $m = 0.1$ in plot (b). Panel (a) demonstrates when virus dynamics are fast, the maximum tumour shrinkage under therapy is possible for lower Y_I and higher b values. Panel (b) represents that lower Y_I values will not guarantee the best outcome when virus dynamics are slow. In this case, the smallest tumour size is achieved when parameters b and Y_I are chosen such that $H = 0$.

the solid curve and the dotted curve. However, when the viral timescale is slow, the greatest tumour shrinkage is obtained when the parameters Y_I and b are chosen along the surface $H = 0$, see Figure 2.9b for an illustration. As Figure 2.9b suggests when viral timescale is slow, a high level of virulence has drawbacks on the outcome of viral therapy. When the viral timescale is slow, the best range for parameters Y_I and b is the area between the three curves.

In Figure 2.10, five different values of Y_I are chosen to find out the effective level of virus cytotoxicity for a fixed b value. The value of Y_I for which the red curve is simulated is $Y_I = \dfrac{X_U}{1+b}$. The value of Y_I for which black curve is plotted, when $m = 0.1$, is the value of Y_I for which $H = 0$. In the case of a fast viral timescale, in other words when m is high enough that it is not in the interval (m_1, m_2), no limit cycle exists. In this case as Figure 2.9a and Figure 2.10a suggest for $Y_I \leq \dfrac{X_U}{b+1}$, changes in Y_I does not affect the tumour size much. The blue, black and green

curves in Figure 2.10a are all corresponding to the cases where $Y_I < \frac{X_U}{b+1}$. As Figure illustrates there is very little difference in the eventual tumour sizes of blue, black and green curves with the case when $Y_I = \frac{X_U}{b+1}$, meaning the red curve. However, the tumour size is eventually smaller when $Y_I = \frac{X_U}{b+1}$. Therefore, for higher values of m, and fixed b value, the best range for Y_I is $(0, \frac{X_U}{1+b}]$ and the most tumour shrinkage is achievable at $Y_I = \frac{X_U}{1+b}$.

Figure 2.10b illustrates the tumour size overtime when the viral timescale is slow and parameter b is fixed. When $Y_I < \frac{X_U}{1+b}$, the system shows oscillatory behaviour: both green and black curves are decaying oscillations. The value of Y_I for which the black curve is simulated is when $H = 0$, therefore a Hopf bifurcation occurs at this point, $Y_I = 0.088$. Therefore, the amplitude of the oscillations takes a very long time to tend to zero. Hence, in practice, if solutions are only observed for a short time, the black curve seems like a stable limit cycle. When $Y_I = 0.01 < 0.088$ (the blue curve), the tumour size is periodic with a very high amplitude. As the small box in the right corner of Figure 2.10b suggests, there is not much difference in the eventual tumour size for the black, green and red curves. If the solution is observed for a very long period of time, eventually the red curve would be lower, but in practice, observing the cases for such long period of time is not possible. Therefore, when the viral timescale is slow, for a fixed b value, the best range for Y_I is the region bounded by H and the surface $Y_I = \frac{X_U}{1+b}$. In this case, the most tumour shrinkage is observed at the value of Y_I for which $H = 0$.

2.5 Discussion

This chapter offers a very simple mathematical model, Model (2.1), to analyze the interactions between cancer cells and viruses during an oncolytic viral therapy. Even though Model (2.1) is simple, it captures some important features about oncolytic

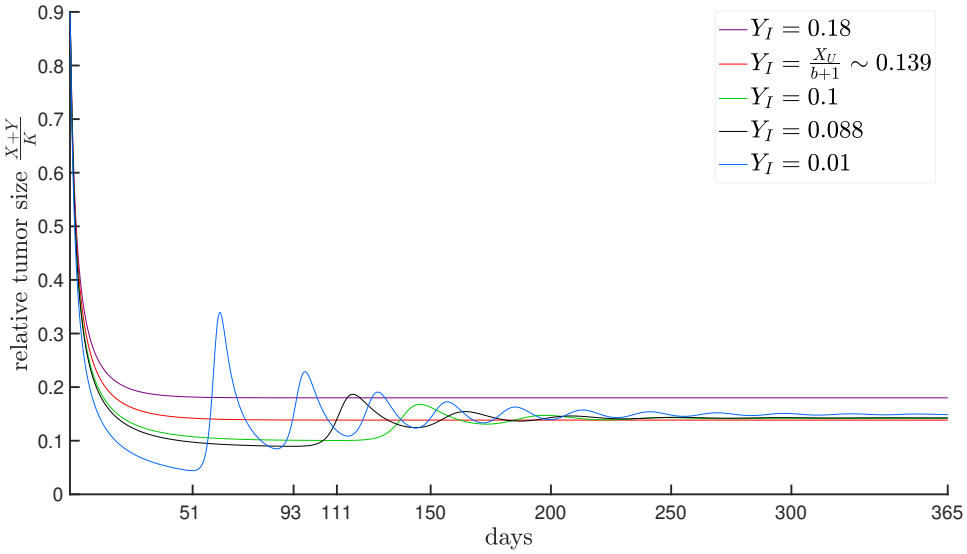

(a)

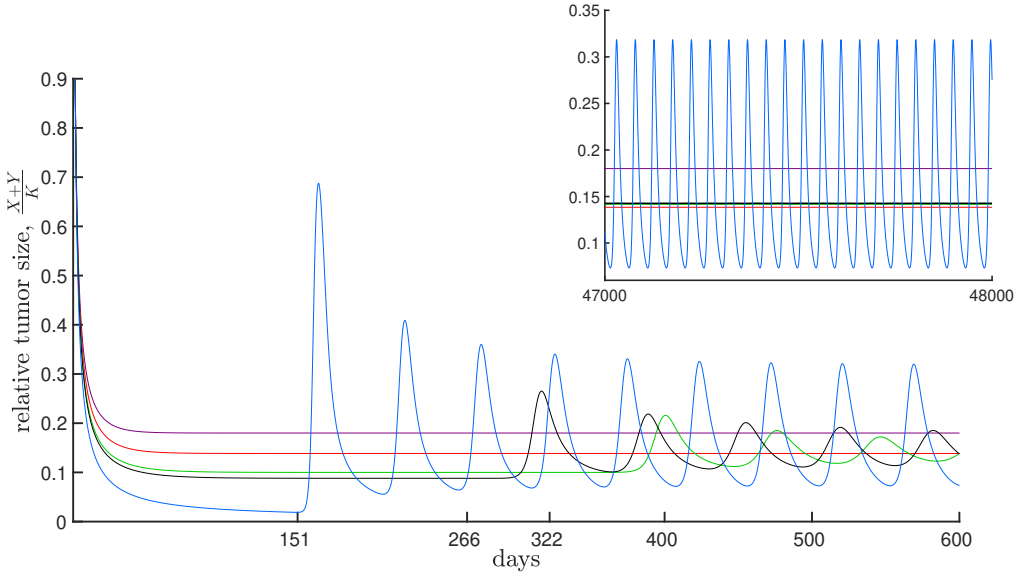

(b)

Figure 2.10: **Effect of cytotoxicity Y_I on the tumour size.** Plot (a) $m = 1$ and Plot (b) $m = 0.1$. As Plot (a) shows for higher values of m, when $Y_I \leq \frac{X_U}{b+1}$, eventually the tumour size is smaller. Therefore, the best range for parameter Y_I, $0 < Y_I < \frac{X_U}{1+b}$. For $m = 0.1$, as plot (b) suggest when values of Y_I decrease, dynamics becomes oscillatory and the amplitude of oscillation increase by decreasing Y_I. For $Y_I = 0.01$ stable oscillation occurs with a very high amplitude. As the small panel at the right top corner of plot (b) shows, both green and black curve or decaying oscillation but it takes very long time for the amplitude of the black curve to tends to zero. When $m = 0.1$, the best range for $0.088 < Y_I \leq \frac{X_U}{b+1}$. This simulation is conducted under the set of parameters $\bar{r} = 1$, $X_U = 0.9$, $\bar{s} = 0.5$, and $b = 5.5$.

viral therapy: features that help to set expectations about the outcome of the treatment and how to engineer the virus in order to get better results. For example, Lemma 2.6, which shows the tumour eradication steady state, E_0, is always unstable, implying that tumour eradication is not possible. This suggests an oncolytic virus that only has an oncolysis effect cannot be used as a cure for cancer. However, Theorem 2.2 implies that the tumour size under therapy over time is always smaller than it would have been without therapy. Therefore, oncolytic viral therapy can be used to control the speed of growth of a tumour. Theorem 2.4 and Lemma 2.6 together show that oncolytic viral therapy can be used to reduce tumour size considerably. The proposition suggests oncolytic viral therapy may be used as an intervention method to control the size of the tumour before a conventional therapy can be followed up.

One of our goals in this study was to optimize the therapy by recommending the parameter regions in which the therapy has the best outcome. To do this, we focused our analysis on some parameter combinations: an indication of virulence, Y_I, a rescaled horizontal transmission rate, b, and the viral clearance rate relative to the mitotic rate of uninfected cancer cells, m.

To ease the communication with the reader throughout this chapter, we denoted the stable, steady state tumour size when therapy fails, or if no treatment occurs, by X_U and the minimal steady state tumour size under the therapy by Y_I. In Theorem 2.4, we showed that the interval $[Y_I, X_U]$ is a global attracting set for the tumour size. Specifically, for a specific virus, i.e., for a fixed set of parameters, the tumour size under therapy is eventually at least Y_I. Therefore, Y_I is the minimum possible tumour size under the therapy.

Lemma 2.6 and Theorem 2.8 specify two possible outcomes for the treatment: (1) failure, and (2) partial success or tumour control. Partial success means a consider-

able reduction in tumour size. Partial success includes two scenarios: (2a), partial tumour infection, and (2b) 100% infection prevalence.

(1) Failure: Treatment fails when the horizontal rate of infection transmission is smaller than the control threshold. In this case, therapy has no impact, and the tumour grows to the maximum size X_U, the same as when no therapy would take place. Long-term tumour reduction will be possible when the horizontal rate of infection transmission is above of control threshold.

2-Partial success:

2(a). **partial infection:** This scenario occurs when the horizontal transmission rate is between the control threshold and optimal threshold. In this case, there are two possible scenarios: if the viral timescale is slow, the positive steady state is unstable, and every solution starting from a positive point that is not on the stable manifold of the positive steady state tends to the stable limit cycle. When the viral timescale is fast, the positive steady state is globally stable, and no limit cycle exists. See Figures 2.4 and 2.5. In this case, as Theorems 2.2 and 2.4, and Lemma 2.5 suggest since horizontal infection transmission is above the control threshold, therapy reduces the tumour size, in comparison with the case that no therapy occurs, but it is not the minimum possible tumour size under the therapy.

2(b). **100% infection prevalence:** The maximum tumour shrinkage by therapy is obtained in this scenario which happens if infection horizontal transmission is equal to the optimal threshold.

In Model (2.1), we assumed (Assumptions (A2) and (A4)) that cancer cells are mitotic and the growth rate of infected cancer cells is lower than their apoptosis rate. If we relax these assumptions, meaning either the infected cells do not self-renew or the self-renewal rate of infected cancer cells be lower than their apoptosis rate, then 100% infection prevalence will not be possible. Therefore, only two scenarios

would be possible: failure or partial infection. Furthermore, the tumour shrinkage by therapy will be less than our model predicts, since the model considers two pathways to infection transmission.

In this study, interactions with immune cells and spatial heterogeneity (neither morphological nor phenotypical) are not discussed. Model (2.1) can be extended to consider the effect of virus specific immune response that seems to be one of the main barriers in the success of oncolytic viral therapy. In our work in progress, by extending the model to also consider interactions of virus specific immune responses with cancer cells and the virus, in most cases, no longer oscillatory behaviour is observable. In the presence of virus specific immune responses, the reduction in tumour size will be lower in comparison with the case no interaction with immune cells is taken into account. However, oncolytic therapy seems yet promising as a considerable reduction in tumour size is still observable.

One of the assumptions under which we started the study was Assumption (A5). One might question how virulent the virus should be? As we discussed before, parameter Y_I, the minimum tumour size, can also be used as an indication of the level of cytotoxicity of the virus. Lower values of Y_I mean the virus is more virulent. As Figures 2.9 and 2.10 illustrate, selecting the best range for virulence also depends on the parameter m. Parameter m is the relative clearance rate of the virus and gives the timescale of the virus dynamics. When parameter m is large, meaning $\bar{m} >> \bar{r}$, as earlier studies by Komarova and Wodarz [61] suggested the system is in quasi-steady state. Meaning, v rapidly approaches y, therefore Model (2.1) can be reduced to the "slow" x-y subsystem, with $v = y$. The maximum level for cytotoxicity recommended by Komarova and Wodarz [61] in terms of parameters of Model (2.3) is equivalent to $Y_I = \dfrac{X_U}{b+1}$ (notice that maximum level of cytotoxicity means lowest value recommended for Y_I). However, our results show that if the parameter m is high enough and does not belong to the interval (m_1, m_2) (see Theorem 2.8 for m_1,

and m_2), then $0 < Y_I \leq \dfrac{X_U}{b+1}$. We recommend the highest value for Y_I is $X_U/(b+1)$ based on our simulations in Figures 2.9 and 2.10. Although, there is not a huge difference in the amount of tumour shrinkage corresponding to Y_I values within the interval $(0, X_U/(b+1))$. If $m \in (m_1, m_2)$, then Y_I should be chosen between the values of Y_I for which the Routh function, H, is zero (see Eq. (2.21)), and $\dfrac{X_U}{b+1}$. This suggest when virus dynamics is slow, in other terms, m is lower, a very high level of virulence is not recommended.

As we mentioned above, oncolytic viral therapy can be used as a method for controlling tumour size. What we suggested above about parameter regions is mainly considered when the viral therapy is going to be used alone. Therefore, we recommend that parameters are chosen in a way that sustained oscillations do not occur. Specifically, parameters should be chosen so that $H \geq 0$. In contrast, if oncolytic viral therapy is going to be followed by another therapy, one may reconsider the lower values of Y_I for which sustained oscillations occur. As we observed in Figure 2.10b, when the virus is highly virulent and the proper initial dosage of the virus is applied, early tumour shrinkage occurs to less than 11% of the initial tumour size, and the tumour remains in this size for almost a year before starting to relapse. For example, when $Y_I = 0.088$ (the black curve), tumour size reaches 9.8% of the initial tumour size at $t = 266$ or the most aggressive case when $Y_I = 0.01$ tumour size reaches 2% of the initial tumour size at $t = 150$. This raises multiple questions, such as, what happens if the treatment switches to another therapy before tumour relapse? Which treatment would be best as the followed-up treatment? We suggest that a virulent virus can be used, but before the tumour relapses, the second therapy must be followed up.

2.6 Appendix

2.6.1 Derivation of dimensionless Model (2.3)

Here we derive the dimensionless Model (2.3). First we recall Model (2.1).

$$\begin{aligned}
\frac{dX}{d\tau} &= \bar{r}X(1-\frac{X+Y}{K}) - \bar{d}X - \beta XV \\
\frac{dY}{d\tau} &= \bar{s}Y(1-\frac{X+Y}{K}) - \bar{d}Y - \bar{a}Y + \beta XV \\
\frac{dV}{d\tau} &= (\bar{d}+\bar{a})\bar{q}Y - \bar{m}V
\end{aligned}$$

Now let $x = \frac{X}{K}$, $y = \frac{Y}{K}$, $v = \frac{\bar{m}}{K\bar{q}(\bar{d}+\bar{a})}V$ and $t = \bar{r}\tau$, then

$$\begin{aligned}
\frac{d(Kx)}{dt} &= Kx(1-x-y) - \frac{\bar{d}}{\bar{r}}Kx - \frac{\beta}{\bar{r}}(Kx)\left(\frac{K\bar{q}(\bar{d}+\bar{a})}{\bar{m}}v\right), \\
\frac{d(Ky)}{dt} &= \frac{\bar{s}}{\bar{r}}Ky(1-x-y) - \frac{\bar{d}}{\bar{r}}Ky - \frac{\bar{a}}{\bar{r}}Ky + \frac{\beta}{\bar{r}}(Kx)\left(\frac{K\bar{q}(\bar{d}+\bar{a})}{\bar{m}}v\right), \\
\frac{d\left(\frac{K\bar{q}(\bar{d}+\bar{a})}{\bar{m}}v\right)}{dt} &= \frac{(\bar{d}+\bar{a})\bar{q}}{\bar{r}}Ky - \frac{\bar{m}}{\bar{r}}\left(\frac{K\bar{q}(\bar{d}+\bar{a})}{\bar{m}}v\right).
\end{aligned}$$

After some algebraic simplifications the above system of equations turns to

$$\begin{aligned}
\frac{dx}{dt} &= x(1-x-y) - \frac{\bar{d}}{\bar{r}}x - \frac{\beta}{\bar{r}}\left(\frac{K\bar{q}(\bar{d}+\bar{a})}{\bar{m}}\right)xv, \\
\frac{dy}{dt} &= \frac{\bar{s}}{\bar{r}}y(1-x-y) - \frac{\bar{d}}{\bar{r}}y - \frac{\bar{a}}{\bar{r}}y + \frac{\beta}{\bar{r}}\left(\frac{K\bar{q}(\bar{d}+\bar{a})}{\bar{m}}\right)xv, \\
\frac{dv}{dt} &= \frac{\bar{m}}{\bar{r}}y - \frac{\bar{m}}{\bar{r}}v.
\end{aligned}$$

Now we will call dimensionless parameters as follows:

$$X_U = 1 - \frac{\bar{d}}{\bar{r}}, \quad s = \frac{\bar{s}}{\bar{r}}, \quad Y_I = 1 - \frac{\bar{d}+\bar{a}}{\bar{s}}, \quad m = \frac{\bar{m}}{\bar{r}}, \quad b = \frac{\beta}{\bar{r}}\left(\frac{K\bar{q}(\bar{d}+\bar{a})}{\bar{m}}\right).$$

Using the new dimensionless parameters Model (2.1) gets the following dimensionless form.

$$\begin{aligned}
\frac{dx}{dt} &= x\big(X_U - (x+y)\big) - bxv, \\
\frac{dy}{dt} &= sy\big(Y_I - (x+y)\big) + bxv, \\
\frac{dv}{dt} &= m(y-v).
\end{aligned}$$

Chapter 3

Effect of virus-specific immune response on outcome of oncolytic viral therapy

Virus-specific immune responses that block viral infection are suspected to render oncolytic viral therapy relatively ineffective. Here, we consider two different types of virus-specific immune responses: (1) antibody (Ab) immune responses that block the attachment of a free virus to a cell; and (2) cytotoxic T cell (CTL) responses that kill infected cancer cells. We use mathematical modelling to assess the impact of each of these virus-specific immune responses on the treatment outcomes. Our results show that activation of an immune response either renders the therapy relatively ineffective, has no effect on the treatment outcome, or enhances the result of the therapy. The latter only occurs with activation of CTL responses. We formulate parameter constraints within which each of the mentioned scenarios is observable. We show that activation of virus-specific immune responses does not affect the treatment's control threshold. We identify when the establishment of a CTL immune response

reduces the tumour size: the establishment of antibodies does not affect the optimal tumour size, but the establishment of a CTL immune response may reduce the optimal tumour size, enhancing the therapy. Our results show that the effect of a virus-specific immune response on the optimal threshold depends on the virulence level of the virus. We show that when a less aggressive virus is used, activation of a virus-specific immune response increases the optimal threshold. However, when an aggressive virus is administrated, activation of the immune response does not affect the treatment's optimal threshold and optimal tumour size.

3.1 Introduction

Oncolytic viral therapy was introduced as a treatment for cancer in the late nineteenth century [55]. Oncolytic viruses are natural or engineered viruses that specifically target cancer cells and do not harm healthy cells. Unfortunately, despite some promising clinical trials, oncolytic viral therapy has still not reached its expected level of success [24, 124, 125]. The primary goal of this chapter is to investigate whether the failure of oncolytic viral therapy could be due to the activation of an immune response (IR). Here we establish when a virus-specific immune response could be a barrier to treatment success. In addition, we also discuss how to overcome this barrier.

The viral replication cycle may vary between different species, but generally includes six stages: attachment, penetration, disassembly (uncoating), replication, assembly, and release [2,23,71,94]. First, a virus attaches itself to a host cell and penetrates the host cell membrane. Then, the virus capsid is disassembled, and the viral genome is released in the intracellular area of the host cell. Then the viral genome manipulates the host cell machinery and imposes it to produce the viral genome. Then, the viral proteins, together with the newly replicated genome, assemble into new virions.

Finally, new virions are released from the host cell either by lysing the host cell (bursting the host cell membrane) or by apoptosis (meaning, they wait till infected cells die). If a virus is released by lysing the host cell, then the replication cycle of such a virus is also called the lytic cycle of the virus. Oncolytic viruses are viruses that follow a lytic cycle. For the success of oncolytic viral therapy, each part of this cycle must be completed successfully.

When a virus enters a host body, the immune system activates various cells, cytokines, and proteins to prevent infection of the host cells. This type of immune response is called a virus-specific immune response. Different types of virus-specific immune responses can block different stages of the viral replication cycle. For example, antibodies (Abs) can prevent attachment. They can remove a virus from the body before it encounters the target cell [81].

Cytotoxic T lymphocytes (CTL) are a type of white blood cell that can kill cancer cells or infected cells. Here, we only focus on their virus-specific ability, i.e., killing infected cancer cells. An infected cell should live long enough to spread the infection through cancer cells. If the lifespan of an infected cell is too short, then the infected cell dies before enough copies of the virus are produced. Therefore, CTLs, by killing infected cells, can prevent the success of oncolytic viral therapy.

As per the preceding discussion, a virus-specific immune response can be a barrier to the success of oncolytic viral treatment. Our goal in this chapter is to investigate the effect of the virus-specific immune response on the efficacy of oncolytic viral therapy. Here we use mathematical approaches to respond to the following questions. Activation of which kind of virus-specific immune response renders the therapy ineffective? Activation of which type of immune response enhances the result of the therapy? Activation of which type of immune response has no impact on the optimal tumour size under the therapy? Do the treatment optimal threshold (the threshold above

which tumour size post-therapy is optimal) and control threshold (the threshold above which treatment starts to work) change in the presence of a virus-specific immune response? Furthermore, we determine how virulent an oncolytic virus should be engineered to overcome this barrier. We assign a parameter that measures the virulence level of the oncolytic virus, and we discuss how changes in this parameter impact the activation of an immune response and the treatment outcome.

Many mathematical models have been introduced to study the immune system's interactions with cancer cells during oncolytic viral therapy. Some of them [57,61,88] only focus on the virus-specific effect of CTL immune response on the cancer cell, and some [42, 48, 72] additionally discuss how an oncolytic virus can trigger a tumour-specific immune response. Here, we consider two different types of virus-specific immune responses: antibodies that block attachment by clearing free virus, and a CTL response that kills the infected cells. None of the previous models in the literature that discuss the effect of an immune response on oncolytic viral therapy consider two pathways for infection, except Komarova and Wodarz [61]. However, they assume that the turnover of viruses is rapid enough that viral concentration remains in a quasi-steady state. Hence, no equation showing virus dynamics is provided. Here we are interested in showing the effect of blocking attachment by antibodies that directly clear free virus. Hence, we include the dynamics of the virus in our model in order to understand the effect of attachment blocking antibodies.

3.2 Modelling

In chapter 2 we introduce a basic model, Model (2.1) to study the interaction between uninfected cancer cells, X, infected cancer cells, Y, and the virus, V, during oncolytic viral therapy. Wodarz and Nowak [119] introduced several models to assess how virus-specific immune responses affect viral load. Using similar ideas, we extend

Model (2.1) to study the impact of two different virus-specific immune responses on oncolytic viral therapy: Model (3.1) considers an antibody response; and Model (3.4) includes mediated cytotoxicity.

Since models that we study in this chapter are extensions of Model (2.1), to be able to compare predictions of Models (3.1) and (3.4) with the results of Model (2.1), we make the same assumptions as assumptions (A1)-(A7) that we assess Model (2.1) under, in this chapter. Furthermore, for simplicity, we also make the following extra assumption in this chapter:

(B1): We showed that when $m_v/\bar{r}$ in Model (2.1) is within a certain interval, Model (2.1) predicts sustained oscillations (see Theorem 2.8), where m_v is the clearance rate of the virus and $\bar{r}$ is the mitosis rate of uninfected cancer cells. Here we assume, $m_v/\bar{r}$ is chosen outside that interval, hence, Model (2.1) shows no sustained oscillations.

3.2.1 Antibody response

Assume Z denotes the density of antibody response. Antibodies are produced at the rate $\bar{c}$ per virus; secretion of antibodies saturates at the rate $\bar{c}/\varepsilon$ per virus, and antibodies are removed at the rate m_z. Furthermore, antibodies clear free virus at a rate $\bar{p}$. Therefore, we can model the effect of an antibody response on the oncolytic viral therapy by the following model:

$$\dot{X} = \bar{r}X(1 - \frac{X+Y}{K}) - \bar{d}X - \beta XV \tag{3.1a}$$

$$\dot{Y} = \bar{s}Y(1 - \frac{X+Y}{K}) - \bar{d}Y - \bar{a}Y + \beta XV \tag{3.1b}$$

$$\dot{V} = \bar{q}Y - m_vV - \bar{p}VZ \tag{3.1c}$$

$$\dot{Z} = \frac{\bar{c}VZ}{1+\varepsilon Z} - m_zZ, \tag{3.1d}$$

where X, Y, V and Z denote the densities of uninfected cancers, infected cancer cells, the virus and antibodies, respectively. $\bar{q}$ is the rate of replication of new virions per infected cell. Note that in the absence of an antibody response Model (3.1) is the same as Model (2.1). Hence, the interpretation of the rest of parameters are the same as mentioned in Chapter 2

We rescale variables and parameters as follows:

$$x = \frac{X}{K}, \qquad y = \frac{Y}{K}, \qquad v = \frac{m_v}{K\bar{q}}V, \qquad t = \bar{r}\tau, \tag{3.2a}$$

$$X_U = 1 - \frac{\bar{d}}{\bar{r}}, \qquad Y_I = 1 - \frac{\bar{a}+\bar{d}}{\bar{s}}, \qquad s = \frac{\bar{s}}{\bar{r}}, \qquad m = \frac{m_v}{\bar{r}}, \qquad b = \frac{K\bar{q}\beta}{\bar{r}m_v}, \tag{3.2b}$$

$$z = \varepsilon Z, \quad p = \frac{\bar{p}}{m_v\varepsilon}, \qquad c = \frac{K\bar{q}\bar{c}}{\bar{r}m_v}, \quad n = \frac{m_v m_z}{K\bar{q}\bar{c}}. \tag{3.2c}$$

After imposing these changes Model (3.1) turns to

$$\dot{x} = x\Big(X_U - (x+y)\Big) - bvx, \tag{3.3a}$$

$$\dot{y} = sy\Big(Y_I - (x+y)\Big) + bvx, \tag{3.3b}$$

$$\dot{v} = m\Big(y - v - pvz\Big), \tag{3.3c}$$

$$\dot{z} = cz\Big(\frac{v}{1+z} - n\Big). \tag{3.3d}$$

For details on derivation of Model (3.3) see Section 3.6.1. To assess the effect of the antibody immune response on the treatment efficacy, we study the dynamics of Model (3.3).

3.2.2 Cytotoxic T cells

Cytotoxic T cells are lytic, meaning that they prevent the spread of infection by killing the infected cells. Assume Z represents the density of CTL immune cells.

CTLs are produced at the rate $\bar{c}$ per infected cell. CTLs production saturates at the rate $\bar{c}/\mu$ per infected cell. CTL immune cells die at the rate m_z and kill the infected cells at rate $\bar{L}$. Hence, we use the following model to assess the effect of the CTL immune cell on the therapy.

$$\dot{X} = \bar{r}X(1 - \frac{X+Y}{K}) - \bar{d}X - \beta XV, \tag{3.4a}$$

$$\dot{Y} = \bar{s}Y(1 - \frac{X+Y}{K}) - \bar{d}Y - \bar{a}Y + \beta XV - \bar{L}YZ, \tag{3.4b}$$

$$\dot{V} = \bar{q}Y - \bar{m}_v V, \tag{3.4c}$$

$$\dot{Z} = \frac{\bar{c}YZ}{1+\mu Z} - m_z Z. \tag{3.4d}$$

In the absence of a CTL immune response, the above model simplifies to Model (2.1). Hence, the interpretations of the rest of the parameters are the same as before.

Note that in the rescalling (3.2), the first two rows are the rescaling of the parameters of Model (2.1). Both Models (3.1) and (3.4) in the absence of an immune response simplify to Model (2.1). Hence, we adopt the same rescaling as (3.2) for the parameters of Model (3.4) which are shared with Model (2.1) and rescale the rest of the parameters as follows.

$$z = \mu Z, \qquad n = \frac{m_z}{\bar{c}K}, \qquad c = \frac{\bar{c}K}{\bar{r}}, \qquad L = \frac{\bar{L}}{\bar{r}\mu}. \tag{3.5}$$

After implying the rescalling, Model (3.4) turns to the following dimensionless form.

$$\dot{x} = x(X_U - (x + y)) - bvx, \tag{3.6a}$$

$$\dot{y} = sy(Y_I - (x + y)) + bvx - Lyz, \tag{3.6b}$$

$$\dot{v} = m(y - v), \tag{3.6c}$$

$$\dot{z} = cz(\frac{y}{1 + z} - n). \tag{3.6d}$$

For details on derivation of Model (3.6) see Section 3.6.2. To investigate the impact of the CTL immune response with the functionality of killing infected cells on treatment efficacy, we study the dynamics of Model (3.6).

As we showed in Chapter 2 Assumptions (A4) and (A5) in the terms of dimensionless parameter can be interpreted as inequalities (H1) and (H2). Since assumptions (A4) and (A5) are valid here as well, inequalities (H1) and (H2) also hold in this chapter.

The control threshold of the therapy is a threshold for horizontal infection rate above which treatment starts to work. In other words, when the b value is smaller than the treatment's control threshold, some early tumour shrinkage may be observable, but the tumour follows the same dynamics as in the absence of therapy. The optimal threshold of the therapy is a threshold on horizontal infection rate above which all the tumour cells are infected, and tumour size under the therapy is minimum. In this work, to discuss the effect of the virus-specific immune response, we show how activation of a virus-specific immune response affects the therapy's control threshold and optimal threshold.

The more virulent virus causes more damage to cell viability. Hence, a more aggressive virus causes an increased reduction in the mitosis rate of a cell and a higher death rate. Therefore, a more aggressive virus means a lower s and a higher a value.

Recall parameter $Y_I = 1 - \frac{a+d}{s}$. Increase in a and decrease in s yields a smaller Y_I value. Therefore, a smaller Y_I value corresponds to a more aggressive virus. Hence, we use Y_I as a measure of the virulence level of the virus. We will discuss how changes in Y_I values impact the activation of immune response and treatment outcome.

One may think that if the decay rate of immune response is much faster than their production rate, then immune response will be short, and hence, it cannot be strong. Hence, it cannot be a barrier for oncolytic viral therapy. Here, we discuss how changes in n can affect the outcome of the treatment.

As mentioned above, to respond to our questions, in our analysis, we mainly focus on three parameters b, Y_I, and n. We identify constraints and boundaries on these parameters for specific treatment outcomes.

3.3 Steady States

3.3.1 Common steady states of Model (3.3) and Model (3.6)

The dynamics of Models (3.3) and (3.6) in the absence of immune response ($z(0) = 0$) are given by Model (2.3) which is the rescaled form of Model (2.1). Hence, the steady states of Model (2.3) are also steady states of Models (3.3) and (3.6). Hence, the followings are possible steady states of the treatment suggested by Model (3.3) and Model (3.6) when no immune response is active.

- Complete tumour eradication steady state: $\mathrm{E_0} = (0, 0, 0, 0)$.
- Treatment failure steady state: $\mathrm{E_U} = (X_U, 0, 0, 0)$.
- 100% infection prevalence with no active immune response : $\mathrm{E_I} = (0, Y_I, Y_I, 0)$.
- Partially infected tumour with no active immune response : $\mathrm{E_p} = (x_p, y_p, v_p, 0)$,

where

$$x_p = \frac{s(-Y_I b + X_U - Y_I)}{b(b+1-s)}, \tag{3.7a}$$

$$y_p = \frac{X_U b - s(X_U - Y_I)}{b(b+1-s)}, \tag{3.7b}$$

$$v_p = y_p. \tag{3.7c}$$

Since the $z = 0$ boundary of Models (3.3) and (3.6) share the dynamics of Model (2.3), the condition for existence of E_U, E_I, E_p in both models are identical and are given by Lemma 2.5.

3.3.2 Steady states of Model (3.3) with an established antibody response

Model (3.3) has a unique steady state in which all the tumour cells are infected, and an antibody immune response is established; we denote this steady state by $\mathrm{E_I^{Ab}}$.

$\mathrm{E_I^{Ab}} = \left(0, Y_I, n(1+z_I^{Ab}), z_I^{Ab}\right)$ where $z_I^{Ab} = \frac{1}{2}\left(\sqrt{(1-\frac{1}{p})^2 + \frac{4Y_I}{np}} - (1+\frac{1}{p})\right)$.

Model (3.3) has a unique steady state in which tumour cells are partially infected and also an antibody immune response is established; we denote this steady-state by $\mathrm{E_p^{Ab}}$. $\mathrm{E_p^{Ab}} = (x_p^{Ab}, y_p^{Ab}, v_p^{Ab}, z_p^{Ab})$ can be formulated as

$$x_p^{Ab} = X_U - n(1+z_p^{Ab})(1+b+pz_p^{Ab}), \tag{3.8a}$$

$$y_p^{Ab} = n(1+z_p^{Ab})(1+pz_p^{Ab}), \tag{3.8b}$$

$$v_p^{Ab} = n(1+z_p^{Ab}), \tag{3.8c}$$

where z_p^{Ab} is a positive solution to the next equation.

$$\begin{aligned} G(z) := \quad & (1-s)pbz^2 + \Big(b^2 + (p+1)(1-s)b + \frac{ps}{n}(X_U - Y_I)\Big)z \\ & + b^2 + (1 - s - \frac{X_U}{n})b + (X_U - Y_I)\frac{s}{n} = 0. \end{aligned} \tag{3.9}$$

Existence of a steady state in the next theorem means all the nonzero components of that steady state are positive.

Define

$$\delta := (\frac{X_U}{n} + s - 1)^2 - \frac{4s}{n}(X_U - Y_I). \tag{3.10}$$

We use the notation δ herein for simplifying some of the algebraic expressions that are represented in this chapter.

Theorem 3.1. *Assume inequalities (H1) and (H2) hold. The following statements are true.*

(1) Steady state $\mathrm{E_p}$ *exists if and only if*

$$\frac{s(X_U - Y_I)}{X_U} < b < \frac{X_U - Y_I}{Y_I}. \tag{3.11}$$

(2) Steady state $\mathrm{E_I^{Ab}}$ *exists if and only if* $Y_I > n$.

(3) When $Y_I > n$, *the following interval for* b *is nonempty and steady state* $\mathrm{E_p^{Ab}}$ *exists if and only if*

$$\frac{1}{2}\left(\frac{X_U}{n} + s - 1 - \sqrt{\delta}\right) < b < \frac{2(X_U - Y_I)}{n\left(\sqrt{\left(1 - \frac{1}{p}\right)^2 + \frac{4Y_I}{np}} + 1 - \frac{1}{p}\right)}. \tag{3.12}$$

(4) When $Y_I < n$, *steady state* $\mathrm{E_p^{Ab}}$ *exists if and only if all the following conditions*

are satisfied.

(I) $n < \dfrac{X_U}{1-s}$,

(II) $X_U - \dfrac{n}{4s}\left(\dfrac{X_U}{n} + s - 1\right)^2 < Y_I$,

(III) $\left|2b - \left(\dfrac{X_U}{n} + s - 1\right)\right| < \sqrt{\delta}$.

Proof. (2). $\mathrm{E_I^{Ab}} = (0, y_I^{Ab}, v_I^{Ab}, z_I^{Ab})$ is a solution to the following set of equations

$$Y_I - y = 0,$$

$$y - v - pvz = 0,$$

$$\frac{v}{1+z} - n = 0.$$

Hence,

$$y_I^{Ab} = Y_I, \tag{3.13a}$$

$$v_I^{Ab} = n(1+z), \tag{3.13b}$$

$$Y_I - n(1+z_I^{Ab})(1+pz_I^{Ab}) = 0. \tag{3.13c}$$

Therefore, z_I^{Ab} is a positive solution to

$$F(z) := z^2 + (1+\frac{1}{p})z + \frac{1}{np}(n - Y_I) = 0. \tag{3.14}$$

By the set of Equations (3.13) when $z_I^{Ab} > 0$, both y_I^{Ab} and v_I^{Ab} are positive. To find conditions for existence of $\mathrm{E_I^{Ab}}$ it suffices to find the condition under which $z_I^{Ab} > 0$. Since quadratic F is increasing in z, it has a positive root for z if and only if $\frac{n-Y_I}{np} < 0$. Hence, z_I^{Ab} is positive if and only if $Y_I > n$.

Before we continue proving part (3) and part (4) of the theorem, note that $E_p^{Ab} =$

$(x_p^{Ab}, y_p^{Ab}, v_p^{Ab}, z_p^{Ab})$ is a solution to the following set of equations

$$X_U - y - bv = x, \tag{3.15a}$$

$$sy(Y_I - y - x) + bvx = 0, \tag{3.15b}$$

$$y - v - pvz = 0, \tag{3.15c}$$

$$\frac{v}{1+z} - n = 0. \tag{3.15d}$$

Hence,

$$x_p^{Ab} = X_U - n(1 + z_p^{Ab})(1 + pz_p^{Ab}) - n(1 + z_p^{Ab})b, \tag{3.16a}$$

$$y_p^{Ab} = n(1 + z_p^{Ab})(1 + pz_p^{Ab}), \tag{3.16b}$$

$$v_p^{Ab} = n(1 + z_p^{Ab}), \tag{3.16c}$$

Where z_p^{Ab} is a positive root of

$$\begin{aligned} G(z) := \quad & (1-s)pbz^2 + \left(b^2 + (p+1)(1-s)b + \frac{ps}{n}(X_U - Y_I)\right)z \\ & + b^2 + \left(1 - s - \frac{X_U}{n}\right)b + (X_U - Y_I)\frac{s}{n} = 0. \end{aligned}$$

Since $1 - s > 0$ and $X_U - Y_I > 0$, $G(z)$ is increasing in z, so G has a positive root if and only if $G(0) < 0$.

$$G(0) := Q(b) = b^2 + \left(1 - s - \frac{X_U}{n}\right)b + (X_U - Y_I)\frac{s}{n}.$$

When $Y_I \geq n$, by Lemma 3.7, z component of E_p^{Ab} is positive if and only if parameter

b satisfies the following inequality.

$$\left|2b - \left(\frac{X_U}{n} + s - 1\right)\right| < \sqrt{\delta}, \tag{3.17}$$

When z component of steady state E_p^{Ab} is positive, as equations (3.16b) and (3.16c) show y and v components of E_p^{Ab} are also positive. x component of a solution to the set of equations (3.15) is zero if and only if its y value equals to Y_I. From Eq. (3.16a), $x = X_U - Y_I + Y_I - n(1+z)(1+pz) - n(1+z)b$. Hence, x is positive if and only if $Y_I > n$ and

$$b < \frac{2(X_U - Y_I)}{n\left(\sqrt{(1-\frac{1}{p})^2 + \frac{4Y_I}{np}} + 1 - \frac{1}{p}\right)}. \tag{3.18}$$

Hence, when $Y_I \geq n$, a positive steady state exists if parameter b satisfy both inequalities (3.17) and (3.18). On the other hand when $Y_I \geq n$, $\frac{Y_I}{n} \geq 1$. Hence, $\frac{4Y_I}{np} \geq \frac{4}{p}$. Hence,

$$\begin{aligned}
\sqrt{(1-\frac{1}{p})^2 + \frac{4Y_I}{np}} + 1 - \frac{1}{p} \geq& \sqrt{(1-\frac{1}{p})^2 + \frac{4}{p}} + 1 - \frac{1}{p}, \\
\sqrt{(1-\frac{1}{p})^2 + \frac{4Y_I}{np}} + 1 - \frac{1}{p} \geq& \sqrt{(1+\frac{1}{p})^2} + 1 - \frac{1}{p}, \\
\sqrt{(1-\frac{1}{p})^2 + \frac{4Y_I}{np}} + 1 - \frac{1}{p} \geq& 2.
\end{aligned}$$

Hence,

$$\frac{2}{n}\frac{X_U - Y_I}{\sqrt{(1-\frac{1}{p})^2 + \frac{4Y_I}{np}} + 1 - \frac{1}{p}} \leq \frac{X_U - Y_I}{n} \tag{3.19}$$

Hence, when $Y_I \geq n$, from inequality (3.35) and (3.19),

$$\frac{X_U - Y_I}{Y_I} \leq \frac{2}{n} \frac{X_U - Y_I}{\sqrt{\frac{4Y_I}{np} + \left(\frac{1}{p} - 1\right)^2} + 1 - \frac{1}{p}} \leq \frac{X_U - Y_I}{n} \tag{3.20}$$

Since,

$$\begin{aligned} Q\left(\frac{X_U - Y_I}{Y_I}\right) =& \frac{X_U - sY_I}{n} \cdot \left(\frac{X_U - Y_I}{Y_I^2}\right) \cdot (n - Y_I), \\ Q\left(\frac{X_U - Y_I}{n}\right) =& \frac{(X_U - Y_I)(n - Y_I)}{n}. \end{aligned}$$

When $Y_I \geq n$, Q is negative over the interval $\left[\frac{X_U - Y_I}{Y_I}, \frac{X_U - Y_I}{n}\right]$. Since quadratic Q is only negative between its two positive roots

$$\left[\frac{X_U - Y_I}{Y_I}, \frac{X_U - Y_I}{n}\right] \subseteq \left\{b > 0 : \left|2b - \left(\frac{X_U}{n} + s - 1\right)\right| < \sqrt{\delta}\right\}.$$

Hence, by inequality (3.20) and the above statement, when $Y_I \geq n$, the value

$$b = \frac{2(X_U - Y_I)}{n\left(\sqrt{\left(1 - \frac{1}{p}\right)^2 + \frac{4Y_I}{np}} + 1 - \frac{1}{p}\right)}$$

is between two positive zeros of quadratic Q. Hence, when $Y_I \geq n$ there is a unique positive steady state if and only if

$$\frac{1}{2}\left(\frac{X_U}{n} + s - 1 - \sqrt{\delta}\right) < b < \frac{2(X_U - Y_I)}{n\left(\sqrt{\left(1 - \frac{1}{p}\right)^2 + \frac{4Y_I}{np}} + 1 - \frac{1}{p}\right)}. \tag{3.21}$$

As we mentioned above the z component of the positive steady state is positive when quadratic $G(0) = Q(b) < 0$. When $Y_I < n$ as we showed in the proof of Theorem 3.3,

$Q < 0$ if and only if

(I) $n < \dfrac{X_U}{1-s}$,

(II) $X_U - \dfrac{n}{4s}\left(\dfrac{X_U}{n} + s - 1\right)^2 < Y_I$.

(III) $\left|2b - \left(\dfrac{X_U}{n} + s - 1\right)\right| < \sqrt{\delta}$

When $Y_I < n$, x, y, v components are always positive when conditions (I), (II) and (III) are satisfied. Hence, there exists a unique quadratic if and only if the conditions (I), (II) and (III) are satisfied. □

3.3.3 Steady states of Model (3.6) with an established CTL response

$\mathrm{E_I^{CTL}}$ is the steady state in which all the tumour cells are infected and a CTL immune response is established. $\mathrm{E_I^{CTL}}$ can be formulated as

$$\mathrm{E_I^{CTL}} = \left(0, \frac{n(sY_I + L)}{ns + L}, \frac{n(sY_I + L)}{ns + L}, \frac{s(Y_I - n)}{ns + L}\right). \tag{3.22}$$

$\mathrm{E_p^{CTL}}$ is the steady states that tumour cells are partially infected and a CTL immune response is established. $\mathrm{E_p^{CTL}}$ can be formulated as $\mathrm{E_p^{CTL}} = \left(x_p^{\mathrm{CTL}}, y_p^{\mathrm{CTL}}, v_p^{\mathrm{CTL}}, z_p^{\mathrm{CTL}}\right)$

where

$$x_p^{\mathrm{CTL}} = \frac{-b(sY_I + L) + L(\frac{X_U}{n} - 1) + s(X_U - Y_I)}{\frac{L}{n} + b(b + 1 - s)}, \tag{3.23a}$$

$$y_p^{\mathrm{CTL}} = v_p^{\mathrm{CTL}} = \frac{X_U b + L - s(X_U - Y_I)}{\frac{L}{n} + b(b + 1 - s)}, \tag{3.23b}$$

$$z_p^{\mathrm{CTL}} = \frac{-b^2 + b\left(\frac{X_U}{n} + s - 1\right) - \frac{s}{n}(X_U - Y_I)}{\frac{L}{n} + b(b + 1 - s)}. \tag{3.23c}$$

Existence of a steady state in the next theorem means all its nonzero components are positive.

Theorem 3.2. *Assume inequalities (H1) and (H2) hold. Then, the following statements are true.*

1. $\mathrm{E_I^{CTL}}$ *exists if and only if* $Y_I > n$.

2. *When* $Y_I > n$, *then* $\mathrm{E_p^{CTL}}$ *exists if and only if*

$$\frac{1}{2}\left(\frac{X_U}{n} + s - 1 - \sqrt{\delta}\right) < b < \frac{s(X_U - Y_I) + L(\frac{X_U}{n} - 1)}{sY_I + L}. \tag{3.24}$$

3. *When* $Y_I < n$, *then* $\mathrm{E_p^{CTL}}$ *exists if and only if all the following conditions are satisfied.*

   (I) $n < \frac{X_U}{1 - s}$.

   (II) $Y_I > X_U - \frac{n}{4s}(\frac{X_U}{n} + s - 1)^2$.

   (III) $\left|2b - (\frac{X_U}{n} + s - 1)\right| < \sqrt{\delta}$.

Proof. 1. By Eq. (3.22) all the nonzero components of $\mathrm{E_I^{CTL}}$ are always positive except its z components. The z_I^{CTL} is positive if and only if $Y_I > n$.

2. By Eq. (3.23b) when z_p^{CTL} is positive, y_p^{CTL} and v_p^{CTL} are both positive. Hence, to find the condition under which $\mathrm{E_p^{CTL}}$ exists it suffices to find the condition under which both z_p^{CTL} and x_p^{CTL} are positive.

By inequality (H1) $\frac{L}{n} + b(b+1-s)$ is always positive. Hence z_p^{CTL} is positive if and only if $Q(b) < 0$, and x_p^{CTL} is positive if and only if

$$b < \frac{s(X_U - Y_I) + L(\frac{X_U}{n} - 1)}{sY_I + L} \tag{3.25}$$

By Lemma 3.7 when $Y_I > n$, z_p^{CTL} is positive if and only if

$$\left| 2b - \left(\frac{X_U}{n} + s - 1 \right) \right| < \sqrt{\delta} \tag{3.26}$$

On the other hand x_p^{CTL} is positive if and only if b satisfies inequality (3.25). Note that

$$\begin{aligned} Q\left(\frac{s(X_U - Y_I) + L(\frac{X_U}{n} - 1)}{sY_I + L} \right) =& s^2(n - Y_I)\frac{X_U(1-s)(X_U - Y_I)}{(sY_I + L)^2} \\ &+ s(n - Y_I)\left(\frac{sX_U - sY_I - L}{sY_I + L} \right)^2 \\ &+ s(n - Y_I)\frac{LX_U(X_U - n + ns)}{n(sY_I + L)^2} \end{aligned} \tag{3.27}$$

When $Y_I > n$, by inequality (H2), $X_U - n + ns > 0$. Hence, when $Y_I > n$, by inequalities (H1) and (H2)

$$Q\Big(\frac{s(X_U - Y_I) + L(\frac{X_U}{n} - 1)}{sY_I + L} \Big) < 0.$$

Therefore,

$$\frac{1}{2}\left(\frac{X_U}{n}+s-1-\sqrt{\delta}\right)<\frac{s(X_U-Y_I)+L(\frac{X_U}{n}-1)}{sY_I+L}<\frac{1}{2}\left(\frac{X_U}{n}+s-1+\sqrt{\delta}\right)$$

Hence, b satisfies both inequalities (3.25) and (3.26) if and only if

$$\frac{1}{2}\left(\frac{X_U}{n}+s-1-\sqrt{\delta}\right)<b<\frac{s(X_U-Y_I)+L(\frac{X_U}{n}-1)}{sY_I+L}$$

Thus, when $Y_I > n$, the steady state E_p^{CTL} exists if and only if b satisfies inequality (3.24).

3. When $Y_I < n$, by Lemma 3.7 Q is negative if and only if all the conditions (I), (II) and (III) are satisfied. In addition, When Y_I is greater than n, $Q(\frac{s(X_U-Y_I)+L(\frac{X_U}{n}-1)}{sY_I+L}) < 0$. When Y_I equals n, $b = \frac{s(X_U-Y_I)+L(\frac{X_U}{n}-1)}{sY_I+L}$ is the bigger zero of Q and since Q is a continuous function, and when $Y_I < n$, $Q(\frac{s(X_U-Y_I)+L(\frac{X_U}{n}-1)}{sY_I+L})$ is positive. Thus, when Y_I is smaller than n, $\frac{s(X_U-Y_I)+L(\frac{X_U}{n}-1)}{sY_I+L}$ is bigger than the bigger zero of Q. Hence, when $Y_I < n$, if b satisfies inequality (3.26), it also satisfies inequality (3.25). Therefore, when $Y_I < n$, z_p^{CTL} exists if and only if all the following conditions are satisfied.

$n < \dfrac{X_U}{1-s}$,

$X_U - \dfrac{n}{4s}(\dfrac{X_U}{n}+s-1)^2 < Y_I$,

$\left|2b-\left(\dfrac{X_U}{n}+s-1\right)\right| < \sqrt{\delta}$. □

3.3.4 The possible treatment outcome when an immune response is considered

The size of the tumour post-therapy is a crucial factor in identifying how successful a treatment is. When a steady state is globally stable, all the solutions will eventually

tend to it, and the tumour size post-therapy is the same as the $x + y$ value corresponding to the stable steady state. Therefore, it is vital to identify the parameter space for which a specific steady state is stable.

The following theorem indicates the parameter spaces under which the steady states with no active immune response are locally stable.

Theorem 3.3. *Assume inequalities (H1) and (H2) hold. Then, the following statements are true.*

1. $\mathrm{E_0}$ *is always unstable.*
2. $\mathrm{E_U}$ *is locally asymptotically stable if and only if* $b < \dfrac{s(X_U - Y_I)}{X_U}$.
3. $\mathrm{E_I}$ *is locally asymptotically stable if and only if* $\dfrac{X_U}{b+1} < Y_I < n$.
4. *When* $Y_I > n$, $\mathrm{E_p}$ *is locally asymptotically stable if and only if*

$$\frac{s(X_U - Y_I)}{X_U} < b < \frac{1}{2}\left(\frac{X_U}{n} + s - 1 - \sqrt{\delta}\right). \tag{3.28}$$

5. *When* $Y_I < n$ *and* $\dfrac{s(X_U - Y_I)}{X_U} < b < \dfrac{X_U - Y_I}{Y_I}$, $\mathrm{E_p}$ *is locally asymptotically stable if and only if any of the following conditions fail.*

   (I) $n < \dfrac{X_U}{1-s}$.

   (II) $Y_I > X_U - \dfrac{n}{4s}\left(\dfrac{X_U}{n} + s - 1\right)^2$.

   (III) $\left|2b - \left(\dfrac{X_U}{n} + s - 1\right)\right| < \sqrt{\delta}$.

Proof. 1. The Jacobian of Model (3.3)(Model (3.6)) at E_0 is

$$\begin{pmatrix} X_U & 0 & 0 & 0 \\ 0 & sY_I & 0 & 0 \\ 0 & m & -m & 0 \\ 0 & 0 & 0 & -cn \end{pmatrix}.$$

The eigenvalues of the above at E_0 are sY_I, X_U,$-m$, and $-cn$. Since $Y_I, X_U > 0$, this Jacobian always has two positive eigenvalues, E_0 is always unstable.

2. The Jacobian of Model (3.3) at E_U is the same as the Jacobian of Model (3.6) at E_U. This Jacobian is

$$\begin{pmatrix} -X_U & -X_U & -bX_U & 0 \\ 0 & -s(X_U - Y_I) & bX_U & 0 \\ 0 & m & -m & 0 \\ 0 & 0 & 0 & -cn \end{pmatrix}.$$

The above matrix always has two negative eigenvalues, $-X_U$ and $-cn$ and the other two eigenvalues are eigenvalues of the following matrix.

$$A_U = \begin{bmatrix} -s(X_U - Y_I) & bX_U \\ m & -m \end{bmatrix}.$$

By Assumption (H2), $X_U - Y_I > 0$. So, trace of matrix A_U is always negative. If $\det(A_U) > 0$, then both eigenvalues of A_U have negative real parts and in this case E_U is stable. When $\det(A_U) < 0$, then A_U has one eigenvalue with positive real part. Hence, in this case E_U is unstable. In other words, E_U is a locally asymptotically stable steady state for Model (3.3) and Model (3.6) if and only if $b < \frac{s(X_U - Y_I)}{X_U}$.

Part (3). The Jacobians of Model (3.3) and Model (3.6) at E_I have the following

eigenvalues: $-m$, $-sY_I$, $c(Y_I - n)$, and $-Y_I(b+1) + X_U$. Hence, $\mathrm{E_I}$ is a stable steady state for Model (3.3) and Model (3.6) if and only if $Y_I - n < 0$ and $-Y_I(b+1) + X_U < 0$, or equivalently, $\mathrm{E_I}$ is a stable steady state for Model (3.3) and Model (3.6) if and only if $\frac{X_U}{b+1} < Y_I < n$.

Part 4. One of the eigenvalues of the Jacobians of Model (3.3) and Model (3.6) at $\mathrm{E_p}$ is $c(v_p - n)$ and the other eigenvalues are eigenvalues of the following matrix.

$$J_p = \begin{pmatrix} -x_p & -x_p & -bx_p \\ (b-s)y_p & -bx_p - sy_p & bx_p \\ 0 & m & -m \end{pmatrix}.$$

This is the same as the Jacobian of Model (2.3) at the projection of $\mathrm{E_p}$ on xyv space. By Assumption (B1), $m > m_2$. Hence, by Theorem 2.8 the real part of all the eigenvalues of J_p is negative. Hence, $\mathrm{E_p}$ is a stable steady state for Model (3.3) and Model (3.6) if and only if $v_p - n < 0$.

$$v_p - n = \frac{-nc}{b(b+1-s)}\left(b^2 + b\left(1 - s - \frac{X_U}{n}\right) + \frac{s}{n}(X_U - Y_I)\right).$$

Let $Q(b) = b^2 + b(1 - s - \dfrac{X_U}{n}) + \dfrac{s}{n}(X_U - Y_I)$. $v_p - n < 0$ if and only if $Q(b) > 0$. On the other hand, $\mathrm{E_p}$ exists if and only if $\frac{s(X_U - Y_I)}{X_U} < b < \frac{X_U - Y_I}{Y_I}$. Hence, by Lemma 3.7 when $Y_I \geq n$, quadratic Q is positive if and only if

$$\frac{s(X_U - Y_I)}{X_U} < b < \frac{1}{2}\left(\frac{X_U}{n} + s - 1 - \sqrt{\delta}\right).$$

Hence, when $Y_I \geq n$, $\mathrm{E_p}$ is locally asymptotically stable if and only if the above inequality holds.

Part (5). When $Y_I < n$, by Lemma 3.7 $\mathrm{E_p}$ is unstable if and only if all the conditions

(I), (II) and (III) are satisfied. □

The following theorem constrains rescaled infectivity rate b, when this constraint is met the tumour becomes fully infected.

Theorem 3.4. *Assume inequalities (H1) and (H2) hold, and $Y_I > n$, then*

1. $\mathrm{E_I^{Ab}}$ *is locally asymptotically stable if and only if*

$$b > \frac{2(X_U - Y_I)}{n\left(\sqrt{(1-\frac{1}{p})^2 + \frac{4Y_I}{np}} + 1 - \frac{1}{p}\right)}. \tag{3.29}$$

2. $\mathrm{E_I^{CTL}}$ *is locally asymptotically stable if and only if*

$$b > \frac{s(X_U - Y_I) + L(\frac{X_U}{n} - 1)}{sY_I + L}. \tag{3.30}$$

Proof.

1. Jacobian of Model (3.3) at $\mathrm{E_I^{Ab}}$ has four eigenvalues, two are determined explicitly; $X_U - Y_I - b\frac{n}{2}\left(1 - \frac{1}{p} + \sqrt{(1-\frac{1}{p})^2 + \frac{4Y_I}{np}}\right)$ and $-sY_I$. The other two are eigenvalues of the following matrix

$$A_I^{Ab} = \begin{pmatrix} -m(1+pz_I^{Ab}) & -mpv_I^{Ab} \\ \dfrac{cz_I^{Ab}}{1+z_I^{Ab}} & \dfrac{-cnz_I^{Ab}}{1+z_I^{Ab}} \end{pmatrix}.$$

Since $\mathrm{tr}(A_I^{Ab}) < 0$ and $\det\left(A_I^{Ab}\right) > 0$, A_I^{Ab} has two eigenvalues with negative real parts. Therefore, $\mathrm{E_I^{Ab}}$ is stable if and only if

$$X_U - Y_I - \frac{bn}{2}\left(1 - \frac{1}{p} + \sqrt{\left(1-\frac{1}{p}\right)^2 + \frac{4Y_I}{np}}\right) < 0$$

In other words, $\mathrm{E_I^{Ab}}$ is stable if and only if

$$b > \frac{2(X_U - Y_I)}{n\left(1 - \frac{1}{p} + \sqrt{\left(1 - \frac{1}{p}\right)^2 + \frac{4Y_I}{np}}\right)}.$$

2. Jacobian of Model (3.6) at $\mathrm{E_I^{CTL}}$ has four eigenvalues, two of them are determined explicitly; $X_U - (1+b)\frac{n(sY_I + L)}{ns + L}$, and $-m < 0$. The other two are eigenvalues of the following matrix.

$$A_I^{CTL} = \begin{pmatrix} -sy_I^{CTL} & -Ly_I^{CTL} \\ \frac{cz_I^{CTL}}{1 + z_I^{CTL}} & \frac{-cnz_I^{CTL}}{1 + z_I^{CTL}} \end{pmatrix}.$$

$\mathrm{tr}(A_I^{CTL}) < 0$ and $\det\big(A_I^{CTL}\big) > 0$. Hence, A_I^{CTL} has two eigenvalues with negative real part. Hence, $\mathrm{E_I^{CTL}}$ is stable if and only if

$$b > \frac{s(X_U - Y_I) + L(\frac{X_U}{n} - 1)}{sY_I + L}.$$

□

Our numerical simulations suggest that when a steady state is locally stable, it is almost every where globally stable, i.e. it attracts all the solutions starting from a positive initial point, i.e., an initial point that all its four components are positive.

Results of Theorems 3.1, 3.2, 3.3, and 3.4 help identify the possible outcomes of the treatment, based on the parameters b, Y_I and n. When an steady state with no active immune response such as $\mathrm{E_U}$, $\mathrm{E_I}$, or $\mathrm{E_p}$ is stable, the immune response has no effect on the treatment outcome. An immune response is only established when steady states $\mathrm{E_p^{Ab}}$ or $\mathrm{E_I^{Ab}}$, or steady states $\mathrm{E_p^{CTL}}$ or $\mathrm{E_I^{CTL}}$ are stable. See Figure 3.1a for illustration: the horizontal axis is Y_I and the vertical axis is b, and the vertical

black curve is where Y_I equals n; an immune response is only established in the shaded blue areas labelled by IV and V, and no immune response is established in the areas labelled by I, II, and III.

By part 2 of Theorem 3.3 when $b < \frac{s(X_U - Y_I)}{X_U}$, treatment failure steady state is stable. As we mentioned before, our numerical simulations show that when a steady state is locally stable, it is almost everywhere globally stable, i.e. every solution starting from a positive initial condition tends to it. Hence, when $b < \frac{s(X_U - Y_I)}{X_U}$, $\mathrm{E_U}$ is almost everywhere globally stable and treatment fails. Hence, for treatment to start working $b > \frac{s(X_U - Y_I)}{X_U}$. Hence, $b = \frac{s(X_U - Y_I)}{X_U}$ is the control threshold. The value for the control threshold when no immune response is taken into account is the same (see Lemma 2.6). Hence, an immune response does not affect the control threshold of the treatment. Note that by part 2 of Theorem 3.3, stability of $\mathrm{E_U}$ does not depend on the value of n. The green curve in Figure 3.1a is $b = s(X_U - Y_I)/X_U$ and the area labelled by I is corresponding to treatment failure in Y_I–b parameter space. Note that the area labelled by I does not depend on the sign$(Y_I - n)$. We use b_c to denote treatment control threshold. Hence,

$$b_c = \frac{s(X_U - Y_I)}{X_U} \tag{3.31}$$

By part 2 of Theorem 3.1 and the part 1 of Theorem 3.2, the steady state in which all the tumour cells are infected and also an immune response is established, is only observable when $Y_I > n$. When b and Y_I satisfy the inequality (3.29) (inequality (3.30)) $\mathrm{E_I^{Ab}}$ ($\mathrm{E_I^{CTL}}$) is stable (respectively). See Figure 3.1a for an illustration: in the area labelled V, starting the therapy from almost any tumour size, eventually all the tumour cells become infected and also an immune response is established. When an antibody (CTL) immune response is established, area labelled by V corresponds to the case when steady state $\mathrm{E_I^{Ab}}$ ($\mathrm{E_I^{CTL}}$) is stable. Hence, the blue line in the

Figure 3.1a, in the case of an antibody response is corresponding to

$$b = \frac{2(X_U - Y_I)}{n\left(\sqrt{(1-\frac{1}{p})^2 + \frac{4Y_I}{np}} + 1 - \frac{1}{p}\right)},$$

and in the case of a CTL immune response is corresponding to

$$b = \frac{s(X_U - Y_I) + L(\frac{X_U}{n} - 1)}{sY_I + L}.$$

Our numerical simulations suggest that the positive steady state $\mathrm{E_p^{Ab}}$ ($\mathrm{E_p^{CTL}}$) when exists, attracts all the solutions starting from a positive initial point. The condition for the existence of the positive steady state is stated in Theorem 3.1 parts 3 and 4 for an antibody immune response, and in Theorem 3.2 parts 2 and 3 for a CTL immune response (see Figure 3.1a).

3.4 Effect of virus-specific immune response on the optimal tumour size under therapy.

3.4.1 Effect of activation of an antibody immune response on the tumour size

Model (3.3) in the absence of an antibody immune response is the same as Model (2.3). The rate of change of tumour size under therapy by Model (3.3) is give by

$$\frac{d(x+y)}{dt} = x(X_U - (x+y)) + sy(Y_I - (x+y)). \tag{3.32}$$

By Theorem 2.4, when the rate of change of tumour size is given by Eq. (3.32), the tumour size under the therapy ranges from the minimum value Y_I to the maximum

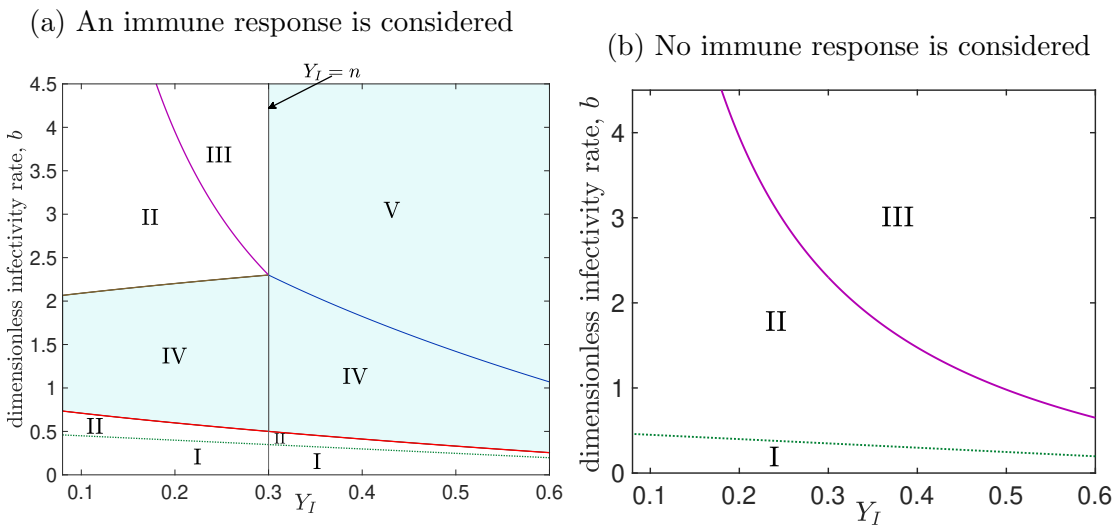

Figure 3.1: **The effect of the virus-specific immune response on treatment outcome depends on the virulence level of the virus**. (a) An immune response is taken into account. In the shaded area, an immune response is established. The black line is where (dimensionless) removal rate n of an immune response is equal to the virulence level Y_I of the virus. When $Y_I < n$, an immune response is only established in the area labelled IV and has no effect on the optimal threshold. The purple curve shows the optimal threshold when $Y_I < n$. When $Y_I > n$, an immune response is established in the areas labelled by IV and V. In this scenario, establishment of an immune response changes the optimal threshold to the blue line, which is higher than the optimal threshold when no immune response is active for the same values of b and Y_I. In the area labelled by I (III) the steady state $\mathrm{E_U}$ ($\mathrm{E_I}$ is stable, respectively), and in the area labelled by II, $\mathrm{E_p}$ is stable. In the area labelled IV, tumour is partially infected and an immune response is established; meaning, the steady state $\mathrm{E_p^{Ab}}$ ($\mathrm{E_p^{CTL}}$) in the case of an antibody (a CTL) response is stable. In the area labelled by V, tumour is completely infected and also an immune response is established, i.e. the steady state $\mathrm{E_I^{Ab}}$ ($\mathrm{E_I^{CTL}}$) in the case of an antibody (a CTL) response is stable. See Theorem 3.3 (Theorem 3.4) for an antibody response (CTL response, respectively) to see the equations of the boundaries of each labelled area. This simulation is conducted under the set of parameters $s = 0.5$, $d = 0.01$, $X_U = 0.99$, $m = 1$. In plot (a) $n = 0.3$, $p = 1$ ($L = 1$), and $c = 1$.

value X_U. Therefore, establishment of an antibody immune response by functionality of clearing the virus does not affect the optimal tumour size by the therapy. Hence, the optimal tumour size under the therapy in the presence of an antibody immune response is Y_I (see Figure 3.2 for an illustration).

The tumour size in the presence of an antibody immune response becomes Y_I when either E_I or E_I^{Ab} is stable. By Theorem 3.4 part 1, when $Y_I \geq n$, this occurs at $b = 2(X_U - Y_I)/n(\sqrt{(1-\frac{1}{p})^2 + \frac{4Y_I}{np}} + 1 - \frac{1}{p})$ and when $Y_I < n$, at $b = \frac{X_U - Y_I}{Y_I}$. Hence, when an antibody is taken into account, the optimal threshold of therapy b_o^{Ab} can be defined as:

$$b_o^{Ab} = \begin{cases} \dfrac{2(X_U - Y_I)}{n\left(\sqrt{(1-\dfrac{1}{p})^2 + \dfrac{4Y_I}{np}} + 1 - \dfrac{1}{p}\right)}, & Y_I \geq n, \\ \dfrac{X_U - Y_I}{Y_I}, & Y_I < n. \end{cases} \tag{3.33}$$

Let b_o denote the optimal threshold of the therapy when no immune response is involved. According to [44], $b_o = \frac{X_U - Y_I}{Y_I}$. Hence, by Eq. (2.12) when $Y_I < n$, $b_o^{Ab} = b_o$, see Figure 3.2a and Figure 3.2b for clarification; b_o is shown by yellow marker and b_o^{Ab} is shown by red marker on the b axis.

Theorem 3.5. *When $Y_I > n$, an antibody immune response adversely affects the treatment by increasing the treatment's optimal threshold. Mathematically, this is equivalent to*

$$b_o^{Ab} > b_o, \qquad \textit{if } \ Y_I > n. \tag{3.34}$$

Proof. To prove the theorem it suffices to show that when $Y_I > n$, the following

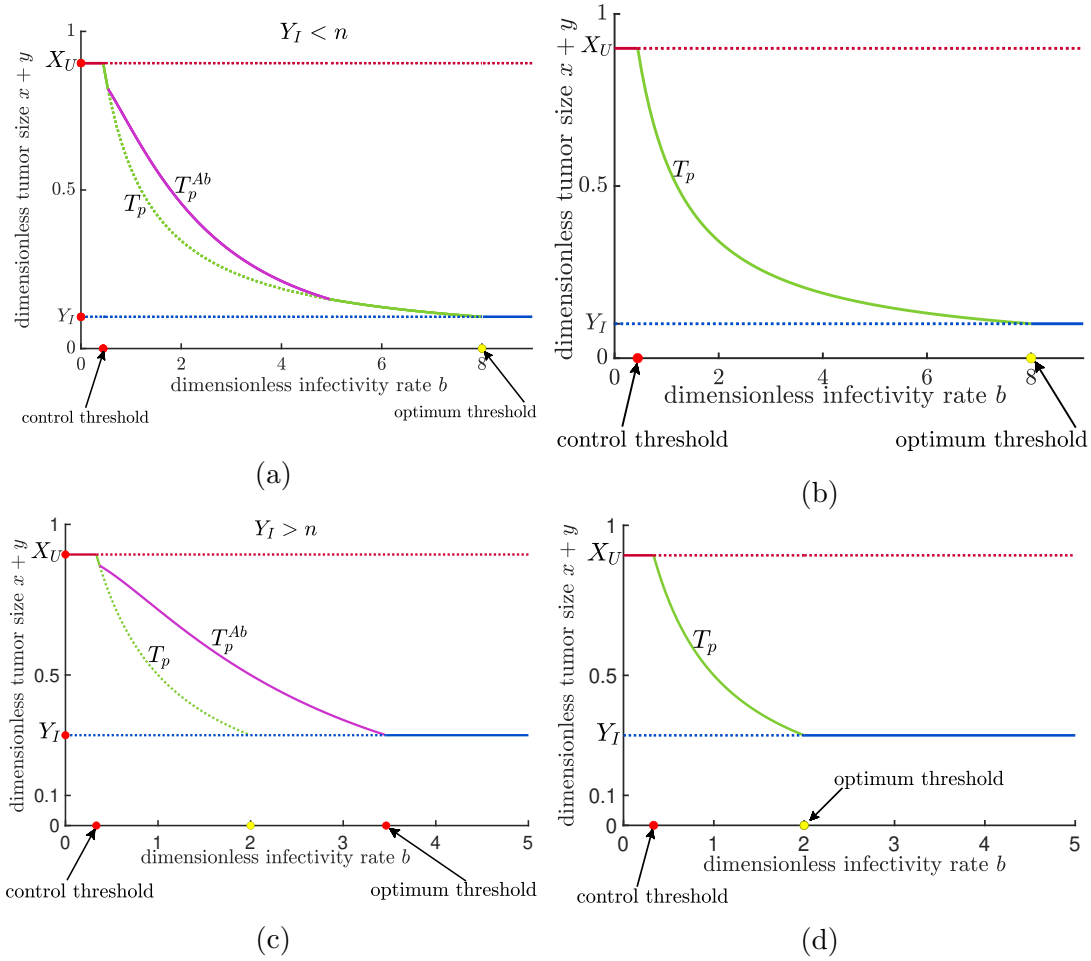

Figure 3.2: **Establishment of an antibody response affects optimal tumour size and optimal threshold of the treatment.** This Figure provides a comparison on the change in steady state tumour size as rescaled infectivity rate b varies, when an antibody immune response is considered (plots (a) and (c)) versus when no immune response is considered (plots (b) and (d)). In fact in plot (a) an antibody immune response is considered and (b) is plotted for the same set of parameters but no immune response is considered. Same is true for plots (c) and (d). In plot (a) $n > Y_I$ and in plot (c) $n < Y_I$. A comparison between plots (a) and (b) shows when $Y_I < n$, an antibody immune response does not affect the optimal threshold of therapy which is marked by the green circle in these two plots. Comparing plots (c) and (d), we learn that the treatment's optimal threshold when an antibody immune response is considered is higher than the case with no immune response. The minimum tumour size in all the plots is Y_I, meaning that activation of an antibody immune response does not change the optimal tumour size. T_p^{Ab} denotes the tumour size in steady state E_p^{Ab} and T_p denotes the tumour size in steady state E_p. This figure suggests regardless of sign$(Y_I - n)$, when both steady states of E_p and E_p^{Ab} exist, $T_p^{Ab} > T_p$. In plots (a) and (b) parameter $Y_I = 0.1$, and in plots (c) and (d) parameter $Y_I = 0.3$. The rest of parameters are as follows: $n = 0.15$, $s = 0.5$, $X_U = 0.9$, $m = 1$ and $c = 1$, $p = 1$.

inequality holds.

$$\frac{2(X_U - Y_I)}{n\left(\sqrt{(1-\frac{1}{p})^2 + \frac{4Y_I}{np}} + 1 - \frac{1}{p}\right)} > \frac{X_U - Y_I}{Y_I}. \tag{3.35}$$

The above inequality holds because all the following inequalities are equivalent.

$$\begin{aligned}
Y_I &> n, \\
-\frac{Y_I}{n} &< -1, \\
\frac{1}{p} - \frac{Y_I}{n} &< \frac{1}{p} - 1, \\
\frac{4Y_I}{n}\left(\frac{1}{p} - \frac{Y_I}{n}\right) &< \frac{4Y_I}{n}\left(\frac{1}{p} - 1\right), \\
\frac{4Y_I}{np} &< \left(\frac{2Y_I}{n}\right)^2 + \frac{4Y_I}{n}\left(\frac{1}{p} - 1\right), \\
\frac{4Y_I}{np} + \left(\frac{1}{p} - 1\right)^2 &< \left(\frac{2Y_I}{n}\right)^2 + \frac{4Y_I}{n}\left(\frac{1}{p} - 1\right) + \left(\frac{1}{p} - 1\right)^2, \\
\frac{4Y_I}{np} + \left(\frac{1}{p} - 1\right)^2 &< \left(\frac{2Y_I}{n} + \left(\frac{1}{p} - 1\right)\right)^2, \\
\sqrt{\frac{4Y_I}{np} + \left(\frac{1}{p} - 1\right)^2} &< \frac{2Y_I}{n} + \left(\frac{1}{p} - 1\right), \\
\sqrt{\frac{4Y_I}{np} + \left(\frac{1}{p} - 1\right)^2} + 1 - \frac{1}{p} &\leq \frac{2Y_I}{n}, \\
\frac{2}{n}\frac{X_U - Y_I}{\sqrt{\frac{4Y_I}{np} + \left(\frac{1}{p} - 1\right)^2} + 1 - \frac{1}{p}} &< \frac{X_U - Y_I}{Y_I}.
\end{aligned}$$

□

As we mentioned before, there are two steady states in which tumour is partially infected: one with an active antibody response $\mathrm{E_p^{Ab}}$ and one with no active IR, $\mathrm{E_p}$. Our numerical simulations suggest that when the tumour is partially infected, the steady-state tumour size with an active antibody immune response is higher than

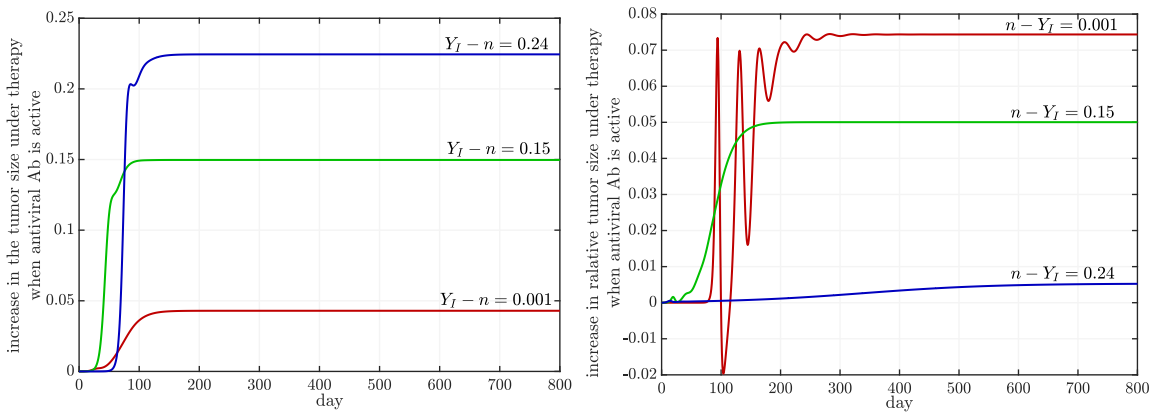

(a) $Y_I > n$ (b) $Y_I < n$

Figure 3.3: **The degree of negativity of the establishment of an antibody response on treatment outcome depends on magnitude of $|Y_I - n|$.** Difference between the tumour size $x(t) + y(t)$ of the two solutions is plotted; one starting from a point $(X_U, 0, v_0, z_0)$ with nonzero antibody, i.e. $z_0 \neq 0$ and the other starting from $(X_U, 0, v_0, 0)$. The parameters are chosen in the way that both $\mathrm{E_p}$ and $\mathrm{E_p^{Ab}}$ exist. The solution starting from $(X_U, 0, v_0, 0)$ eventually tends to E_p and the solution starting from $(X_U, 0, v_0, z_0)$ eventually tends to E_p^{Ab}. Therefore, each plotted curve eventually tends to $T_p^{Ab} - T_p$. As illustrated in panel (a) when $Y_I > n$ by increase in magnitude of $|Y_I - n|$, $T_p^{Ab} - T_p$ becomes larger. In other words, when $Y_I > n$, if $|Y_I - n|$ increases, the activation of an antibody immune response has more negative effect on the treatment outcome. In contrast panel (b) highlights that when $Y_I < n$ and the magnitude of $|Y_I - n|$ increases, the detrimental effect of activation of an antibody reduces. The parameters are $X_U = 0.9$, $s = 0.5$, $m = 1$, $c = 1$, $p = 1$. $Y_I = 0.3$ in plot (a) and $Y_I = 0.08$ in plot (b). Parameter b is chosen the midpoint of the interval on which $\mathrm{E_p^{Ab}}$ exist(see Theorem 3.1).

the steady-state tumour size with no active immune response. In other words if T_p^{Ab} denotes the tumour size corresponding to E_p^{Ab} and T_p denotes the tumour size corresponding to E_p, then $T_p < T_p^{Ab}$ (see Figure 3.2 for an illustration). Hence, when E_p^{Ab} exists, activation of an antibody immune response affects the treatment negatively. However, our simulations recommend that the degree to which this effect is negative strongly depends on the magnitude of the difference $|Y_I - n|$: if $Y_I > n$ and $|Y_I - n|$ increases, $T_p^{Ab} - T_p$ increases (see Figure 3.3(a)); if $Y_I < n$ and $|Y_I - n|$ increases, $T_p^{Ab} - T_p$ decreases (see Figure 3.3(b)).

3.4.2 Effect of activation of a CTL immune response on tumour size

First, we compare the possible steady state tumour sizes under Model (3.6). By Theorem 3.2 when $Y_I < n$, only steady states $\mathrm{E_p}$, $\mathrm{E_p^{CTL}}$, $\mathrm{E_I}$, E_U could exist. Let T_p^{CTL}, T_p, T_I and T_U denote the tumour size at the steady states $\mathrm{E_p^{CTL}}$, $\mathrm{E_p}$, $\mathrm{E_I}$, and $\mathrm{E_U}$, respectively. $T_I = Y_I$ and $T_U = X_U$, and by Theorem 2.4, $Y_I < T_p < X_U$.

Assuming parameters Y_I and b are chosen in the way that both steady states $\mathrm{E_p}$ and $\mathrm{E_p^{CTL}}$ exist

$$T_p^{CTL} - T_p = z_p^{CTL}\left(\frac{1}{b+1-s}\right) > 0.$$

$$T_U - T_p^{CTL} = b\frac{n(sY_I + L)}{ns + L} > 0.$$

Hence, when $Y_I < n$, in the areas of parameter space Y_I–b that both $\mathrm{E_p}$ and $\mathrm{E_p^{CTL}}$ exist,

$$Y_I \leq T_p \leq T_p^{CTL} < X_U, \qquad \text{if } Y_I < n. \tag{3.36}$$

Hence, when $Y_I < n$, the optimal tumour size by Model (3.6) is Y_I (see Figure 3.4a for an illustration).

When $Y_I > n$, the steady state $\mathrm{E_I^{CTL}}$ could also exist. Let T_I^{CTL} denote the steady state tumour size corresponding to $\mathrm{E_I^{CTL}}$. Then,

$$T_I - T_I^{CTL} = \frac{p(Y_I - n)}{ns + L} > 0, \qquad \text{if } Y_I > n. \tag{3.37}$$

Hence, when $Y_I > n$, and b and Y_I are chosen in the way that both $\mathrm{E_p}$ and $\mathrm{E_p^{CTL}}$

exist, the following is true.

$$T_I^{CTL} \leq Y_I \leq T_p \leq T_p^{CTL} < X_U, \qquad \text{if } Y_I > n. \tag{3.38}$$

Hence, when $Y_I > n$, the optimal tumour size under the therapy is T_I^{CTL} which corresponds to the steady state $\mathrm{E_I^{CTL}}$ (see Figure 3.4b). Let $\mathrm{T_o^{CTL}}$ be the optimal tumour size by therapy suggested by Model (3.6). As in the preceding discussion, $\mathrm{T_o^{CTL}}$ is defined as follows:

$$\mathrm{T_o^{CTL}} = \begin{cases} \dfrac{n(sY_I + L)}{ns + L}, & Y_I \geq n, \\ \\ Y_I, & Y_I < n. \end{cases} \tag{3.39}$$

The steady state tumour size Y_I corresponds to the steady state E_I. When $Y_I < n$, by Theorem 3.3, E_I is stable if and only if $b > \frac{X_U - Y_I}{Y_I}$. Hence, the optimal threshold of the therapy in this case is $b = \frac{X_U - Y_I}{Y_I}$. By part 2 of Theorem 3.4, $\mathrm{E_I^{CTL}}$ is stable if and only if b satisfies the inequality (3.30). Hence, when $Y_I > n$, the optimal threshold of the therapy is $b = \left(s(X_U - Y_I) + L(\dfrac{X_U}{n} - 1)\right)/(sY_I + L)$.

Let b_o^{CTL} denote the optimal threshold of the therapy under Model (3.6); per the above discussion b_o^{CTL} is defined as follows:

$$b_o^{CTL} = \begin{cases} \dfrac{s(X_U - Y_I) + L(\dfrac{X_U}{n} - 1)}{sY_I + L}, & Y_I \geq n, \\ \\ \dfrac{X_U - Y_I}{Y_I}, & Y_I < n. \end{cases} \tag{3.40}$$

Lemma 3.6. When $Y_I > n$, in the presence of a CTL immune response the optimal threshold is higher, i.e. $b_o^{CTL} > b_o$.

Proof. To prove the lemma, it suffices to show that when $Y_I > n$, the following

inequality holds.

$$\frac{s(X_U - Y_I) + L(\frac{X_U}{n} - 1)}{sY_I + L} > \frac{X_U - Y_I}{Y_I}. \tag{3.41}$$

The above inequality holds because all the following inequalities are equivalent.

$$\begin{aligned}
Y_I &> n, \\
\frac{Y_I X_U}{n} &> X_U, \\
\frac{Y_I X_U}{n} - Y_I &> X_U - Y_I, \\
L(\frac{X_U}{n} - 1) &> \frac{L(X_U - Y_I)}{Y_I}, \\
s(X_U - Y_I) + L(\frac{X_U}{n} - 1) &> \frac{L(X_U - Y_I)}{Y_I} + s(X_U - Y_I), \\
s(X_U - Y_I) + L(\frac{X_U}{n} - 1) &> \frac{(sY_I + L)(X_U - Y_I)}{Y_I}, \\
\frac{s(X_U - Y_I) + L(\frac{X_U}{n} - 1)}{sY_I + L} &> \frac{X_U - Y_I}{Y_I}.
\end{aligned}$$

□

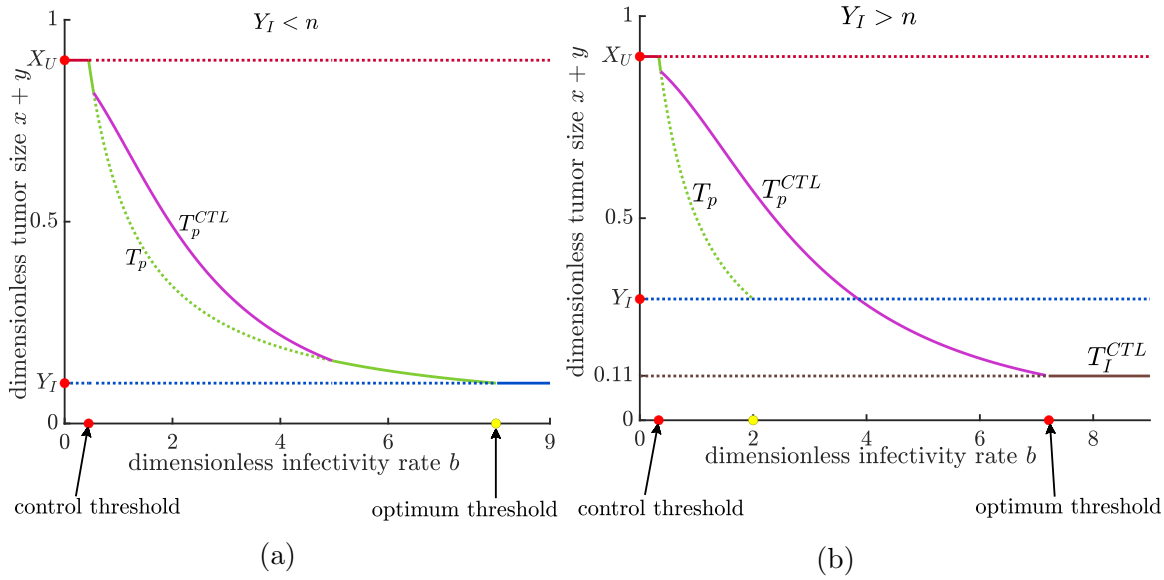

Figure 3.4: **The establishment of a CTL affects the optimal tumour size and treatment optimal threshold.** This figure illustrates that effect of CTL response depends on virulence of virus, denoted by parameter Y_I, and rescaled removal rate of the virus, denoted by n. When $Y_I < n$, as plot (a) suggests establishment of a CTL response does not change the optimal threshold and the optimal tumour size by therapy. The point marked by square shows $b_o = (X_U - Y_I)/Y_I$. When $Y_I > n$, as plot (b) illustrates activation of a CTL immune response enhances the therapy by reducing the optimal tumour size; however, there is also a drawback that the optimal threshold is increased. The optimal threshold b_o^{CTL} is marked by triangle in plot (b). In plots (a) $Y_I = 0.1$, and in plots (b) $Y_I = 0.3$. The rest of parameters are as follows: $n = 0.15$, $s = 0.5$, $X_U = 0.9$, $m = 1$, $L = 1$, and $c = 1$.

By the set of equations (3.23) T_p^{CTL} equals Y_I at

$$b_e^{CTL} = \frac{n(L + Y_I - X_U) + \sqrt{n^2(L + Y_I - X_U)^2 + 4nLY_I(X_U - Y_I)}}{2nY_I}. \tag{3.42}$$

If an oncolytic virus is administrated with (rescaled) transmissibility rate b such that $b_o < b < b_e^{CTL}$, when a CTL immune response is active the minimum tumour size is Y_I, which is the same as optimal tumour size when no immune response is considered. However, when an oncolytic virus with (rescaled) transmissibility rate b such that $b > b_e^{CTL}$ is administrated, when a CTL immune response is active the tumour size is always lower than Y_I. Hence, in this case activation of a CTL

immune response enhances the treatment's outcome. This value of b, is the minimum (rescaled) transmission rate that if any virus with higher transmission rate activates a CTL immune response the result of therapy enhances.

When $Y_I > n$ and a CTL immune response is active, the optimal tumour size T_o^{CTL} is smaller than the optimal tumour size when no immune response is active (see Eq. (3.37) and Eq. (3.39)). Hence, when $Y_I > n$ activation of a CTL immune response could enhance the treatment's outcome. However, by Eq. (3.37), $Y_I - T_o^{CTL}$ depends strongly on $Y_I - n$. When $Y_I - n$ tends to zero, $Y_I - T_o^{CTL}$ tends to zero (see Figure 3.5 for an illustration). In other words, when the Y_I value is very close to the n value, CTL immune response almost does not affect the optimal tumour size and the optimal threshold.

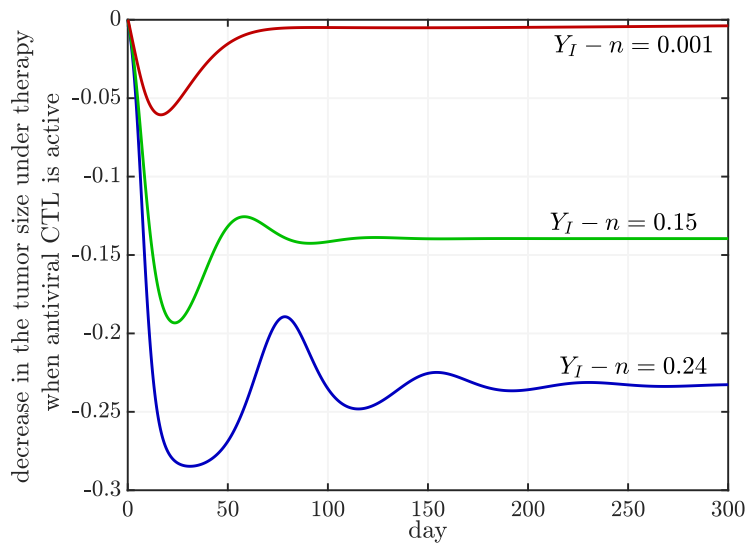

Figure 3.5: **When $Y_I - n$ increases, the positive impact of CTL establishment is stronger.** In this figure difference between the value of $x + y$ of two solutions of Model (3.6) is plotted, for different values of n: one solution starts from $(X_U, 0, v_0, z_0)$ with nonzero CTL, $z_0 \neq 0$ and another solution starting from $(X_U, 0, v_0, 0)$. The solution starting from $(X_U, 0, v_0, z_0)$ eventually tends to E_I^{CTL} and the solution starting from $(X_U, 0, v_0, 0)$ eventually tends to E_I. Hence, the end point of each curve shows $T_I^{CTL} - Y_I$. By increase in $Y_I - n$, $|Y_I - T_I^{CTL}|$ increases, meaning T_I^{CTL} is much lower than Y_I. Hence, when $Y_I - n$ is maximum, activation of a CTL immune response enhances the therapy the most.

3.5 Discussion

A wide range of research suggests that virus-specific immune responses, specifically neutralizing antibodies, are an obstacle to the success of oncolytic viral therapy; some researchers suggest combining oncolytic viral therapy with immune checkpoint inhibitors overcomes this barrier [45, 66, 83]. Instead of using combination therapy, our main focus was to use mathematical modelling to formulate all the effects of a virus-specific immune response such as an antibody or cytotoxic T lymphocyte on oncolytic viral therapy. We studied models of two different immune responses: Model (3.1) demonstrates the effect of the establishment of an antibody by the functionality of clearing the virus; Model (3.4) represents the effect of the establishment of a cytotoxic T lymphocyte by the functionality of killing the infected cells. We proposed some hypotheses, assumptions (A1)-(A7) and (B1), concerning viral therapy. Under these assumptions, the activation of a virus-specific immune response has three types of effects on the treatment's outcomes: detrimental, beneficial or neutral. It is detrimental when the establishment of a virus-specific immune response increases tumour size in comparison with the case where no immune response is active. Establishment of a virus-specific immune response may not affect the steady-state tumour size and hence does not affect the treatment outcome. Lastly, the establishment of a virus-specific immune response may enhance the result of the therapy by decreasing the tumour size. The latter scenario is only observable by establishment of a CTL immune response.

Note that in the previous paragraph, we mentioned that the establishment of a virus-specific immune response has three general effects: sometimes, no virus-specific immune response is established during an oncolytic viral therapy, it may be activated, but it is a very short response and does not last for a long time. An important finding of this chapter is that we found all the necessary and sufficient conditions under

which, during an oncolytic viral therapy, an antibody or a CTL immune response is established. This crucial finding could be used to engineer an oncolytic virus that does not trigger a virus-specific immune response. Alternatively, it could be used to engineer a virus that only triggers a particular virus-specific immune response during therapy, or to determine before administrating which oncolytic viruses if pretreating a patient with an immunosuppressive medicine is beneficial. There are available data that suggest combining oncolytic viruses with immunosuppressive medicines could enhance the result of the therapy [59]. In a glioma model, pretreatment of a rat with cyclophosphamide increased the burst size in the injected tumours by suppressing immune activity [107]. For the constraint on the parameter space within which during an oncolytic viral therapy, an antibody (a CTL) is established, see Theorem 3.1 (see Theorem 3.2, respectively). One of the interesting facts is that when $Y_I < n$, the constraint on the parameter space for the establishment of an antibody response and a CTL immune response is the same, where Y_I is a marker that we use to measure the virulence level of the virus, and n is a rescaled parameter which is proportional to the ratio of removal to production rates of the immune response (see Eq. (3.2c) and Eq. (3.5)). The mentioned similarity is because we assume that both types of immune responses once reach their abundance saturate (see Eq. (3.3d) and Eq. (3.6d)), and also the functional response of both types of immune response is considered to be linear.

Another interesting observation is that the rate at which antibodies clear virus, or the rate at which CTLs kill infected cells, does not affect the tumour size under the therapy as much as changes in the ratio of removal rate over production rate of the immune response affects the tumour size after the therapy. Our results suggest that not only the ratio of removal to production rates of an immune response identifies when that immune response can be established, but it also affects the tumour size under therapy once an immune response is established: if the tumour is partially

infected and an immune response is also established, increase in the ratio of removal to production rates of that immune response decreases the tumour size under therapy, if the tumour is fully infected and also an immune response is established (which is only observable by the establishment of a CTL), then decrease in the ratio of removal to production rates of an immune response decreases the tumour size (see Figures 3.3 and 3.5). Note that smaller values of the ratio removal to production rates of an immune response represent longer lasting response and bigger values of ratio removal to the production rates represent shorter response. Our results are a proof of concept in the terms that when tumour is partially infected and immune response is established, a longer immune system by blocking spread of infection is a burden, but if the tumour is completely infected and also a CTL immune response is established, since infection has already invaded the tumour, a longer CTL response causes more death of infected cells, hence tumour load becomes less, enhancing the result of the therapy.

Our results show that activation of a virus-specific immune response does not affect the treatment's control threshold: the treatment's control threshold when a virus-specific immune response is activated is the same as when no immune response is active (see Eq. (3.31)). We showed that when the effect of an immune response is ignored, the optimal tumour size under therapy is obtained when the tumour under therapy becomes fully infected [44]. It is essential to discuss how considering a virus-specific immune response can affect this scenario. Our results show that even when a virus-specific immune response becomes active during the therapy, the optimal tumour size by therapy is obtained when the steady states in which 100% infection prevalence is obtained are stable. The optimal threshold of therapy may or may not change by activation of a virus-specific immune response. When $Y_I \leq n$, then activation of a virus-specific immune response does not affect the optimal tumour size and the optimal threshold. However, when $Y_I > n$ and an immune response is

active, the treatment optimal threshold is always higher, meaning that a virus with a higher transmission rate must be administrated for infection to fully invade the tumour in comparison with the case that no immune response gets established (see Theorem 3.5 and Lemma 3.6).

Komarova and Wodarz [61] studied the effect of a virus-specific CTL immune response by the functionality of the killing infected cells. They showed that if in the absence of a CTL immune response the tumour is partially infected, then the establishment of a CTL immune response is only detrimental because tumour size is bigger in the presence of a CTL immune response; however, they do not discuss to which extent it is harmful. Our result supports their findings. In our earlier work we identify the constraint on the transmission rate and the virulence level of the virus within which the treatment yields to partial infection [44] when no virus-specific immune response is considered. Our result shows within that constraint if a virus-specific immune response (Ab or CTL) becomes established, the tumour size is always higher than the tumour size when tumour is partially infected but no immune response is active (see Figure 3.2, and Figure 3.4). Hence, in this case, activation of an immune response is detrimental. However, the extent to which it is detrimental depends on the virulence level of the virus and the ratio removal rate over production rate of the immune response. To be precise, the increase in the tumour size caused by establishment of an immune response (antibody or CTL) decreases when $Y_I < n$ and $|Y_I - n|$ increases. When $Y_I < n$ and $|Y_I - n|$ is maximum, the activation of the immune response has the lowest effect, which can be ignored. In other words, there are some boundaries on Y_I and n values for which an immune response can be established; within those ranges when $Y_I < n$ and $|Y_I - n|$ is maximum, the immune response has the lowest negative effect on the treatment that its effect can be ignored (see Figure 3.3). In contrast when $Y_I > n$, the negative effect of establishment of a virus specific immune response on the treatment becomes stronger as the magnitude

of $|Y_I - n|$ increases.

The models that we propose in this chapter do not include the dynamics of the memory B cells that secrete antibody molecules. Our model can be extended similar to those proposed in [28, 116] to include the dynamics of memory B cells, however, including that equation in our model does not affect the results of this work and all the results remain valid.

3.6 Appendix

Lemma 3.7. Assume $\dfrac{s(X_U - Y_I)}{X_U} < b < \dfrac{X_U - Y_I}{Y_I}$. Define

$$Q(b) := b^2 + b\left(1 - s - \frac{X_U}{n}\right) + \frac{s}{n}(X_U - Y_I), \tag{3.43}$$

and denote the discriminant of Q with δ i.e., $\delta = \left(\dfrac{X_U}{n} + s - 1\right)^2 - \dfrac{4s}{n}(X_U - Y_I)$.

(I) When $Y_I \geq n$, Q is negative if and only if

$$\frac{1}{2}\left(\frac{X_U}{n} + s - 1 - \sqrt{\delta}\right) < b < \frac{X_U - Y_I}{Y_I}. \tag{3.44}$$

(II) When $Y_I < n$, Q is negative if and only if all the followings are satisfied.

(a) $n < \dfrac{X_U}{1-s}$,

(b) $X_U - \dfrac{n}{4s}\left(\dfrac{X_U}{n} + s - 1\right)^2 < Y_I$,

(c) $\left|2b - \left(\dfrac{X_U}{n} + s - 1\right)\right| < \sqrt{\delta}$.

Proof. (I) When $Y_I \geq n$, by inequalities (H1) and (H2), $\frac{X_U}{1-s} > Y_I$. Since $Y_I \geq n$, $\frac{X_U}{1-s} > n$. In other words, $1 - s - \frac{X_U}{n} < 0$.

In addition when $Y_I \geq n$, discriminant of Q is always positive. Otherwise, $\delta \leq 0$.

Since $Y_I \geq n$,

$$\left(\frac{X_U}{n} + s - 1\right)^2 \leq \frac{4s}{n}(X_U - Y_I) \leq \frac{4s}{n}(X_U - n).$$

After algebraic simplification, the above inequality can be rewritten as

$$\left(1 + s - \frac{X_U}{n}\right)^2 \leq 0,$$

which is a contradiction (note that in this case $1+s-\frac{X_U}{n} \neq 0$). Hence, when $Y_I \geq n$, discriminant of Q is always positive.

Hence, when $Y_I \geq n$, quadratic Q always has two positive zeros. On the other hand,

$$Q(\frac{s(X_U - Y_I)}{X_U}) = (X_U - sY_I) \cdot \frac{s(X_U - Y_I)}{X_U^2} > 0. \tag{3.45a}$$

$$Q(\frac{X_U - Y_I}{Y_I}) = \frac{X_U - sY_I}{n} \cdot \left(\frac{X_U - Y_I}{Y_I^2}\right) \cdot (n - Y_I). \tag{3.45b}$$

Since $Q(\frac{X_U-Y_I}{Y_I}) < 0$ and $Q(\frac{s(X_U-Y_I)}{X_U}) > 0$, only one of the zeros of Q is within the interval $\frac{s(X_U-Y_I)}{X_U} < b < \frac{X_U-Y_I}{Y_I}$. Hence, when $Y_I \geq n$, quadratic Q is negative for all the b values within the interval

$$\frac{1}{2}\left(\frac{X_U}{n} + s - 1 - \sqrt{\delta}\right) < b < \frac{X_U - Y_I}{Y_I}. \tag{3.46}$$

(II) When $Y_I > n$, the right root of $Q(b)$ is bigger than $\frac{X_U-Y_I}{Y_I}$, and when $Y_I = n$, $b = \frac{X_U-Y_I}{Y_I}$ is the right root of quadratic Q. Since Q is a continuous function, when $Y_I < n$, both roots of Q if they exist are within the interval $\frac{s(X_U-Y_I)}{X_U} < b < \frac{X_U-Y_I}{Y_I}$. Since, Q is a concave up quadratic and $Q(0) > 0$, Q can have two positive zeros within the interval $\frac{s(X_U-Y_I)}{X_U} < b < \frac{X_U-Y_I}{Y_I}$ if and only if

(I) $n < \dfrac{X_U}{1-s}$,

(II) $X_U - \dfrac{n}{4s}\left(\dfrac{X_U}{n} + s - 1\right)^2 < Y_I$.

Condition (I) is equivalent to $1 - s - \frac{X_U}{n} < 0$ and condition (II) holds if and only if discriminant of quadratic Q is positive. Under the assumption (I) and (II) Q is negative only between the two roots. Precisely, when $Y_I < n$ and both (I) and (II) are satisfied, Q is negative if and only if

$$\left|2b - (\frac{X_U}{n} + s - 1)\right| < \sqrt{\delta}. \tag{3.47}$$

□

3.6.1 Derivation of dimensionless Model (3.3)

Here we derive the dimensionless Model (3.3). First we recall Model (3.1).

$$\begin{aligned}
\frac{dX}{d\tau} &= \bar{r}X(1 - \frac{X+Y}{K}) - \bar{d}X - \beta XV, \\
\frac{dY}{d\tau} &= \bar{s}Y(1 - \frac{X+Y}{K}) - \bar{d}Y - \bar{a}Y + \beta XV, \\
\frac{dV}{d\tau} &= \bar{q}Y - m_v V - \bar{p}VZ, \\
\frac{dZ}{d\tau} &= \frac{\bar{c}VZ}{1+\varepsilon Z} - m_z Z.
\end{aligned}$$

Now let $x = \dfrac{X}{K}$, $y = \dfrac{Y}{K}$, $v = \dfrac{m_v}{K\bar{q}}V$, $z = \varepsilon Z$ and $t = \bar{r}\tau$, then

$$\begin{aligned}
\frac{d(Kx)}{dt} &= Kx(1-x-y) - \frac{\bar{d}}{\bar{r}}Kx - \frac{\beta}{\bar{r}}Kx\left(\frac{K\bar{q}}{m_v}v\right),\\
\frac{d(Ky)}{dt} &= \frac{\bar{s}}{\bar{r}}Ky(1-x-y) - \frac{\bar{d}}{\bar{r}}Ky - \frac{\bar{a}}{\bar{r}}Ky + \frac{\beta}{\bar{r}}Kx\left(\frac{K\bar{q}}{m_v}v\right),\\
\frac{d\left(\frac{K\bar{q}}{m_v}v\right)}{dt} &= \frac{\bar{q}}{\bar{r}}Ky - \frac{m_v}{\bar{r}}\left(\frac{K\bar{q}}{m_v}v\right) - \frac{\bar{p}}{\bar{r}}\left(\frac{K\bar{q}}{m_v}v\right)\frac{z}{\varepsilon},\\
\frac{d\left(\frac{z}{\varepsilon}\right)}{dt} &= \frac{\frac{\bar{c}}{\bar{r}}\left(\frac{K\bar{q}}{m_v}v\right)\left(\frac{z}{\varepsilon}\right)}{1+\varepsilon\left(\frac{z}{\varepsilon}\right)} - \frac{m_z}{\bar{r}}\left(\frac{z}{\varepsilon}\right).
\end{aligned}$$

After some algebraic simplifications the above system of equations turns to

$$\begin{aligned}
\frac{dx}{dt} &= x(1-x-y) - \frac{\bar{d}}{\bar{r}}x - \left(\frac{K\bar{q}\beta}{\bar{r}m_v}\right)xv,\\
\frac{dy}{dt} &= \frac{\bar{s}}{\bar{r}}y(1-x-y) - \frac{\bar{d}}{\bar{r}}y - \frac{\bar{a}}{\bar{r}}y + \left(\frac{K\bar{q}\beta}{\bar{r}m_v}\right)xv,\\
\frac{dv}{dt} &= \frac{m_v}{\bar{r}}\left(y - v - \frac{\bar{p}}{m_v\varepsilon}vz\right),\\
\frac{dz}{dt} &= \left(\frac{K\bar{q}\bar{c}}{\bar{r}m_v}\right)z\left(\frac{v}{1+z} - \frac{m_v m_z}{K\bar{q}\bar{c}}\right).
\end{aligned} \tag{3.48}$$

Now we will call dimensionless parameters as follows:

$$X_U = 1 - \frac{\bar{d}}{\bar{r}}, Y_I = 1 - \frac{\bar{a}+\bar{d}}{\bar{s}}, s = \frac{\bar{s}}{\bar{r}}, m = \frac{m_v}{\bar{r}}, b = \frac{K\bar{q}\beta}{\bar{r}m_v}, \tag{3.49a}$$

$$c = \frac{K\bar{q}\bar{c}}{\bar{r}m_v}, n = \frac{m_v m_z}{K\bar{q}\bar{c}}, p = \frac{\bar{p}}{m_v\varepsilon}. \tag{3.49b}$$

Using the new dimensionless parameters Model (3.1) gets the following dimensionless form.

$$\begin{aligned}
\dot{x} &= x\big(X_U - (x+y)\big) - bvx, \\
\dot{y} &= sy\big(Y_I - (x+y)\big) + bvx, \\
\dot{v} &= m\big(y - v - pvz\big), \\
\dot{z} &= cz\big(\frac{v}{1+z} - n\big).
\end{aligned}$$

3.6.2 Derivation of dimensionless Model (3.6)

First we recall Model (3.4).

$$\begin{aligned}
\frac{dX}{d\tau} &= \bar{r}X(1 - \frac{X+Y}{K}) - \bar{d}X - \beta XV, \\
\frac{dY}{d\tau} &= \bar{s}Y(1 - \frac{X+Y}{K}) - \bar{d}Y - \bar{a}Y + \beta XV - \bar{L}YZ \\
\frac{dV}{d\tau} &= \bar{q}Y - \bar{m}_v V \\
\frac{dZ}{d\tau} &= \frac{\bar{c}YZ}{1+\mu Z} - m_z Z,
\end{aligned}$$

Now let $x = \frac{X}{K}$, $y = \frac{Y}{K}$, $v = \frac{m_v}{K\bar{q}}V$, $z = \mu Z$ and $t = \bar{r}\tau$, then

$$\begin{aligned}
\frac{d(Kx)}{dt} &= Kx(1-x-y) - \frac{\bar{d}}{\bar{r}}Kx - \frac{\beta}{\bar{r}}Kx\left(\frac{K\bar{q}}{m_v}v\right), \\
\frac{d(Ky)}{dt} &= \frac{\bar{s}}{\bar{r}}Ky(1-x-y) - \frac{\bar{d}}{\bar{r}}Ky - \frac{\bar{a}}{\bar{r}}Ky + \frac{\beta}{\bar{r}}Kx\left(\frac{K\bar{q}}{m_v}v\right) - \frac{\bar{L}}{\bar{r}}(Ky)(\frac{z}{\mu}), \\
\frac{d\left(\frac{K\bar{q}}{m_v}v\right)}{dt} &= \frac{\bar{q}}{\bar{r}}Ky - \frac{m_v}{\bar{r}}\left(\frac{K\bar{q}}{m_v}v\right), \\
\frac{d\left(\frac{z}{\mu}\right)}{dt} &= \frac{\frac{\bar{c}}{\bar{r}}(Ky)\left(\frac{z}{\mu}\right)}{1+\mu\left(\frac{z}{\mu}\right)} - \frac{m_z}{\bar{r}}\left(\frac{z}{\mu}\right).
\end{aligned}$$

After some algebraic simplifications the above system of equations turns to

$$\begin{aligned}
\frac{dx}{dt} &= x(1-x-y) - \frac{\bar{d}}{\bar{r}}x - \left(\frac{K\bar{q}\beta}{\bar{r}m_v}\right)xv, \\
\frac{dy}{dt} &= \frac{\bar{s}}{\bar{r}}y(1-x-y) - \frac{\bar{d}}{\bar{r}}y - \frac{\bar{a}}{\bar{r}}y + \left(\frac{K\bar{q}\beta}{\bar{r}m_v}\right)xv - \frac{\bar{L}}{\bar{r}\mu}yz, \\
\frac{dv}{dt} &= \frac{m_v}{\bar{r}}(y-v), \\
\frac{dz}{dt} &= \left(\frac{K\bar{c}}{\bar{r}}\right)z\left(\frac{y}{1+z} - \frac{m_z}{K\bar{c}}\right).
\end{aligned} \tag{3.50}$$

Model (3.50) is the same as Model (3.48) is the absence of an immune response, meaning when z is equal to zero. Hence, we use the same notation as (3.49) to represent the dimensionless parameters. The rest of dimensionless parameters of Model (3.50) are called as follows.

$$c = \frac{K\bar{c}}{\bar{r}}, \quad n = \frac{m_z}{K\bar{c}}, \quad L = \frac{\bar{L}}{\bar{r}\mu}.$$

Using the new dimensionless parameters Model (3.4) gets the following dimensionless form.

$$\begin{aligned}
\dot{x} &= x(X_U - (x+y)) - bvx, \\
\dot{y} &= sy(Y_I - (x+y)) + bvx - Lyz, \\
\dot{v} &= m(y-v), \\
\dot{z} &= cz\left(\frac{y}{1+z} - n\right).
\end{aligned}$$

Chapter 4

Targeting cancer stem cells with oncolytic viral therapy

Cancer stem cells have a predominant role in forming a tumour even though differentiated cells are the prevalent cells in a tumour. Oncolytic viruses act as agents that enter a tumour through infection and target both cancer stem cells and differentiated cells. In this work, we extend previous mathematical models of viral and tumour dynamics in order to analyze the effectiveness of targeting cancer stem cells with oncolytic viruses. We model interactions between uninfected and infected cancer cells, within stem cell-differentiated cell hierarchy, during an oncolytic viral therapy. We calculate the basic reproduction number and use it to constrain the infectivity rates of initiating and differentiated cancer cells. When this constraint is met, long-term tumour shrinkage is observable; otherwise, treatment fails. Our results suggest that stem cell specificity of oncolytic virus depends both on the average infectivity and mitotic rates of infected cells. There is a positive correlation between the average infectivity rate and stem cell specificity for nonmitotic infected cells. When average infectivity is high, an oncolytic virus with higher stem cell specificity leads to smaller tumours. In contrast, when average infectivity is low, the minimum tumour size is

obtained when an oncolytic virus with higher potency targeting differentiated cells is used. Perfect stem cell targeting obtains the minimum tumour size when infected cells are mitotic, and the basic reproduction number is above one. When mitotic rates of infected cells are greater than their apoptosis rates, we derive a value for stem cell infectivity rate for minimizing tumour size.

4.1 Introduction

Tumour heterogeneity, which renders many conventional therapies ineffective, has been an important subject of research for several decades [11, 22, 27, 33, 56, 58, 75–78, 102, 110]. The phenotypic heterogeneity inside a tumour is both morphological and functional. One of the most important features of epigenetic heterogeneity inside a tumour is that only a small subpopulation of cells, known as cancer-initiating cells, or so-called cancer stem cells, can create a tumour clone. These tumour initiating phenotypes have the potential to self-renew and differentiate via both symmetric and asymmetric proliferation events. This pluripotential capacity leads to various heterogeneities inside a tumour.

The phenotypic heterogeneity of tumours has a significant impact on the effectiveness of treatment strategies. Tumour initiating cells have some common properties, such as long-lasting quiescence, high levels of multi-drug resistance expression, and high DNA repair capability [89, 90, 106], which cause conventional therapies like chemotherapy [123] and radiotherapy [97] to fail in eradicating cancer stem cells. Hence, cancer stem cells are causative for tumour recurrence. It seems therapies that are not affected by the common properties of cancer-initiating cells lead to more effective results. Oncolytic viruses enter tumour cells through infection; therefore, they target both proliferating and quiescent stem cells [18]. On the other hand, most of these properties are common to both cancer-initiating cells and intact normal

stem cells. Using tumour specific promoters, oncolytic viruses can be engineered to only target cancer cells and do not replicate in the healthy normal cells. Therefore, oncolytic viral therapy has fewer side effects in comparison to conventional therapies.

Despite some promising results from in vitro and in vivo clinical trials [6,8,19,29,95], many questions remain unanswered about the overall promise of targeting tumour initiating cells using an oncolytic virus. Moreover, the treatment strategy and goal of such viral therapy could affect the design of the regimen. In principle, one can tune such treatment to target pre-cancerous small tumours or use it in combination with other anti-cancer therapies during a treatment course or just after/before remission to assure the leftover tumour initiating cells are eradicated [91, 108]. To do this, one needs a comprehensive yet simple model that incorporates a hierarchy of cells, including tumour initiating cells and differentiated cells in the presence of a cytotoxic oncolytic virus that targets different tumour cell types with different specificities and killing rates. Our modelling effort aims to address the following questions.

- Is it possible to reach complete tumour eradication for a given oncolytic therapy that targets both stem cells and their progenitors?
- Can we identify limits on infectivity of stem and differentiated cells that lead to successful treatment?
- Which phenotype should preferentially be targeted to enhance the efficiency of therapy? In other words, does a higher specificity in targeting stem-like cancer cells increase the overall efficacy of the oncolytic viral therapy, or is a higher specificity in targeting differentiated tumour cells necessary?
- If this is the case, what is the optimal stem cell specificity to obtain the lowest tumour burden?
- What factors affect the optimal stem cell specificity?

- How do the infected cells' mitotic (self-renewal and differentiation) rates affect the therapeutic outcome?
- Does the stem cell fraction increase or decrease after oncolytic therapy?

Cancer initiating cells were first defined in acute myeloid leukaemia (AML) in 1994 [65]. A subpopulation with marker $CD34^+/CD38^-$, which has been used to mark stem cells, was observed in leukaemia in vivo in nude mice [65]. Later experiments identified a similar subpopulation with tumour initiating potential for solid tumours. For breast cancer, Al Hajj et al. [5] showed a subpopulation with marker CD44+/CD24- were operating as tumourigenic cells. For brain tumours, $CD133^+$ cells are identified as a stem-like subpopulation [54]. There are several different opinions on how such subpopulations of cancer stem cells arise. One hypothesis is that they come from epigenetic alterations in a normal stem cell, and thus we can expect the appearance of tumour initiating cells inside stem cell niche areas. However, this hypothesis is questioned since inside a tumour, cells are highly phenotypically plastic, and there are de-differentiation events during which non-cancer stem cells transform into cancer stem cells [36]. In this work, we make the simplifying assumptions that the cancer stem cell population remains in the stem cell niche area, and the size of this area limits cancer stem cells' growth.

By engineering a category of adenoviral vectors, Eriksson et al. [29] conducted a proof of concept study to show the effectiveness of oncolytic viruses against cancer stem cells. They prevented a sorted subpopulation of breast cancer tumour initiating cells from forming a tumour in mouse mammary fat pads by infecting them with Ad5/3-Δ24 and Ad5.pK7-Δ24. Their result was promising both in vitro and in vivo. In vivo, they measured the tumour initiating capability of infected subpopulations of cancer-initiating cells versus uninfected ones. The infected ones could not establish a tumour in any of the cases, while the uninfected CD44+/CD24- subpopulation

presented strong tumour initiating capability. Moreover, they showed that oncolytic viruses with E1A-CR2 capsid-modified adenoviruses could kill both quiescent and committed cancer stem cells [68]. Hence, a model that captures dynamics of cancer stem cells during oncolytic virotherapy, captures dynamics of both quiescent and committed cancer stem cells.

In recent years, many in vivo and in vitro experiments have been conducted for targeting tumour initiating cells with oncolytic viruses in different types of cancers. For example, Sagara et al. [95] showed that a Coxsackievirus B3 (CVB3) infection caused effective oncolytic activity against lung cancer-initiating cells. For clone cancer, Yoo et al. [122] developed cancer favouring oncolytic virus that could efficiently infect and replicate in colon cancer-initiating cells because it was not affected by drug-resistance pathways. They concluded that this oncolytic virus efficaciously suppresses cancer-initiating cells, and by co-treatment with anti-cancer drug 5-Fu, therapy can be more successful.

In the past two decades, some mathematical models have been introduced to describe each phenotype dynamics in the hierarchical structure of a tumour [50,51,73,100]. In addition, several mathematical models have been introduced to investigate oncolytic viral therapy [3,61,86,114]. However, there has not been a mathematical model that describes the regimen in which cells from different phenotypes are targeted with different specificity. Here we build a mathematical model that describes interactions between populations of infected and uninfected cancer cells, where each of these populations is a hierarchical structure of stem cell-differentiated cell as illustrated in Figure 4.2.

The outcomes of treatment depend extensively on the extent to which infection invades the tumour. An important measure widely used in epidemiology to identify transmissibility of infection is basic reproduction number [105]. Here, we use the

basic reproduction number to find the constraint needed on the infectivity rates of stem and differentiated cells for the therapy to work. When this constraint is not satisfied, therapy fails.

To assess cancer stem cell selectivity by oncolytic viruses, Bauerschmitz et al. [8] used oncolytic viruses equipped with tumour specific promoters such as Rb, a-lactalbumin (ala), cyclo-oxygenase 2 (Cox-2), telomerase (hTERT), and multi-drug resistance (MDR) promoters. They constructed respective capsid modified, promoter-controlled adenoviruses and observed their oncolytic efficiency in vitro and in vivo experiments. They found out the viruses Ad5/3-hTERT-Δgp, Ad5/ 3-Cox2L-Δ24 and Ad5/3-mdr-Δ24 had higher potency and selectivity for CD44+/CD24- subpopulations while Ad5/ 3ala-Δ24 was less effective. In vitro, all of the above viruses with various efficacy could kill 100% of the CD44+/CD24- populations. For in vivo experiments, a subpopulation of FAC sorted CD44+/CD24- cells are injected into (immunodeficient) mice and were left for a tumour to establish. The virus was injected intratumourally every second day, starting at day 14. The treatment resulted in smaller tumours and much slower growth (or complete stagnation). However, the eradication of the tumour was never observed in vivo. On day 17 of treatment, the tumour population was sorted for subpopulations of CD44 +/- and CD24 -/-. Interestingly, the fraction of CD44+/CD24- is not significantly changed versus mock. The best result is obtained by using Ad5/3-MDR-d24, in which CD44+/CD24- is 2.6% of population fraction versus 3.4% in mock. Our numerical simulation illustrates that tumour size under therapy decreases when infection partially or fully spreads in a tumour. However, stem cell fraction increases once the tumour becomes infected.

The above in vivo and in vitro experiments make us confident that oncolytic viruses can be engineered with different levels of sensitivity and specificity in targeting tumour stem-like subpopulations, motivating us to analytically and numerically investigate optimal stem cells specificity and its dependence on the spread of infection.

Specifically, we consider two different scenarios: mitotic and nonmitotic infected cells. We refer to an infected cell that cannot self-renew and differentiate as a nonmitotic infected cell. When infected cells are nonmitotic, virus transmission is only horizontal, meaning infection only is transmitted when an uninfected cell encounters an infected cell and becomes infected. We will show that in this case, tumours can only be partially infected. We refer to an infected cell that can self-renew and differentiate as an infected mitotic cell. When infected cells are mitotic, infection transmission occurs both horizontally and vertically. Vertical transmission occurs during self-renewal or differentiation. During self-renewal, an infected stem cell divides into two infected daughter stem cells, and during (symmetric) differentiation, an infected stem cell gives birth to two infected differentiated cells. We will show that infection can fully invade the tumour when the basic reproduction number is above one, and the reproduction number of uninfected cancer cells is less than one. As we will show, mitotic rates of infected cells significantly impact optimal stem cell specificity.

4.2 Model: Oncolytic viruses targeting tumour initiating cells

Cancer stem cells are pluripotent because they can produce phenotypically different progenies from the original mother stem cell; this can be achieved through symmetric and asymmetric divisions where the daughter cell is either a stem cell or an early progenitor [26]. Progenitor or partially differentiated cells which divide through a chain of proliferation events give rise to a larger population of fully-differentiated cells [109]. In this work, we only consider symmetric cell divisions. During the self-renewal process, a stem cell gives rise to two identical daughter stem cells, as illustrated in Figure 4.1(a). During the symmetric differentiation process, a stem cell

divides into two differentiated cells, see Figure 4.1(b) for a schematic representation.

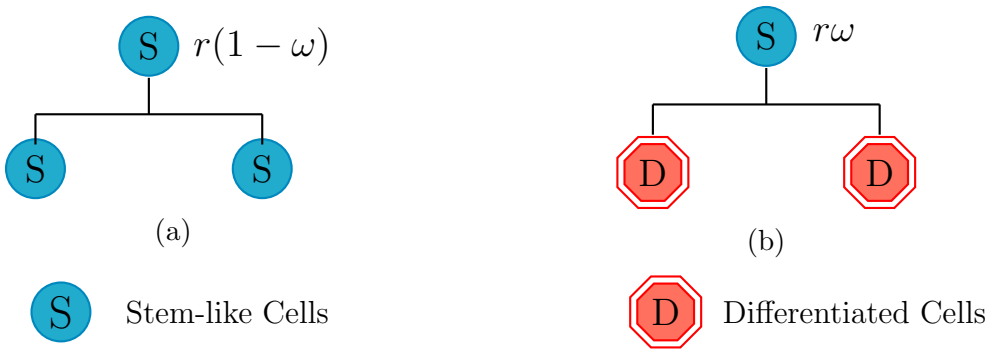

Figure 4.1: **A simplified hierarchy of symmetric divisions of tumour initiating cells.** This figure is a schematic representation of symmetric cell divisions of stem cells. Here we assume stem cell division rate is r and $(1-\omega)$ is the self-renewal probability. **Plot (a)** represents self-renewal, meaning a stem cell divides into two daughter stem cells with rate $r_{\mathrm{S}} = r(1-\omega)$. **Plot (b)** shows differentiation process in which a stem cell divides symmetrically into two differentiated cells with rate $r_{\mathrm{D}} = 2r\omega$.

For simplicity, we use a simplified two-compartment model where stem cells are collected in one compartment and partially or fully differentiated cells are in another. The following system of equations gives this simplified model.

$$\begin{aligned} \frac{\mathrm{d}x_{\mathrm{S}}}{\mathrm{d}t} &= L_{\mathrm{S}}(x_{\mathrm{S}}, x_{\mathrm{D}})x_{\mathrm{S}}, \\ \frac{\mathrm{d}x_{\mathrm{D}}}{\mathrm{d}t} &= L_{\mathrm{D}}(x_{\mathrm{D}})x_{\mathrm{S}} + \hat{L}_{\mathrm{D}}(x_{\mathrm{D}})x_{\mathrm{D}}, \end{aligned} \tag{4.1}$$

where x_{S} and x_{D} are the population densities of stem cells and differentiated cells, respectively. The function L_{S} is the rate of turnover of stem cells and includes self-renewal, death and differentiation events. Hence,

$$L_{\mathrm{S}}(x_{\mathrm{S}}, x_{\mathrm{D}}) = r_{\mathrm{S}}(1 - b_S x_{\mathrm{S}}) - \bar{d}_{\mathrm{S}} - r\omega(1 - b_{\mathrm{D}} x_{\mathrm{D}}),$$

where $r_{\mathrm{S}} = r(1-\omega)$ is the rate at which stem cells self-renew. r denotes the stem cell division rate and ω is the differentiation probability. b_{S} is the inverse carrying capacity in the stem cell niche/compartment, and $\bar{d}_{\mathrm{S}}$ is the apoptosis rate of stem

cells.

$L_D(X_{\mathrm{D}})$ denotes reproduction of fully differentiated cells via symmetric differentiation. Hence, $L_{\mathrm{D}}(x_{\mathrm{D}}) = r_{\mathrm{D}}(1 - b_{\mathrm{D}}x_{\mathrm{D}})$ where $r_{\mathrm{D}} = \alpha r\omega$ is the rate of differentiation in which $\alpha \geq 2$ is a variable denoting the final number of fully differentiated cells that are reproduced by a stem cell that is undergone a differentiation. The term $\hat{L}_{\mathrm{D}} = d_{\mathrm{D}}$ denotes the apoptosis rate of fully-differentiated cells. b_{D} is the inverse carrying capacity of differentiated cells. Using two different carrying capacities for stem cells and differentiated cells is because stem cells are assumed to be confined to stem cell niches. In practice carrying capacity of stem cells is much lower than the carrying capacity of differentiated cells; hence, $b_{\mathrm{D}} \ll b_{\mathrm{S}}$. Therefore, we can assume $b_{\mathrm{D}} = 0$, this assumption yields

$$L_{\mathrm{S}}(x_{\mathrm{S}}, x_{\mathrm{D}}) = r_{\mathrm{S}}(1 - b_S x_{\mathrm{S}}) - \bar{d}_{\mathrm{S}} - r\omega.$$

As of now for simplicity we show $\bar{d}_{\mathrm{S}} + r\omega$ by d_{S}. Notice that when $b_{\mathrm{D}} = 0$, d_{S} denotes the removal rate of cancer stem cells.

This simple model encapsulates the main features of a hierarchical structure of stem cell-differentiated cell proliferation inside a tumour. We use the above simple stem cell-differentiated cell hierarchy to model the cancer cell dynamics during oncolytic therapy. The primary function of oncolytic viruses is to infect and lyse tumour cells. However, an oncolytic viral therapy in which both stem and differentiated cells are targeted involves many complexities. For example, tumour initiating cells and differentiated cells might become infected at different rates. The number of copies that a virus makes in a host infected cell may vary depending on the phenotype of the infected cell. The timescale of virus dynamics may be fast or slow. Here, our goal is to introduce a very simple model that describes the dynamics of both cancer stem cells and differentiated cells during an oncolytic viral therapy that targets both

stem cells and differentiated cells. Therefore, we make some simple assumptions that ignore some of these complexities.

We begin by writing a four-compartment model which includes target stem cells, x_{S}, target differentiated cells, x_{D}, infected stem cells, y_{S}, and infected differentiated cells, y_{D}, see Figure 4.2. The stem cells and differentiated cells in the absence of treatment follow the dynamics discussed in the previous section. A stem cell when encountering an infected cell, becomes infected with rate β_{S}. A differentiated cell when encountering an infected cell becomes infected with rate β_{D}. The self-renewal rates of infected stem cells are denoted by l_{S} and the differentiation rate of infected stem cells is denoted by l_{D}, see Figure 4.2. a_{S} denotes the sum of apoptosis rate and differentiation rate of infected stem cells. The apoptosis rate of infected differentiated cells is denoted by a_{D}. A summary of all the parameters with their corresponding biological interpretations is provided in Table 4.1.

The above dynamics are given by the following system of equations,

$$\frac{\mathrm{d}x_{\mathrm{S}}}{\mathrm{d}t} = r_{\mathrm{S}}x_{\mathrm{S}}(1 - b_{\mathrm{S}}(x_{\mathrm{S}} + y_{\mathrm{S}})) - d_{\mathrm{S}}x_{\mathrm{S}} - \beta_{\mathrm{S}}x_{\mathrm{S}}(y_{\mathrm{S}} + y_{\mathrm{D}}), \tag{4.2a}$$

$$\frac{\mathrm{d}x_{\mathrm{D}}}{\mathrm{d}t} = r_{\mathrm{D}}x_{\mathrm{S}} - d_{\mathrm{D}}x_{\mathrm{D}} - \beta_{\mathrm{D}}x_{\mathrm{D}}(y_{\mathrm{S}} + y_{\mathrm{D}}), \tag{4.2b}$$

$$\frac{\mathrm{d}y_{\mathrm{S}}}{\mathrm{d}t} = l_{\mathrm{S}}y_{\mathrm{S}}(1 - b_{\mathrm{S}}(x_{\mathrm{S}} + y_{\mathrm{S}})) - a_{\mathrm{S}}y_{\mathrm{S}} + \beta_{\mathrm{S}}x_{\mathrm{S}}(y_{\mathrm{S}} + y_{\mathrm{D}}), \tag{4.2c}$$

$$\frac{\mathrm{d}y_{\mathrm{D}}}{\mathrm{d}t} = l_{\mathrm{D}}y_{\mathrm{S}} - a_{\mathrm{D}}y_{\mathrm{D}} + \beta_{\mathrm{D}}x_{\mathrm{D}}(y_{\mathrm{S}} + y_{\mathrm{D}}). \tag{4.2d}$$

The followings are the assumptions under which we will study the dynamics of the above Model:

C1: Here, we assume virus turnover is much faster than the turnover of infected cells, so the virus is in a quasi-steady state; that is why there is no equation describing the dynamics of the virus explicitly.

C2: For simplicity, we assume that the burst size of the virus is the same per both

cancer stem cells and cancer differentiated cells.

C3: We assume the carrying capacity of differentiated cancer cells is much higher than one's for cancer stem cells. Therefore, $b_{\mathrm{D}} \ll b_{\mathrm{S}}$. Hence, we assume $b_{\mathrm{D}} = 0$.

C4: Here, we assume vertical infection transmission is perfect. In other words, an infected cell during self-renewal or differentiation does not produce any uninfected daughter cells.

C5: We assume per capita growth rates of target cancer cells are greater than their removal rates. Therefore, $r_{\mathrm{S}} > d_{\mathrm{S}}$ and $r_{\mathrm{D}} > d_{\mathrm{D}}$.

C6: Herein we assume virus is virulent, meaning it will make the host cells less functional by inducing infection on them, in other words:

- infection reduces cell growth; $l_{\mathrm{S}} < r_{\mathrm{S}}$ and $l_{\mathrm{D}} < r_{\mathrm{D}}$. In many cases, infected cells are not replicating, $l_{\mathrm{S,D}} = 0$.
- infection elevates apoptosis; $a_{\mathrm{S}} > d_{\mathrm{S}}$ and $a_{\mathrm{D}} > d_{\mathrm{D}}$.

Earlier research on oncolytic viral therapy that does not take phenotypic heterogeneity into account suggests that by an increase in transmission rate, therapy is enhanced. To be precise, the tumour size under therapy decreases [44, 61]. Numerical simulations of Model (4.2) in which cancer cells are being randomly targeted, meaning $\beta_{\mathrm{S}} = \beta_{\mathrm{D}} = \beta$, supports the result of earlier papers. Figure 4.3 is a numerical simulation of Model (4.2) where $\beta_{\mathrm{S}} = \beta_{\mathrm{D}} = \beta$. In plots (a) and (b) infected cells are nonmitotic, i.e. $l_{\mathrm{S}} = l_{\mathrm{D}} = 0$, and in plots (c) and (d) infected cells are mitotic, but mitotic rates are low, $l_{\mathrm{S}} = 0.25$, and $l_{\mathrm{D}} = 0.5$. In Figure 4.3 the tumour growth parameters are $r = 2, \omega = 0.5$,where $r_{\mathrm{S}} = r(1-\omega), r_{\mathrm{D}} = 2r\omega$. The treatment is modelled by assuming $\beta_{\mathrm{S,D}}$ as step-wise functions of time and at $t = t_0 = 30$ they turn on to their non-zero value. For initial conditions a small value of initial infected cells are assumed, however the results are not sensitive to the initial condi-

Table 4.1: Biological interpretations of parameters of Model (4.2).

Symbol	Biological interpretation	Units
b_{S}	inverse maximum load of cancer stem cells (due to the size of stem cell niche)	$\frac{1}{[\text{cell}]}$
b_{D}	inverse carrying capacity of tumour (differentiated) cells	$\frac{1}{[\text{cell}]}$
β_{S}	infectivity rate per stem cell	$\frac{1}{[\text{time}]\ [\text{cell}]}$
β_{D}	infectivity rate per differentiated cell	$\frac{1}{[\text{time}]\ [\text{cell}]}$
r_{S}	self-renewal rate for target stem cells	$\frac{1}{[\text{time}]}$
l_{S}	self-renewal rate for infected stem cells	$\frac{1}{[\text{time}]}$
r_{D}	rate of symmetric differentiation for target stem cells	$\frac{1}{[\text{time}]}$
l_{D}	rate of symmetric differentiation for infected stem cells	$\frac{1}{[\text{time}]}$
d_{D}	apoptosis rate of target differentiated cells	$\frac{1}{[\text{time}]}$
a_{D}	apoptosis rate of infected differentiated cells	$\frac{1}{[\text{time}]}$
d_{S}	removal rate (i.e. sum of apoptosis rate and differentiation rate) of target stem cells	$\frac{1}{[\text{time}]}$
a_{S}	removal rate (i.e. sum of apoptosis rate and differentiation rate) of infected stem cells	$\frac{1}{[\text{time}]}$
r	stem cell division rate	$\frac{1}{[\text{time}]}$
ω	differentiation probability	
α	final number of fully differentiated cells	

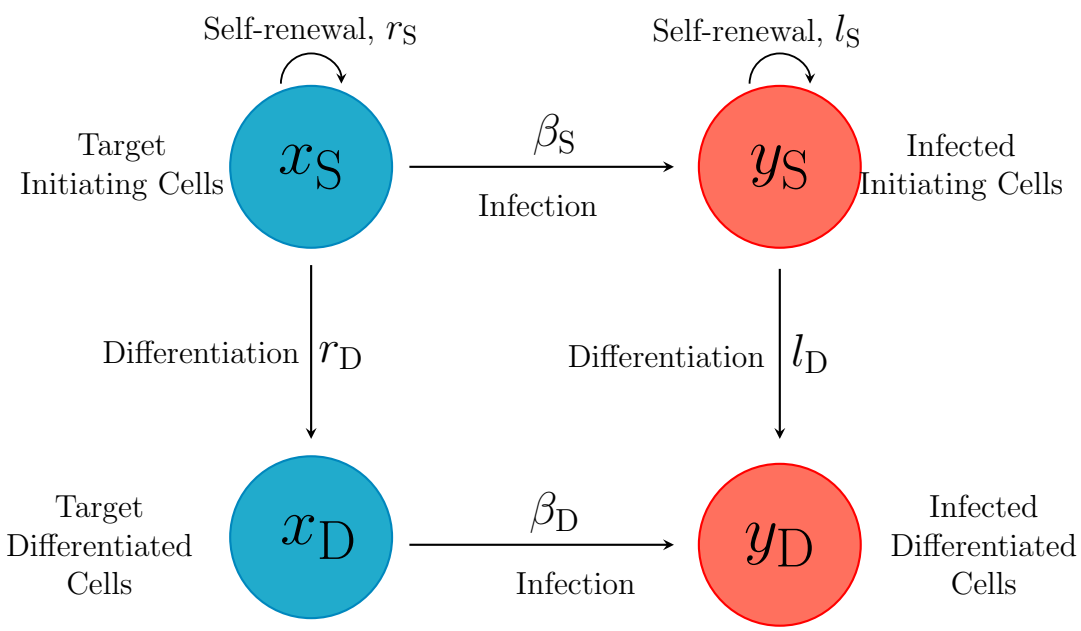

Figure 4.2: **Schematic representation of vertical and horizontal transmission of infection within a tumour.** x_S, x_D, y_S, y_D, represent target stem cells, target differentiated cells, infected stem cells and infected differentiated cells, respectively.

tions. For the plots we assumed the tumour is in its virus-free steady state before the start of treatment. The results are plotted for various values of average infectivity: $\beta = 0.2, 0.4, 0.6, 0.8, \cdots, 1$. Figures 4.3(a) and 4.3(c) illustrate that very small values of β do not affect tumour size. By increasing β, tumour size post therapy decreases, in both case of mitotic and nonmitotic infected cells (see Figure 4.3 caption for the rest of model parameters).

Figures 4.3(b) and 4.3(d) suggest that stem cell fraction increases when average infectivity increases.

In section 4.4 we show that in the case of mitotic infected cells an increase in average infectivity does not reduce the tumour size all the time. We show that virus specificity in preferentially targeting a phenotype over the other strongly affects the treatment outcome. In the case of mitotic infected cells, we will show there is a threshold for the transmission rate of infection to stem cells; once that transmission

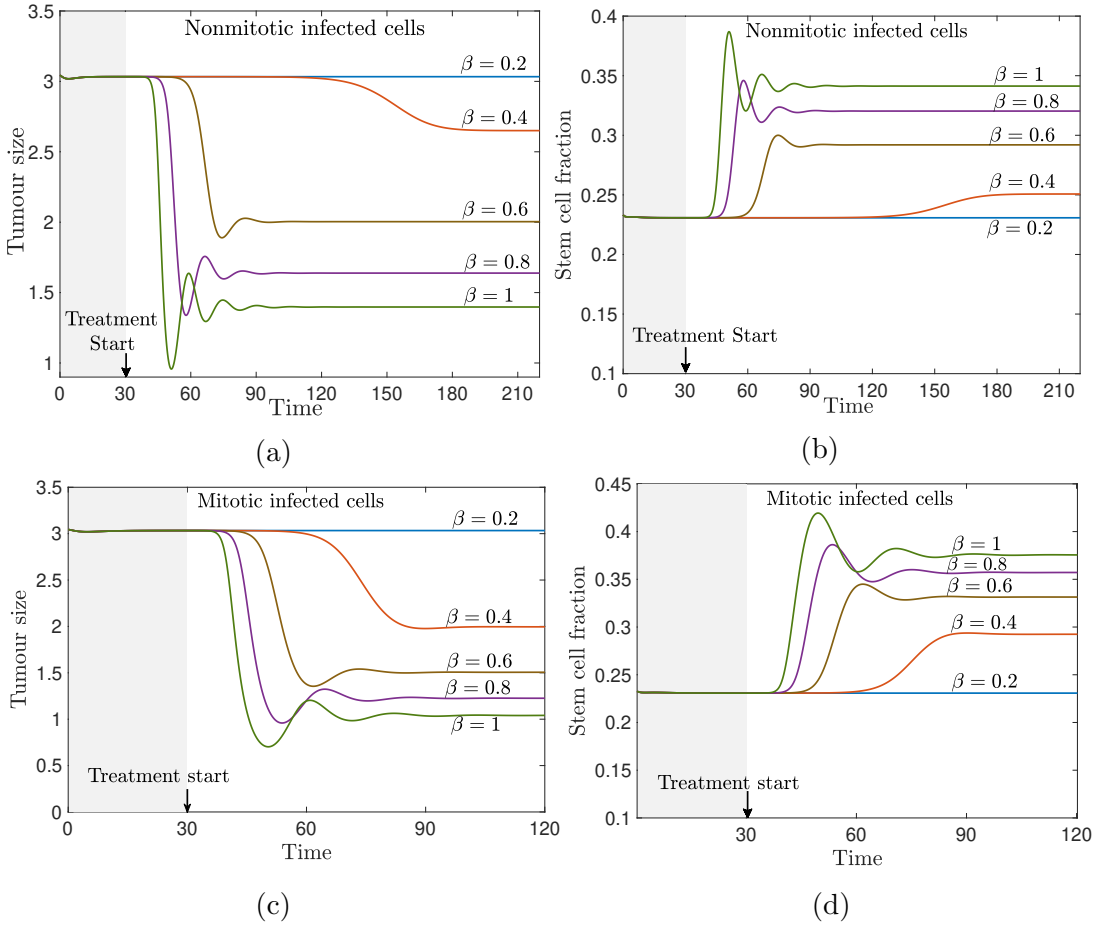

Figure 4.3: **(a,c) An increase in average infectivity decreases tumour size. (b,d) An increase in average infectivity increases stem cell fraction.** Plots (a) and (c) illustrate that tumour size becomes smaller when average infectivity increases. Plots (b) and (d) suggest that stem cell fraction increases by an increase in average infectivity. In plots (a) and (b) infected cells are nonmitotic $l_{\mathrm{S,D}} = 0$ and in plots (c) and (d) infected cells are mitotic $l_{\mathrm{S}} = 0.25$ and $l_{\mathrm{D}} = 0.5$. However, even in the case of mitotic infected cells, mitotic rates of infected cells are still low. As we will show in Section 4.4, an increase in average infectivity rate does not always reduce the tumour size in the case of mitotic infected cells. These plots are conducted for Model (4.2). Treatment is applied at $t = 30$ with an initial dose of virus injected ($y_{\mathrm{S}} = 0.01x_{\mathrm{S}}$ is used to represent this). $\beta_{\mathrm{S}} = \beta_{\mathrm{D}} = \beta$. $\beta = 0.2, 0.4, \cdots, 1.0$. Other model parameters are: $r = 2, \omega = 0.5, r_{\mathrm{S}} = r\omega = 1, r_{\mathrm{D}} = 2r(1-\omega) = 2, d_{\mathrm{S}} = 0.3, d_{\mathrm{D}} = 0.6, a_{\mathrm{S}} = d_{\mathrm{S}} + 0.01, a_{\mathrm{D}} = d_{\mathrm{D}} + 0.01, b_{\mathrm{S}} = 1, b_{\mathrm{D}} = 0$.

rate is obtained, tumour size becomes minimum.

The main question of this chapter is how hierarchical phenotypic variability affects the mechanism of tumour infection by the virus. The engineered virus used in the experiments targets some common tumour suppressor gene promoters. To engineer viruses with the capability of targeting stem cells, an additional stem cell marker is added to increase the specificity of the virus while the infectivity to the non-stem-like tumour cells is not changed. Specificity and infectivity of the virus encountering tumour initiating (tumour differentiated) cells are incorporated in β_{S} (β_{D}). In this work, we will focus on how changes in β_{S} and β_{D} affect the outcome of the therapy.

In the next section, we identify all the steady states of the model and the conditions under which each exists.

4.3 Steady states

Possible outcomes of Model (4.2) depends on the stability of its steady states. When a steady state is globally stable, and almost all the solutions eventually tend to it. Hence, the tumour size post-therapy will be the total population of both infected and uninfected cancer cells from both kinds of fully differentiated and tumour initiating cells corresponding to that steady state. Since the tumour size post-therapy is a measure of the success of the therapy, it is important to identify the steady states of the model. We denote the steady state with vector $E = (x_{\mathrm{S}}, x_{\mathrm{D}}, y_{\mathrm{S}}, y_{\mathrm{D}})$. In principle, there are four distinct steady states. Each steady state corresponds to a different outcome and is as follows:

- Complete tumour eradication steady state, $E_0 = (0, 0, 0, 0)$. When this steady state is globally stable means, the therapy fully eradicates the tumour.
- Treatment failure steady state, $E_{\mathrm{T}} = (x_{\mathrm{TS}}, x_{\mathrm{TD}}, 0, 0)$. This steady state is

globally stable when infection fails to spread across the tumour and eventually the infected tumour cells die out. The steady state population of target stem cell and differentiated cells, x_{TS} and x_{TD} depend on the original stem cell dynamics model and are independent of the infection parameters:

$$x_{\mathrm{TS}} = b_{\mathrm{S}}^{-1} \cdot (1 - \frac{d_{\mathrm{S}}}{r_{\mathrm{S}}}),$$
$$x_{\mathrm{TD}} = \frac{r_{\mathrm{D}}}{d_{\mathrm{D}}} \cdot x_{\mathrm{TS}} \tag{4.3}$$

- 100% infection prevalence steady state, $X_{\mathrm{I}} = (0, 0, y_{\mathrm{IS}}, y_{\mathrm{ID}})$. 100% infection prevalence occurs when infection is successfully spread across the tumour and all tumour cells have been infected with oncolytic virus. Populations of infected stem and differentiated cells of this steady state are given by:

$$y_{\mathrm{IS}} = b_{\mathrm{S}}^{-1} \cdot (1 - \frac{a_{\mathrm{S}}}{l_{\mathrm{S}}}),$$
$$y_{\mathrm{ID}} = \frac{l_{\mathrm{D}}}{a_{\mathrm{D}}} \cdot y_{\mathrm{IS}} \tag{4.4}$$

- Partially infected steady state, $E_P = (x_{\mathrm{S}}^*, x_{\mathrm{D}}^*, y_{\mathrm{S}}^*, y_{\mathrm{D}}^*)$. When E_p is globally stable, the virus has partially spread; this happens when the virus is weakly transmissive and uninfected cells outgrow the infected ones. However, at the steady state, the rate of new infections balances the uninfected cells higher

fitness. The closed forms for x_{S}^*, $x_{\mathrm{D}}^*, y_{\mathrm{S}}^*$ and y_{D}^* are as follows.

$$x_{\mathrm{S}}^* = \frac{(r_{\mathrm{S}} - d_{\mathrm{S}} - \beta_{\mathrm{S}}T)(a_{\mathrm{S}}r_{\mathrm{S}} - l_{\mathrm{S}}d_{\mathrm{S}} - l_{\mathrm{S}}\beta_{\mathrm{S}}T)}{b_{\mathrm{S}}r_{\mathrm{S}}\big((r_{\mathrm{S}} - l_{\mathrm{S}})\beta_{\mathrm{S}}T + a_{\mathrm{S}}r_{\mathrm{S}} - l_{\mathrm{S}}d_{\mathrm{S}}\big)}, \tag{4.5a}$$

$$x_{\mathrm{D}}^* = x_{\mathrm{S}}^* \frac{r_{\mathrm{D}}}{\beta_{\mathrm{D}}T + d_{\mathrm{D}}}, \tag{4.5b}$$

$$y_{\mathrm{S}}^* = \frac{\beta_{\mathrm{S}}T(r_{\mathrm{S}} - d_{\mathrm{S}} - \beta_{\mathrm{S}}T)}{b_{\mathrm{S}}\big((r_{\mathrm{S}} - l_{\mathrm{S}})\beta_{\mathrm{S}}T + a_{\mathrm{S}}r_{\mathrm{S}} - l_{\mathrm{S}}d_{\mathrm{S}}\big)}, \tag{4.5c}$$

$$y_{\mathrm{D}}^* = T - y_{\mathrm{S}}^*, \tag{4.5d}$$

where T has one of the following forms:

$$\begin{aligned}
T &= -\frac{B}{2A} + \sqrt{\left(\frac{B}{2A}\right)^2 - \frac{C}{A}}, && \text{if } A > 0 \text{ and } C < 0,\\
T &= -\frac{B}{2A} - \sqrt{\left(\frac{B}{2A}\right)^2 - \frac{C}{A}}, && \text{if } A < 0 \text{ and } C < 0,\\
T &= -\frac{C}{B}, && \text{if } A = 0 \text{ and } C < 0,
\end{aligned}$$

where A, B and C are defined as,

$$\begin{aligned}
A :=& \beta_{\mathrm{S}}\beta_{\mathrm{D}}\Big(\beta_{\mathrm{S}}\big((l_{\mathrm{D}} + a_{\mathrm{D}})r_{\mathrm{S}} - r_{\mathrm{D}}l_{\mathrm{S}}\big) + b_{\mathrm{S}}a_{\mathrm{D}}r_{\mathrm{S}}(r_{\mathrm{S}} - l_{\mathrm{S}})\Big),\\
B :=& d_{\mathrm{D}}r_{\mathrm{S}}(l_{\mathrm{D}} + a_{\mathrm{D}})\beta_{\mathrm{S}}^2 + b_{\mathrm{S}}a_{\mathrm{D}}r_{\mathrm{S}}\beta_{\mathrm{D}}(r_{\mathrm{S}}a_{\mathrm{S}} - l_{\mathrm{S}}d_{\mathrm{S}}) + b_{\mathrm{S}}d_{\mathrm{D}}r_{\mathrm{S}}a_{\mathrm{D}}(r_{\mathrm{S}} - l_{\mathrm{S}})\beta_{\mathrm{S}}\\
&+ \Big((r_{\mathrm{S}} - d_{\mathrm{S}})\big(r_{\mathrm{D}}l_{\mathrm{S}} - (l_{\mathrm{D}} + a_{\mathrm{D}})r_{\mathrm{S}}\big) + r_{\mathrm{D}}(r_{\mathrm{S}}a_{\mathrm{S}} - l_{\mathrm{S}}d_{\mathrm{S}})\Big)\beta_{\mathrm{D}}\beta_{\mathrm{S}}.\\
C :=& -(a_{\mathrm{D}} + l_{\mathrm{D}})(r_{\mathrm{S}} - d_{\mathrm{S}})r_{\mathrm{S}}d_{\mathrm{D}}\beta_{\mathrm{S}} + (a_{\mathrm{S}}r_{\mathrm{S}} - d_{\mathrm{S}}l_{\mathrm{S}})\big(b_{\mathrm{S}}d_{\mathrm{D}}a_{\mathrm{D}}r_{\mathrm{S}} - \beta_{\mathrm{D}}r_{\mathrm{D}}(r_{\mathrm{S}} - d_{\mathrm{S}})\big).
\end{aligned}$$

Theorem 4.1 states the constraints on β_{S} and β_{D} values, under which the above steady states exist.

Theorem 4.1.

(I): E_U always exist under assumption (C5) .

(II): E_I exists if and only if infected cells are mitotic and the self-renewal rate of infected cancer stem cells is greater than their removal rate, meaning $l_{\mathrm{S}} \neq 0$ and $l_{\mathrm{D}} \neq 0$, i.e. $l_{\mathrm{S}} > a_{\mathrm{S}}$.

(III): When $a_{\mathrm{S}} < l_{\mathrm{S}}$ and $1 < \dfrac{r_{\mathrm{D}}}{a_{\mathrm{D}} + l_{\mathrm{D}}} < \dfrac{r_{\mathrm{S}}}{l_{\mathrm{S}}}$, there exists a unique interior steady state if

$$\left(\frac{a_{\mathrm{S}} r_{\mathrm{S}} - d_{\mathrm{S}} l_{\mathrm{S}}}{a_{\mathrm{D}} + l_{\mathrm{D}}}\right) \frac{b_{\mathrm{S}} d_{\mathrm{D}} a_{\mathrm{D}} r_{\mathrm{S}} - \beta_{\mathrm{D}} r_{\mathrm{D}} (r_{\mathrm{S}} - d_{\mathrm{S}})}{r_{\mathrm{S}} d_{\mathrm{D}} (r_{\mathrm{S}} - d_{\mathrm{S}})} < \beta_{\mathrm{S}} < \frac{b_{\mathrm{S}} a_{\mathrm{D}} (r_{\mathrm{S}} a_{\mathrm{S}} - l_{\mathrm{S}} d_{\mathrm{S}})}{(l_{\mathrm{S}} - a_{\mathrm{S}})(a_{\mathrm{D}} + l_{\mathrm{D}})} \tag{4.6}$$

(IV): When $l_{\mathrm{S}} = l_{\mathrm{D}} = 0$, there exists a unique interior steady state if

$$\left(\frac{a_{\mathrm{S}} r_{\mathrm{S}} - d_{\mathrm{S}} l_{\mathrm{S}}}{a_{\mathrm{D}} + l_{\mathrm{D}}}\right) \frac{b_{\mathrm{S}} d_{\mathrm{D}} a_{\mathrm{D}} r_{\mathrm{S}} - \beta_{\mathrm{D}} r_{\mathrm{D}} (r_{\mathrm{S}} - d_{\mathrm{S}})}{r_{\mathrm{S}} d_{\mathrm{D}} (r_{\mathrm{S}} - d_{\mathrm{S}})} < \beta_{\mathrm{S}} \tag{4.7}$$

See 4.7.5 for a proof of the above theorem.

Parts (III) and (IV) of the above theorem give some conditions under which we can analytically prove a unique interior steady state exists. However, our numerical simulations show that interior steady state depends only on the mitotic rate of infected cells and the rate at which stem cells become infected. Part (IV) of the above theorem gives a sufficient condition for the existence of the unique steady state on the infectivity rate of stem cells when infected cells are not mitotic. Our numerical observations suggest that when infected cells are not mitotic inequality (4.7) is the necessary and sufficient condition on β_{S} for the existence of a unique steady state. In part (III) of the above theorem, we identify a part of parameter space, in which a unique interior steady state exists when infected stem cells can survive in the absence of horizontal infection (meaning that $l_{\mathrm{S}} > a_{\mathrm{S}}$). Our numerical observation illustrates that when $l_{\mathrm{S}} > a_{\mathrm{S}}$, there exists a unique interior steady state if and only if β_{S} satisfies

inequality (4.6).

4.4 Reproduction number of cancer cells identifies treatment outcomes

The Jacobian of Model (4.2) at E_0 is

$$\begin{pmatrix} r_{\mathrm{S}} - d_{\mathrm{S}} & 0 & 0 & 0 \\ r_{\mathrm{D}} & -d_{\mathrm{D}} & 0 & 0 \\ 0 & 0 & l_{\mathrm{S}} - a_{\mathrm{S}} & 0 \\ 0 & 0 & l_{\mathrm{D}} & -a_{\mathrm{D}} \end{pmatrix}$$

Eigenvalues of the above are $r_{\mathrm{S}} - d_{\mathrm{S}}$, $l_{\mathrm{S}} - a_{\mathrm{S}}$, $-d_{\mathrm{D}}$, and $-a_{\mathrm{D}}$. According to assumption (C5) $r_{\mathrm{S}} - d_{\mathrm{S}} > 0$, therefore, the Jacobian of Model (4.2) at E_0 always has at least one positive eigenvalue. Therefore, under assumption (C5) E_0 is always unstable. Hence, our model suggests that even an oncolytic viral therapy in which cancer cells from different phenotypes are targeted with different specificity cannot eradicate the tumour. However, long term tumour shrinkage after therapy is observed when the infection spreads through the tumour cells, and the tumour becomes partially or fully infected. For the infection to invade the tumour, the basic reproduction number must be larger than one. The basic reproduction number, R_0, is defined as the expected number of newly infected cells produced by a typical infected cell when the tumour is on E_U steady state. That is the population of infected cells are rare, and the population density of uninfected tumour stem cells is $x_{\mathrm{TS}} = b_{\mathrm{S}}^{-1}(1 - d_{\mathrm{S}}/r_{\mathrm{S}})$ and the population density of uninfected fully differentiated cells is $x_{\mathrm{TD}} = x_{\mathrm{TS}} r_{\mathrm{D}}/d_{\mathrm{D}}$.

To calculate the basic reproduction number, we use the method given by Van den

Driessche and Watmough in 2002 [105]. The basic reproduction number is

$$R_0 = \frac{\mathrm{tr}(\mathscr{N}_I)}{2} + \sqrt{\left(\frac{\mathrm{tr}(\mathscr{N}_I)}{2}\right)^2 - \det(\mathscr{N}_I)}, \tag{4.8}$$

where the next generation matrix $\mathscr{N}_I$ of infected cells for Model (4.2) is

$$\mathscr{N}_I = \begin{pmatrix} \dfrac{l_{\mathrm{S}} d_{\mathrm{S}}}{a_{\mathrm{S}} r_{\mathrm{S}}} + \dfrac{x_{\mathrm{TS}} \beta_{\mathrm{S}}}{a_{\mathrm{S}}} & \dfrac{x_{\mathrm{TS}} \beta_{\mathrm{S}}}{a_{\mathrm{D}}} \\ \\ \dfrac{l_{\mathrm{D}}}{a_{\mathrm{S}}} + \dfrac{x_{\mathrm{TD}} \beta_{\mathrm{D}}}{a_{\mathrm{S}}} & \dfrac{x_{\mathrm{TD}} \beta_{\mathrm{D}}}{a_{\mathrm{D}}} \end{pmatrix} \tag{4.9}$$

See 4.7.1 for the algebraic calculations of $\mathscr{N}_I$ and basic reproduction number.

In the special case when the virus transmission is only horizontal, meaning $l_{\mathrm{S}} = l_{\mathrm{D}} = 0$, R_0 is

$$R_0 = \frac{1}{b_{\mathrm{S}}} \left(\frac{\beta_{\mathrm{S}}}{a_{\mathrm{S}}} + \frac{\beta_{\mathrm{D}}}{a_{\mathrm{D}}} \frac{r_{\mathrm{D}}}{d_{\mathrm{D}}} \right) \left(1 - \frac{d_{\mathrm{S}}}{r_{\mathrm{S}}} \right) \tag{4.10}$$

The above formula shows basic reproduction number is proportional with number of new exposures and new infections as expected. In fact, the life time of an infected CSC is $1/a_{\mathrm{S}}$ and each cancer stem cell produces $\beta_{\mathrm{S}} \frac{1}{b_{\mathrm{S}}} (1 - \frac{d_{\mathrm{S}}}{r_{\mathrm{S}}})$ infected tumour stem cells in its life time and the life time of an infected differentiated cell is $1/a_{\mathrm{D}}$ and each infected differentiated cell produces $\beta_{\mathrm{D}} \frac{1}{b_{\mathrm{S}}} (1 - \frac{d_{\mathrm{S}}}{r_{\mathrm{S}}}) \frac{r_{\mathrm{D}}}{d_{\mathrm{D}}}$ infected differentiated cells in its life time, so each infected cell in its life time produces R_0 infected individuals.

As we mentioned above, we are interested in the case that $R_0 > 1$. As per equation (4.8), it is tedious to calculate R_0, but next lemma gives the constraint in the parameter space under which $R_0 > 1$.

Lemma 4.2. $R_0 > 1$ if and only if

$$\beta_{\mathrm{S}} > \left(\frac{b_{\mathrm{S}} a_{\mathrm{D}}}{r_{\mathrm{S}} - d_{\mathrm{S}}} - \beta_{\mathrm{D}} \frac{r_{\mathrm{D}}}{r_{\mathrm{S}} d_{\mathrm{D}}}\right) \frac{r_{\mathrm{S}} a_{\mathrm{S}} - l_{\mathrm{S}} d_{\mathrm{S}}}{l_{\mathrm{D}} + a_{\mathrm{D}}} \tag{4.11}$$

See 4.7.2 for a proof of the above Lemma 4.2.

It is essential to know that once most of the tumour cells become infected and the population of uninfected cancer cells are rare, is it possible for the population of uninfected cancer cells to regrow again and invade the tumour partially or fully. To know this, we need to calculate the reproduction number of uninfected cancer cells. The reproduction number of an uninfected cancer cell is the number of new uninfected cancer cells that an uninfected cancer cell produces in its lifetime when Model (4.2) is in E_I steady state. Let R_U denote the reproduction number of uninfected cancer cells, so

$$R_U = \left(\frac{r_{\mathrm{S}}}{d_{\mathrm{S}} + \beta_{\mathrm{S}}(y_{\mathrm{IS}} + y_{\mathrm{ID}})}\right) \frac{a_{\mathrm{S}}}{l_{\mathrm{S}}}. \tag{4.12}$$

R_U is the maximum of absolute values of eigenvalues of next generation matrix $\mathscr{N}_U$ of uninfected cancer cells for Model (4.2). $\mathscr{N}_U$ is given by

$$\mathscr{N}_U = \begin{bmatrix} \left(\dfrac{r_{\mathrm{S}}}{d_{\mathrm{S}} + \beta_{\mathrm{S}}(y_{IS} + y_{ID})}\right) \dfrac{a_{\mathrm{S}}}{l_{\mathrm{S}}} & 0 \\ \dfrac{r_{\mathrm{D}}}{d_{\mathrm{S}} + \beta_{\mathrm{S}}(y_{IS} + y_{ID})} & 0 \end{bmatrix} \tag{4.13}$$

See 4.7.3 for details of algebraic calculations of $\mathscr{N}_U$.

Note that R_U is not defined when infected cells are not mitotic. R_U only can be defined when the steady state in which tumour cells are fully infected is possible. As we explained before steady state E_I only exists if infected cells are mitotic, i.e. $l_{\mathrm{S}} \neq 0$ and $l_{\mathrm{D}} \neq 0$, and the net growth rate of infected cancer stem cells is positive in the absence of horizontal infection, i.e. $l_{\mathrm{S}} > a_{\mathrm{S}}$.

We are interested in the case that $R_U < 1$, meaning that when all the tumour cells are infected, and no longer uninfected cells can outgrow the infected ones. Eq. (4.12) shows $R_U < 1$ if and only if

$$\beta_{\mathrm{S}} > \frac{b_{\mathrm{S}} a_{\mathrm{D}}(r_{\mathrm{S}} a_{\mathrm{S}} - l_{\mathrm{S}} d_{\mathrm{S}})}{(l_{\mathrm{S}} - a_{\mathrm{S}})(a_{\mathrm{D}} + l_{\mathrm{D}})}. \tag{4.14}$$

Remark 4.3. Notice from Lemma 4.2 and equation (4.14) we can rewrite the conditions for the existence of interior steady state in the terms of R_0 and R_U as follows:

1. when $a_{\mathrm{S}} < l_{\mathrm{S}}$ and $1 < \dfrac{r_{\mathrm{D}}}{a_{\mathrm{D}} + l_{\mathrm{D}}} < \dfrac{r_{\mathrm{S}}}{l_{\mathrm{S}}}$, there exists a unique interior steady state if $R_0 > 1$ and $R_U > 1$;

2. when $l_{\mathrm{S}} = l_{\mathrm{D}} = 0$, there exists a unique interior steady state if $R_0 > 1$.

Outcomes of the treatment are as follows.

(I) **Treatment failure:** Infection is weakly transmissible such that it cannot invade the tumour, and treatment fails. This occurs when $R_0 < 1$. Figure 4.4 is a heat map of tumour size post-therapy as a function of $\beta_{\mathrm{S}}, \beta_{\mathrm{D}}$. As this figure indicates, the biggest tumour size post-therapy occurs when $R_0 < 1$. The figure suggests that if the rate at which stem cells become infected, β_{S} and the rate at which fully differentiated cells become infected β_{D} belong to the area labelled by $R_0 < 1$, treatment fails. In this case, either there will not be a tumour shrinkage, or there may be a small tumour shrinkage at the beginning of the therapy. However, the tumour eventually follows the same dynamics as in the absence of the therapy. In this case, post-therapy tumour size will be same as tumour size in E_U steady state, i.e.

$$x_{\mathrm{TS}} + x_{\mathrm{TD}} = \frac{(r_{\mathrm{S}} - d_{\mathrm{S}})(d_{\mathrm{D}} + r_{\mathrm{D}})}{r_{\mathrm{S}} b_{\mathrm{S}} d_{\mathrm{D}}}.$$

(II) **Partial success:** Infection partially invades the tumour, some tumour cells become infected, and the size of the tumour gets considerably smaller. When either $R_0 > 1$, $R_U > 1$, and $l_{\mathrm{S}} > a_{\mathrm{S}}$ or $R_0 > 1$ and $l_{\mathrm{S}} < a_{\mathrm{S}}$, our numerical simulations recommend that there exists a unique interior steady state that is globally stable, i.e. post-therapy eventually tumour size will be $x_{\mathrm{S}}^*+x_{\mathrm{D}}^*+y_{\mathrm{S}}^*+y_{\mathrm{D}}^*$ and this result is not sensitive to initial size of tumour. The area corresponding to $R_0 > 1$ and $R_U > 1$ in Figure 4.4 is the area between the two lines. If the net growth rate (the self renewal rate minus removal rate) of infected cancer stem cells is positive, then partial infection occurs when $R_0 > 1$ and $R_U > 1$. This scenario in $\beta_{\mathrm{D}} - \beta_{\mathrm{S}}$ parameter space is corresponding to area between the two lines in Figure 4.4, the dashed line (lower line) is corresponding to $R_0 = 1$ and the solid line (upper line) is corresponding to $R_U = 1$. Notice that as we mentioned before, when infected cells are not mitotic $l_{\mathrm{S}} = l_{\mathrm{D}} = 0$ or when infected cells are mitotic but infected cancer stem cells' net growth rate is negative (i.e. $l_{\mathrm{S}} < a_{\mathrm{S}}$), R_U cannot be defined. In this scenario, partial infection occurs when $R_0 > 1$. When $l_{\mathrm{S}} - a_{\mathrm{S}}$ tends to zero, the probability that the tumour becomes fully infected tends to zero. In Figure 4.4 as $l_{\mathrm{S}} - a_{\mathrm{S}}$ tends to zero, the line $R_U = 1$ tends to infinity and remains there.

(III) **Success:** Infection completely invades the tumour. This is equivalent to the case when $R_U \leq 1$. As we mentioned before, 100% infection prevalence is only possible when net growth rate of infected cancer stem cell is positive, i.e. $l_{\mathrm{S}} > a_{\mathrm{S}}$. When $l_{\mathrm{S}} > a_{\mathrm{S}}$ and $R_0 > 1$, as Figure 4.4 illustrates by increase in β_{S} value, tumour size is reduced and the lowest tumour size is obtained when $\beta_S = \frac{a_{\mathrm{D}} b_{\mathrm{S}}(r_{\mathrm{S}} a_{\mathrm{S}} - l_{\mathrm{S}} d_{\mathrm{S}})}{(l_{\mathrm{S}} - a_{\mathrm{S}})(a_{\mathrm{D}} + l_{\mathrm{D}})}$ (which corresponds to $R_U = 1$). Once β_{S} reaches the value $\frac{a_{\mathrm{D}} b_{\mathrm{S}}(r_{\mathrm{S}} a_{\mathrm{S}} - l_{\mathrm{S}} d_{\mathrm{S}})}{(l_{\mathrm{S}} - a_{\mathrm{S}})(a_{\mathrm{D}} + l_{\mathrm{D}})}$, increases in β_{S} can no longer impact the tumour size. Since when $\beta_{\mathrm{S}} \geq \frac{a_{\mathrm{D}} b_{\mathrm{S}}(r_{\mathrm{S}} a_{\mathrm{S}} - l_{\mathrm{S}} d_{\mathrm{S}})}{(l_{\mathrm{S}} - a_{\mathrm{S}})(a_{\mathrm{D}} + l_{\mathrm{D}})}$ the tumour size post therapy is the same as tumour size at E_I steady state, the tumour size post therapy is $y_{\mathrm{IS}} + y_{\mathrm{ID}} = \frac{(l_{\mathrm{S}} - a_{\mathrm{S}})(a_{\mathrm{D}} + l_{\mathrm{D}})}{l_{\mathrm{S}} b_{\mathrm{S}} a_{\mathrm{D}}}$,

which is independent of values of β_S and β_D.

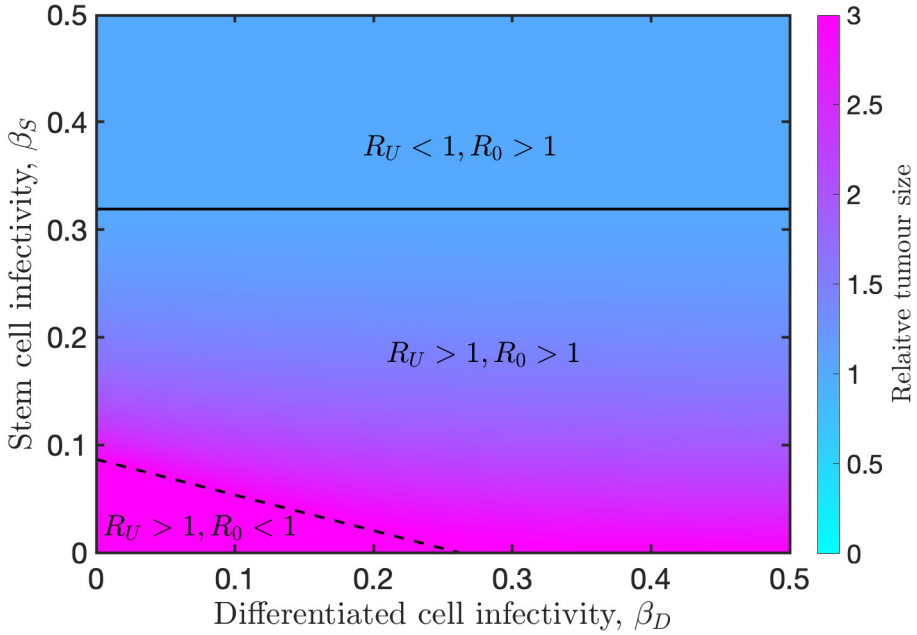

Figure 4.4: **Heat map of tumour burden post therapy as a function of $\boldsymbol{\beta_S, \beta_D}$.** Tumour steady state is plotted as a function of β_D and β_S. This is superimposed with the regions in $(\beta_\mathrm{S}, \beta_\mathrm{D})$ plane that are separated by lines $R_0 = 1$ and $R_U = 1$ where R_0 is the basic reproduction number of the virus Eq.(4.8) and R_U is the reproduction number of uninfected cancer cells Eq.(4.12). The dashed line represents $R_0 = 1$. The maximum tumour size under treatment occurs when $R_0 < 1$. The solid line represents $R_U = 1$. Tumour size reduces as β_S increases, and it becomes minimum when $R_U = 1$. In the area labelled as $R_U < 1$, changes in β_S or β_D does not affect the tumour size. This simulation corresponds to a positive net growth rate (self-renewal rate - removal rate) of infected cancer stem cells. When the net growth rate of infected cancer stem cells tends to zero, the line $R_U = 1$ tends to infinity. (Model parameters are: $r_\mathrm{S} = 0.5, r_\mathrm{D} = 2r_\mathrm{S}, d_\mathrm{S} = 0.3, d_\mathrm{D} = 2r_\mathrm{S}, l_\mathrm{S} = 0.5, l_\mathrm{D} = 2l_\mathrm{S}, a_\mathrm{S} = d_\mathrm{S} + 0.1, a_\mathrm{D} = d_\mathrm{D} + 0.1, b_\mathrm{S} = 1, b_\mathrm{D} = 0.$)

4.5 Optimal stem cell specificity

One of the main questions in engineering a virus is when stem cell targeting has an advantage over random or differentiated cell targeting. When infected cells are mitotic and the net growth rate of infected cancer stem cells is positive, as Figure 4.4 suggests, the minimum tumour size is obtained above the line $R_U \leq 1$, which corresponds to $\beta_\mathrm{S} \geq \frac{b_\mathrm{S} a_\mathrm{D}(r_\mathrm{S} a_\mathrm{S} - l_\mathrm{S} d_\mathrm{S})}{(l_\mathrm{S} - a_\mathrm{S})(a_\mathrm{D} + l_\mathrm{D})}$. This result is not sensitive to the value of β_D

which suggests that when the net growth rate of infected cancer stem cells is positive, the optimal result is obtained by perfect stem cell targeting, in other words, by only targeting stem cells. As equation (4.12) indicates, when the net growth rate of infected cancer stem cells is negative or zero, R_U is not defined, and only partial infection is possible. In this case, Figure 4.4 does not provide a clear answer about the optimal stem cell specificity and how average infectivity may affect that. To respond to these concerns here we re-parametrize $\beta_{\mathrm{S}} = p\beta$, and $\beta_{\mathrm{D}} = (1-p)\beta$, where $0 \leq p \leq 1$ is stem-like specificity and β is an average infectivity. If $p \neq (1/2)$, phenotypic heterogeneity is taken into account and if $p = (1/2)$, phenotypic heterogeneity is not considered and cells are randomly targeted. If $p > (1/2)$ then the engineered oncolytic virus has a higher tendency to infect a stem cell over a differentiated cell. When $p < (1/2)$, the oncolytic virus preferably targets differentiated cells over stem cells. When $p = 1$, only stem cells are targeted and when $p = 0$, only differentiated cells are targeted.

In Figure 4.5 the total tumour size in steady state as a function of stem cell specificity p for different values of β are plotted. In this figure, for a given β value, the minimum steady state tumour size as p varies is denoted by a pink dot. We call this value of p for which the steady state tumour size is minimum the optimal specificity for the given infectivity rate, and we denote it by $p^{\star}_{\beta}$. The optimal specificity depends both on infectivity rate and the type of infected cells (mitotic or non-mitotic). Hence, we consider two separate scenarios: 1) non-mitotic infected cells, i.e. $l_{\mathrm{S,D}} = 0$, Figure 4.5(a) and 2) infected cells are mitotic, but the net growth rate of infected stem cells are negative, i.e. $l_{\mathrm{S,D}} \neq 0$ and $l_{\mathrm{S}} < a_{\mathrm{S}}$, Figure 4.5(b). Notice that, in both Figure 4.5(a) and (b) the net growth rate of infected stem cells are negative. Figure 4.5 recommends that in both scenarios (mitotic and nonmitotic infected cells), as the average infectivity rate β increases, the minimum steady state tumour size decreases.

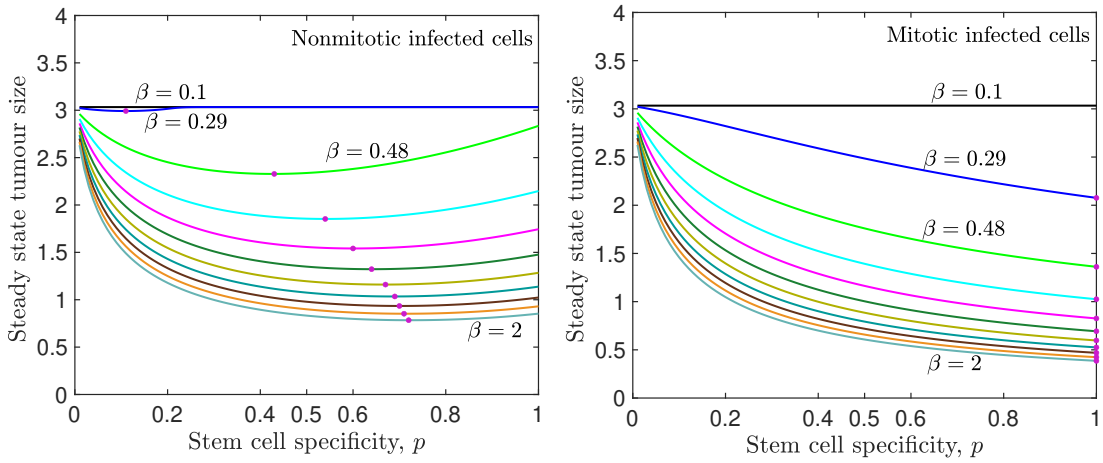

(a) (b)

Figure 4.5: **Perfect stem cell targeting is optimal when infected cells are mitotic; (a) non-mitotic infected cells (b) mitotic infected cells.** The specificity, p, is defined by $\beta_{\mathrm{S}} = p\beta, \beta_{\mathrm{D}} = (1-p)\beta$. Where $\beta/2$ is overall infectivity for uniform system ($p = 1/2$), $\beta_{\mathrm{S}} = \beta_{\mathrm{D}}$. Plots are done for different values of $\beta = 0.1, \ldots, 2$, with the step size of 0.19. for small infectivities, tumour control (weakly) responds to variations in virus-stem cell specificity. Other model parameters are, $r_{\mathrm{S}} = 2, r_{\mathrm{D}} = 4, d_{\mathrm{S}} = 0.3, d_{\mathrm{D}} = 0.6, a_{\mathrm{S}} = d_{\mathrm{S}} + 0.01, a_{\mathrm{D}} = d_{\mathrm{D}} + 0.01, b_{\mathrm{S}} = 1, b_{\mathrm{D}} = 0$. For non-replicating virus $l_{\mathrm{S}} = l_{\mathrm{D}} = 0$ and for replicating virus $l_{\mathrm{S}} = 0.25$ and $l_{\mathrm{D}} = 0.5$.

When the infected cells are non-mitotic, as Figure 4.5(a) represents for lower β values, lower p values are preferred. When β values are low and p values are high, the treatment fails, and the steady state tumour burden is the same as the one in the absence of therapy. As infectivity increases, the optimal p value crosses $p = 1/2$, and for a regime of high infectivities, stem cell targeting is, in fact, a preferred method. For higher values of β, the minimum steady state tumour size is not very sensitive to changes in p and for a wide range of p values, treatment outcomes seem similar. Interestingly for the range of β used here, $0.1 \leq \beta \leq 2$, the optimal p, $p^{\star}_{\beta}$, is less than unity. This means that full stem cell targeting is not the optimal strategy (for model parameters used in this simulation, see caption of Figure 4.5).

The above behaviour changes as we introduce non-zero values of $l_{\mathrm{S,D}}$. When infected cells are mitotic the minimum steady state tumour size occurs for perfect stem cell

targeting. As Figure 4.5(b) shows $p \sim 0$ has almost no effect on tumour burden (no shrinking) and tumour size is optimal at $p \sim 1$. In this figure, the effect of increase in specificity for large infectivity, say $\beta = 2$, is quite strong. In this figure $l_{\mathrm{S}} = 0.25$ and $l_{\mathrm{D}} = \alpha l_{\mathrm{S}}$, $d_{\mathrm{S}} = 0.3$, and $a_{\mathrm{S}} = d_{\mathrm{S}} + 0.01$ (for the rest of parameters see the caption), notice that $l_{\mathrm{S}} < a_{\mathrm{S}}$, therefore, the net growth rate of infected stem cells are negative. Our numerical simulations suggest that the stem cell fraction increases from the beginning of the therapy if the therapy starts when the tumour size is nearly equal to the tumour size at E_U steady state. The same is true under perfect stem cell targeting. In the above paragraph we mentioned that when infected cells self-renewal rate and differentiation rate are nonzero, the minimum tumour size is obtained by the perfect stem cell targeting. Under perfect stem cell targeting, when β_{S} is chosen in the way that $R_0 > 1$, if the therapy starts when tumour size is near E_U steady state always the tumour size, stem cell density and differentiated cell density are reduced. However, the stem cell fraction increases, regardless of the mitotic rate of infected cells and the increase amount in the stem cell fraction depends on the mitotic rate of infected cells; when mitotic rate of infected cell increases, more tumour shrinkage is obtained, but stem cell fraction will be more (see Figure 4.6 for an illustration).

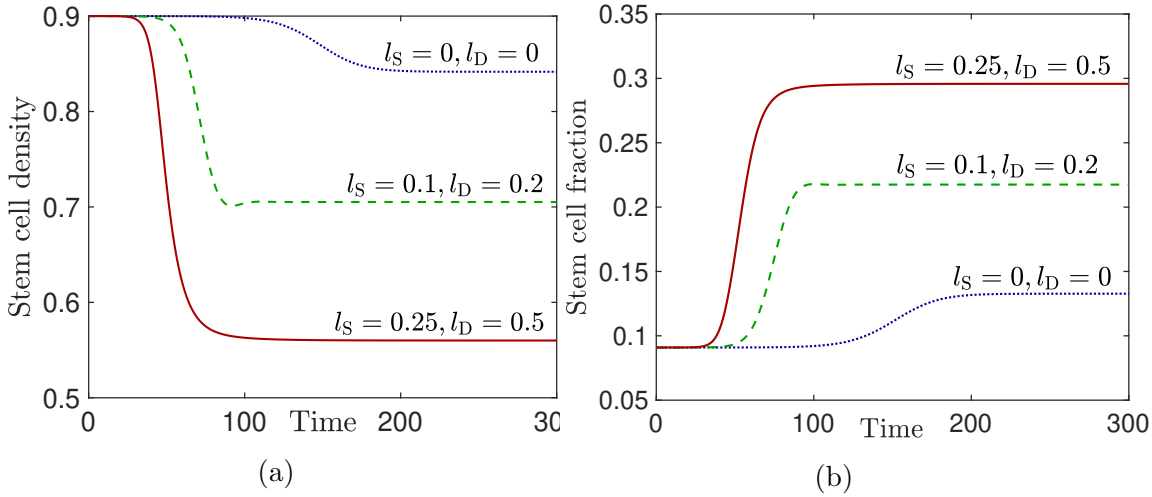

Figure 4.6: **Stem cell fraction increases even under perfect stem cell targeting; (a) Stem cell density (b) Stem cell fraction.** It is assumed that an oncolytic virus that only targets stem cells is administrated. Hence, stem cell specificity $p = 1$. Three different scenarios are considered; 1- The dotted curve corresponds to nonmitotic infected cells, $l_S = 0, l_D = 0$. 2- The dashed curve corresponds to the case where infected cells are mitotic, and the net growth rate of infected cancer stem cells is negative ($l_S < a_S + d_S$) $l_S = 0.1$ and $l_D = 0.2$. 3- The solid curve corresponds to the case where infected cells are mitotic, and the net growth rate of infected cancer stem cells is positive ($l_S > a_S + d_S$) $l_S = 0.25, l_D = 0.5$. Plot (a) demonstrates that when the self-renewal rate and the differentiation rate of infected cancer cell increases, the stem cell density under therapy is reduced. Plot (b) illustrates when the self-renewal rate and the differentiation rate of infected cancer cell increases stem cell fraction increases. Other model parameters are $r_S = 1, r_D = 2, d_S = 0.1, d_D = 0.2, a_S = d_S + 0.01, a_D = d_D + 0.01, \beta_S = p\beta, \beta_D = (1-p)\beta, b_S = 1, b_D = 0, \beta = 0.5$.

4.6 Discussion

Intratumoural heterogeneity is known to be a major cause of tumour relapse, recurrence and failure of many conventional therapies [76, 78, 102]. In fact, most conventional therapies kill the differentiated cells and fail in eliminating cancer stem cells. Cancer stem cells, due to properties such as self-renewal ability and quiescence, are resistant to chemotherapy and radiotherapy [89, 98]. Oncolytic viruses are capable of targeting both quiescent and non-quiescent cancer stem cells and suppressing the growth of cancer stem cells [4, 13, 121]. The complete eradication of cancer stem

cells is observed in some in vitro studies of targeting cancer stem cells with oncolytic viruses [8,29]. However, the complete eradication of cancer stem cells is not reported in most in vivo models of targeting cancer stem cells with oncolytic viruses [6,8]. In this chapter, our primary goal was to propose a simple mathematical model to analyze the efficiency of targeting cancer stem cells with oncolytic viruses. To do this, we disregarded some complexities related to hierarchical tumour structure, and we also considered some hypotheses related to oncolytic virotherapy, assumptions (C1)–(C6). Our promising yet simple model agrees with the results of in-vitro and in-vivo studies of targeting cancer stem cells with oncolytic viruses in that oncolytic viruses can infect all the tumour cells regardless of their phenotypic heterogeneity, reducing the density of both cancer stem cells and differentiated cells. In addition, it agrees with most of the in-vivo studies in the observation that oncolytic viruses cannot eradicate cancer stem cells (see section 4.4).

One of the most important results of this chapter is identifying when targeting stem cells is advantageous over random targeting; our analysis shows that this depends strongly on the mitotic capability of cancer stem cells (see section 4.5). If, after becoming infected, cancer stem cells cannot self-renew or differentiate, then targeting stem cells with oncolytic viruses does not improve the efficiency of the therapy (see Figures 4.4 and 4.5). When cancer stem cells are nonmitotic, higher specificity in targeting cancer stem cells does not enhance the treatment outcome. In fact, in this scenario, average infectivity is more important. Our numerical simulations illustrate that when average infectivity increases, more tumour shrinkage is obtained under treatment (see Figures 4.3, 4.4 and 4.5). When cancer stem cells are mitotic, meaning that they can self-renew and differentiate, targeting cancer stem cells is preferred over random targeting or only targeting differentiated cells. In fact, when cancer stem cells are mitotic, the optimal tumour size by therapy is obtained under perfect stem cell targeting (see Figure 4.5 for an illustration). Moreover, when the

net growth rate of infected cancer stem cells is positive, we obtain optimal infectivity rate of cancer stem cells at which optimal tumour size under therapy is obtained (see Theorem 4.1 and inequality (4.14)).

Our numerical simulations suggest that under Model (4.2), the stem cell fraction always increases (see Figures 4.3 and 4.6) from the beginning of the therapy if the therapy starts when the tumour size is nearly equal to the tumour size at E_U steady state (see Eq. (4.3) for the formulation of E_U steady state).

The success of oncolytic viral therapy depends heavily on the extent to which infection can invade the tumour. Hence, the basic reproduction number R_0 is a valuable marker to know when virotherapy starts to work. We calculated R_0, and treatment starts to work when R_0 is bigger than one: this also gives a linear constraint on the infectivity rates of cancer stem cells and cancer differentiated cells, meaning it formulates to which extent cancer stem cells and cancer differentiated cells must be targeted to see long term tumour shrinkage (see lemma 4.2).

The tumour microenvironment and hierarchical structure within a tumour are very complex. The hierarchical structure starts from a stem cell at the top of the hierarchy and ends in the last row of fully differentiated cells. Stem cells may self-renew or differentiate symmetrically or asymmetrically. Here, for simplicity, we only considered self-renewal and symmetric differentiation. Our model can be extended to a full hierarchical model such as the one discussed in Williams et al. [113] to consider all types of differentiation.

Another assumption ((C2)) that we derived our model under is that the rate of production of virus per infected stem cell and per infected differentiated cell is the same. However, in practice, it may be different. The result of this chapter can also be derived if this assumption is relaxed; just the formulation will be more complicated.

4.7 Appendix

4.7.1 Basic Reproduction Number

Here we use the method given by van den Driessche and Watmough in [105] to calculate basic reproduction number R_0.

Recall basic reproduction number is the number of new infected cells that an infected cell produces in its life time when almost all the cells are susceptible to infection. Therefore, when calculating basic reproduction number we are only interested in dynamics of cancer cells in infected compartments. From Model (4.2),

$$(\dot{y_{\mathrm{S}}}, \dot{y_{\mathrm{D}}}) \quad = \quad \mathscr{F}_I - \mathscr{V}_I,$$

where $\mathscr{F}_I$ refers to appearance of new infections and $\mathscr{V}_I$ refers to removal of infected cells . Therefore,

$$\begin{aligned}
\mathscr{F}_I =& \Big(l_{\mathrm{S}} y_{\mathrm{S}}\big(1 - bs(x_{\mathrm{S}} + y_{\mathrm{S}})\big) + \beta_{\mathrm{S}} x_{\mathrm{S}}\big(y_{\mathrm{S}} + y_{\mathrm{D}}\big), l_{\mathrm{D}} y_{\mathrm{S}} + \beta_{\mathrm{D}} x_{\mathrm{D}}\big(y_{\mathrm{S}} + y_{\mathrm{D}}\big)\Big), \\
\mathscr{V}_I =& \Big(a_{\mathrm{S}} y_{\mathrm{S}}, a_{\mathrm{D}} y_{\mathrm{D}}\Big).
\end{aligned}$$

To calculate the next generation matrix $\mathscr{N}_I$, we should calculate the Jacobians of $\mathscr{F}_I$ and $\mathscr{V}_I$, with respect to y_{S} and y_{D} at infection free steady state $E_U = (x_{TS}, x_{TD}, 0, 0)$ (in other words the steady state in which almost all the cells are susceptible to infection).

$$F_I = \frac{\partial \mathscr{F}_I}{\partial(y_{\mathrm{S}}, y_{\mathrm{D}})} = \begin{bmatrix} l_{\mathrm{S}} \dfrac{d_{\mathrm{S}}}{r_{\mathrm{S}}} + \beta_{\mathrm{S}} x_{TS} & \beta_{\mathrm{S}} x_{TS} \\ l_{\mathrm{D}} + \beta_{\mathrm{D}} x_{TD} & \beta_{\mathrm{D}} x_{TD} \end{bmatrix}, \quad V_I = \frac{\partial \mathscr{V}_I}{\partial(y_{\mathrm{S}}, y_{\mathrm{D}})} = \begin{bmatrix} a_{\mathrm{S}} & 0 \\ 0 & a_{\mathrm{D}} \end{bmatrix}.$$

$\mathscr{N}_I = F_I V_I^{-1}$, hence,

$$\mathscr{N}_I = \begin{bmatrix} \frac{l_{\mathrm{S}}}{a_{\mathrm{S}}}\frac{d_{\mathrm{S}}}{r_{\mathrm{S}}} + \frac{\beta_{\mathrm{S}} x_{TS}}{a_{\mathrm{S}}} & \frac{\beta_{\mathrm{S}} x_{TS}}{a_{\mathrm{D}}} \\ \frac{l_{\mathrm{D}}}{a_{\mathrm{S}}} + \frac{\beta_{\mathrm{D}} x_{TD}}{a_{\mathrm{S}}} & \frac{\beta_{\mathrm{D}} x_{TD}}{a_{\mathrm{D}}} \end{bmatrix}$$

The basic reproduction number is the spectral radius of $\mathscr{N}_I$. The spectral radius of a square matrix is the maximum of absolute values of its eigenvalues. Since $\mathscr{N}_I$ is a matrix with positive entries according to Perron-Forbenius theorem [79], the spectral radius of $\mathscr{N}_I$ is one of its eigenvalues. The eigenvalues of $\mathscr{N}_I$ are roots of quadratic $\lambda^2 - \mathrm{tr}(\mathscr{N}_{\mathrm{I}})\lambda + \det(\mathscr{N}_{\mathrm{I}})$. Since $\mathrm{tr}(\mathscr{N}_I) > 0$, the eigenvalue of $\mathscr{N}_I$ with the biggest magnitude is the following.

$$R_0 = \frac{\mathrm{tr}(\mathscr{N}_I)}{2} + \sqrt{(\frac{\mathrm{tr}(\mathscr{N}_I)}{2})^2 - \det(\mathscr{N}_I)}. \tag{4.15}$$

4.7.2 Proof of Lemma 4.2

From Eq. (4.15) $R_0 > 1$ if and only if

$$\sqrt{\left(\frac{\mathrm{tr}(\mathscr{N}_I)}{2}\right)^2 - \det(\mathscr{N}_I)} \geq 1 - \frac{\mathrm{tr}(\mathscr{N}_I)}{2},$$

If $2 \leq \mathrm{tr}(\mathscr{N}_I)$, then the above inequality is always true, meaning that $R_0 \geq 1$. If $\mathrm{tr}(\mathscr{N}_I) < 2$, then

$$\left(\frac{\mathrm{tr}(\mathscr{N}_I)}{2}\right)^2 - \det(\mathscr{N}_I) \geq (1 - \frac{\mathrm{tr}(\mathscr{N}_I)}{2})^2.$$

After simplification the above inequality is equivalent to

$$1 + \det(\mathscr{N}_I) - \mathrm{tr}(\mathscr{N}_I) \leq 0.$$

Since,

$$\det(\mathscr{N}_I) = \frac{(r_S - d_S)(\beta_D l_S d_S r_D - \beta_S l_D d_D r_S)}{b_S d_D a_D a_S r_S^2},$$
$$\mathrm{tr}(\mathscr{N}_I) = \frac{d_S l_S}{a_S r_S} + \frac{r_S - d_S}{b_S r_S}\left(\frac{\beta_S}{a_S} + \frac{\beta_D r_D}{a_D d_D}\right),$$

after simplification the above inequality turns to

$$\beta_S > \frac{(a_D b_S d_D r_S - \beta_D r_D (r_S - d_S))(a_S r_S - d_S l_S)}{d_D r_S (r_S - d_S)(l_D + a_D)}$$

Let $L_1 : \beta_S = \dfrac{a_D b_S}{r_S - d_S}\dfrac{(a_S r_S - d_S l_S)}{(l_D + a_D)} - \beta_D \dfrac{r_D}{d_D r_S}\dfrac{(a_S r_S - d_S l_S)}{(l_D + a_D)}$

Notice $\mathrm{tr}(\mathscr{N}_I) > 2$ if and only if

$$\beta_S > \frac{b_S d_D (2a_S r_S - d_S l_S) a_D - \beta_D (r_S - d_S) r_D a_S}{a_D d_D (r_S - d_S)}$$

Let $L_2 : \beta_S = \dfrac{b_S(2a_S r_S - d_S l_S)}{(r_S - d_S)} - \beta_D \dfrac{r_D a_S}{a_D d_D}$.

Line l_2 in β_D-β_S plane is always above of line l_1, as shown below.

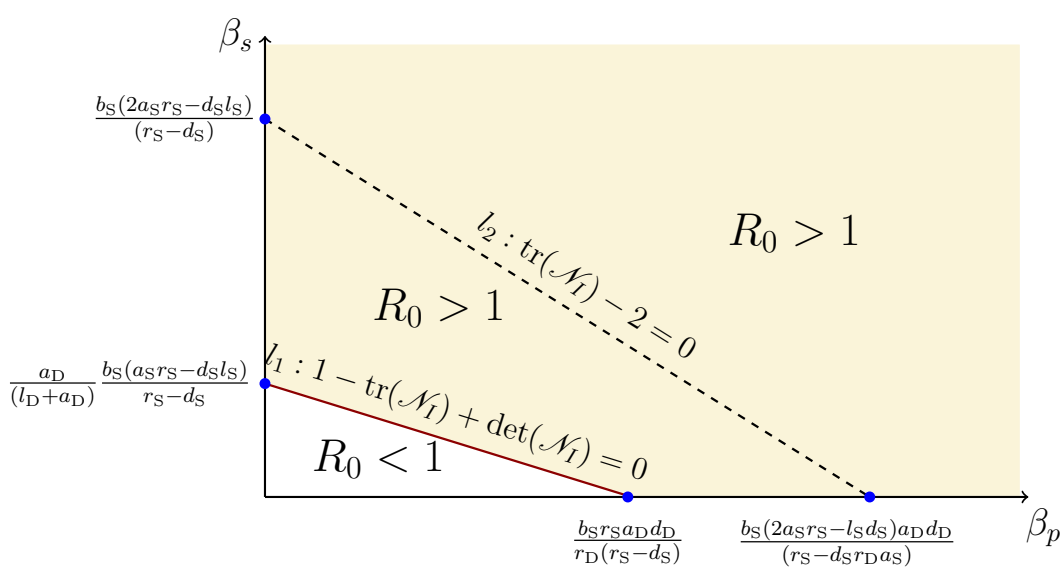

Because $\frac{b_S(2a_S r_S - d_S l_S)}{r_S - d_S} > \frac{a_D b_S}{r_S - d_S}\frac{(a_S r_S - d_S l_S)}{l_D + a_D}$ and $\frac{b_S d_D a_D r_S}{r_D(r_S - d_S)} < \frac{b_S(2a_S r_S - l_S d_S)a_D d_D}{r_S - d_S r_D a_S}$, therefore, line l_2 is always above of line l_1. Therefore, as shown in the above figure, $R_0 - 1$ only is zero along the line l_1. As shown in the above figure $R_0 > 1$ if and only if

$$\beta_S > \frac{(a_S r_S - d_S l_S)(a_D b_S d_D r_S - \beta_D r_D(r_S - d_S))}{d_D r_S(r_S - d_S)(l_D + a_D)}$$

4.7.3 Reproduction number of uninfected cancer cells

Similar to section 4.7.1 we use the method given by van den Driessche and Watmough in [105] to calculate reproduction number R_U of uninfected cancer cells.

Recall reproduction number of uninfected cancer cells are the number of new uninfected cancer cells that an uninfected cancer cell produces during its life time when almost all the tumour cells are already infected. Hence, we only consider the dynamics on the target space, meaning $x_S - x_D$ plane. We rewrite the model as follows

$$(\dot{x_S}, \dot{x_D}) \quad = \quad \mathscr{F}_U - \mathscr{V}_U,$$

where $\mathscr{F}_U$ refers to growth in population of uninfected cancer cells and $\mathscr{V}_U$ refers to removal of cells from uninfected cells' compartments. Thus,

$$\mathscr{F}_U = \big(r_S x_S\big(1 - b_S(x_S + y_S)\big), r_D x_S\big),$$

$$\mathscr{V}_U = (d_S x_S + \beta_S x_S(y_S + y_D), d_D x_D + \beta_D x_D(y_S + y_D)).$$

Next Jacobians of $\mathscr{F}_U$ and $\mathscr{V}_U$ with respect to x_S and x_D are calculated at 100%

infection prevalence steady state $(0, 0, y_{IS}, y_{ID})$.

$$F_U = \frac{\partial \mathscr{F}_U}{\partial(x_{\mathrm{S}}, x_{\mathrm{D}})} = \begin{bmatrix} r_{\mathrm{S}}\dfrac{a_{\mathrm{S}}}{l_{\mathrm{S}}} & 0 \\ r_{\mathrm{D}} & 0 \end{bmatrix}$$

$$V_U = \frac{\partial \mathscr{V}_U}{\partial(x_{\mathrm{S}}, x_{\mathrm{D}})} = \begin{bmatrix} d_{\mathrm{S}} + \beta_{\mathrm{S}}(y_{IS} + y_{ID}) & 0 \\ 0 & d_{\mathrm{D}} + \beta_{\mathrm{D}}(y_{IS} + y_{ID}) \end{bmatrix}.$$

The next generation matrix $\mathscr{N}_U$ of uninfected cells is given by $\mathscr{N}_U = F_U(V_U)^{-1}$, so

$$\mathscr{N}_U = \begin{bmatrix} \left(\dfrac{r_{\mathrm{S}}}{d_{\mathrm{S}} + \beta_{\mathrm{S}}(y_{IS} + y_{ID})}\right)\dfrac{a_{\mathrm{S}}}{l_{\mathrm{S}}} & 0 \\ \dfrac{r_{\mathrm{D}}}{d_{\mathrm{S}} + \beta_{\mathrm{S}}(y_{IS} + y_{ID})} & 0 \end{bmatrix}$$

R_U is the spectral radius of $\mathscr{N}_U$. It is trivial that eigenvalues of $\mathscr{N}_U$ are 0 and $\left(\dfrac{r_{\mathrm{S}}}{d_{\mathrm{S}} + \beta_{\mathrm{S}}(y_{IS} + y_{ID})}\right)\dfrac{a_{\mathrm{S}}}{l_{\mathrm{S}}}$. Therefore,

$$R_U = \left(\frac{r_{\mathrm{S}}}{d_{\mathrm{S}} + \beta_{\mathrm{S}}(y_{IS} + y_{ID})}\right)\frac{a_{\mathrm{S}}}{l_{\mathrm{S}}}. \tag{4.16}$$

4.7.4 Calculation of interior steady state

Let $E_p = (x_{\mathrm{S}}^*, x_{\mathrm{D}}^*, y_{\mathrm{S}}^*, y_{\mathrm{D}}^*)$ be the interior steady state. Hence,

$$\begin{aligned} r_{\mathrm{S}}\big(1 - b_{\mathrm{S}}(x_{\mathrm{S}}^* + y_{\mathrm{S}}^*)\big) - d_{\mathrm{S}} - \beta_{\mathrm{S}}(y_{\mathrm{S}}^* + y_{\mathrm{D}}^*) &= 0 \\ r_{\mathrm{D}}x_{\mathrm{S}}^*\big(1 - b_{\mathrm{D}}(x_{\mathrm{D}}^* + y_{\mathrm{D}}^*)\big) - d_{\mathrm{D}}x_{\mathrm{D}}^* - \beta_{\mathrm{D}}x_{\mathrm{D}}^*(y_{\mathrm{S}}^* + y_{\mathrm{D}}^*) &= 0, \\ l_{\mathrm{S}}y_{\mathrm{S}}^*\big(1 - b_{\mathrm{S}}(x_{\mathrm{S}}^* + y_{\mathrm{S}}^*)\big) - a_{\mathrm{S}}y_{\mathrm{S}}^* + \beta_{\mathrm{S}}x_{\mathrm{S}}^*(y_{\mathrm{S}}^* + y_{\mathrm{D}}^*) &= 0, \\ l_{\mathrm{D}}y_{\mathrm{S}}^*\big(1 - b_{\mathrm{D}}(x_{\mathrm{D}}^* + y_{\mathrm{D}}^*)\big) - a_{\mathrm{D}}y_{\mathrm{D}}^* + \beta_{\mathrm{D}}x_{\mathrm{D}}^*(y_{\mathrm{S}}^* + y_{\mathrm{D}}^*) &= 0. \end{aligned}$$

According to assumption (C3) $b_{\mathrm{D}} = 0$. Upon introducing $T = y_{\mathrm{D}}^* + y_{\mathrm{S}}^*$, the above set of equations simplifies to

$$r_{\mathrm{S}}\big(1 - b_{\mathrm{S}}(x_{\mathrm{S}}^* + y_{\mathrm{S}}^*)\big) - d_{\mathrm{S}} - \beta_{\mathrm{S}} T = 0, \tag{4.17a}$$

$$r_{\mathrm{D}} x_{\mathrm{S}}^* - d_{\mathrm{D}} x_{\mathrm{D}}^* - \beta_{\mathrm{D}} x_{\mathrm{D}}^* T = 0, \tag{4.17b}$$

$$l_{\mathrm{S}} y_{\mathrm{S}}^*\big(1 - b_{\mathrm{S}}(x_{\mathrm{S}}^* + y_{\mathrm{S}}^*)\big) - a_{\mathrm{S}} y_{\mathrm{S}}^* + \beta_{\mathrm{S}} x_{\mathrm{S}}^* T = 0, \tag{4.17c}$$

$$l_{\mathrm{D}} y_{\mathrm{S}}^* - a_{\mathrm{D}}(T - y_{\mathrm{S}}^*) + \beta_{\mathrm{D}} x_{\mathrm{D}}^* T = 0. \tag{4.17d}$$

Solving Eq. (4.17a) for x_{S}^* results in $x_{\mathrm{S}}^* = \dfrac{r_{\mathrm{S}} - d_{\mathrm{S}} - T\beta_{\mathrm{S}}}{b_{\mathrm{S}} r_{\mathrm{S}}} - y_{\mathrm{S}}^*$. Substituting this value for x_{S}^* in Eq. (4.17b) and then solving Eq. (4.17b) for x_{D}^* leads to $x_{\mathrm{D}}^* = x_{\mathrm{S}}^* \dfrac{r_{\mathrm{D}}}{\beta_{\mathrm{D}} T + d_{\mathrm{D}}}$. Now substituting the values of x_{D}^* and x_{S}^* in Eq. (4.17c) and solving Eq. (4.17c) for y_{S}^* yields in $y_{\mathrm{S}}^* = \dfrac{\beta_{\mathrm{S}} T(r_{\mathrm{S}} - d_{\mathrm{S}} - \beta_{\mathrm{S}} T)}{b_{\mathrm{S}}\big((r_{\mathrm{S}} - l_{\mathrm{S}})\beta_{\mathrm{S}} T + a_{\mathrm{S}} r_{\mathrm{S}} - l_{\mathrm{S}} d_{\mathrm{S}}\big)}$. Now by substituting the value of y_{S}^* in formula of x_{S}^*, the above calculation can be summarised as

$$x_{\mathrm{S}}^* = \frac{(r_{\mathrm{S}} - d_{\mathrm{S}} - \beta_{\mathrm{S}} T)(a_{\mathrm{S}} r_{\mathrm{S}} - l_{\mathrm{S}} d_{\mathrm{S}} - l_{\mathrm{S}} \beta_{\mathrm{S}} T)}{b_{\mathrm{S}} r_{\mathrm{S}}\big((r_{\mathrm{S}} - l_{\mathrm{S}})\beta_{\mathrm{S}} T + a_{\mathrm{S}} r_{\mathrm{S}} - l_{\mathrm{S}} d_{\mathrm{S}}\big)}, \tag{4.18a}$$

$$x_{\mathrm{D}}^* = x_{\mathrm{S}}^* \frac{r_{\mathrm{D}}}{\beta_{\mathrm{D}} T + d_{\mathrm{D}}}, \tag{4.18b}$$

$$y_{\mathrm{S}}^* = \frac{\beta_{\mathrm{S}} T(r_{\mathrm{S}} - d_{\mathrm{S}} - \beta_{\mathrm{S}} T)}{b_{\mathrm{S}}\big((r_{\mathrm{S}} - l_{\mathrm{S}})\beta_{\mathrm{S}} T + a_{\mathrm{S}} r_{\mathrm{S}} - l_{\mathrm{S}} d_{\mathrm{S}}\big)}, \tag{4.18c}$$

$$y_{\mathrm{D}}^* = T - y_{\mathrm{S}}^* = \frac{T\Big(T\beta_S\big(\beta_S + b_S(r_S - l_S)\big) + b_S(a_S r_S - l_S d_S) - (r_S - d_S)\beta_S\Big)}{b_S(T(r_S - l_S)\beta_S + a_S r_S - l_S d_S)}, \tag{4.18d}$$

Now by substituting the values of x_{D}^*, y_{S}^* and y_{D}^* in Eq. (4.17d) we have $Q(T) = 0$, where

$$Q(T) = AT^2 + BT + C \tag{4.19}$$

and

$$A := \beta_{\mathrm{S}}\beta_{\mathrm{D}}\Big(\beta_{\mathrm{S}}\big((l_{\mathrm{D}} + a_{\mathrm{D}})r_{\mathrm{S}} - r_{\mathrm{D}} l_{\mathrm{S}}\big) + b_{\mathrm{S}} a_{\mathrm{D}} r_{\mathrm{S}}(r_{\mathrm{S}} - l_{\mathrm{S}})\Big),$$

$$B := d_{\mathrm{D}} r_{\mathrm{S}}(l_{\mathrm{D}} + a_{\mathrm{D}})\beta_{\mathrm{S}}^2 + \Bigg(\Big((r_{\mathrm{S}} - d_{\mathrm{S}})\big(r_{\mathrm{D}} l_{\mathrm{S}} - (l_{\mathrm{D}} + a_{\mathrm{D}}) r_{\mathrm{S}}\big) + r_{\mathrm{D}}(r_{\mathrm{S}} a_{\mathrm{S}} - l_{\mathrm{S}} d_{\mathrm{S}})\Big)\beta_{\mathrm{D}} +$$

$$b_{\mathrm{S}} d_{\mathrm{D}} r_{\mathrm{S}} a_{\mathrm{D}}(r_{\mathrm{S}} - l_{\mathrm{S}})\Bigg)\beta_{\mathrm{S}} + b_{\mathrm{S}} a_{\mathrm{D}} r_{\mathrm{S}} \beta_{\mathrm{D}}(r_{\mathrm{S}} a_{\mathrm{S}} - l_{\mathrm{S}} d_{\mathrm{S}}),$$

$$C := \left(-\beta_{\mathrm{S}} + \frac{(a_{\mathrm{S}} r_{\mathrm{S}} - d_{\mathrm{S}} l_{\mathrm{S}})}{(a_{\mathrm{D}} + l_{\mathrm{D}})} \frac{\big(b_{\mathrm{S}} d_{\mathrm{D}} a_{\mathrm{D}} r_{\mathrm{S}} - \beta_{\mathrm{D}} r_{\mathrm{D}}(r_{\mathrm{S}} - d_{\mathrm{S}})\big)}{r_{\mathrm{S}} d_{\mathrm{D}}(r_{\mathrm{S}} - d_{\mathrm{S}})} \right)(a_{\mathrm{D}} + l_{\mathrm{D}})(r_{\mathrm{S}} - d_{\mathrm{S}}) r_{\mathrm{S}} d_{\mathrm{D}}.$$

According to assumptions (C6) $l_{\mathrm{S}} < r_{\mathrm{S}}$ and $d_{\mathrm{S}} < a_{\mathrm{S}}$. Hence, $r_{\mathrm{S}} - l_{\mathrm{S}} > 0$ and $r_{\mathrm{S}} a_{\mathrm{S}} - l_{\mathrm{S}} d_{\mathrm{S}} > 0$. Therefore, the denominator in the set of equations (4.18) is always positive. Thus, E_p is a strictly positive steady state of Model (4.2) if and only if T is a positive root of Q such that $r_{\mathrm{S}} - d_{\mathrm{S}} - \beta_{\mathrm{S}} T > 0$, $a_{\mathrm{S}} r_{\mathrm{S}} - l_{\mathrm{S}} d_{\mathrm{S}} - l_{\mathrm{S}} \beta_{\mathrm{S}} T > 0$ and $T\beta_S\big(\beta_S + b_S(r_S - l_S)\big) + b_S(a_S r_S - l_S d_S) - (r_S - d_S)\beta_S > 0$.

4.7.5 Proof of Theorem 4.1

Proof of (I). Recall $E_U = \left(b_{\mathrm{S}}^{-1}(1 - \frac{d_{\mathrm{S}}}{r_{\mathrm{S}}}), \frac{r_{\mathrm{D}}}{b_{\mathrm{S}} d_{\mathrm{D}}}(1 - \frac{d_{\mathrm{S}}}{r_{\mathrm{S}}}), 0, 0\right)$. Based of assumption (C5) $d_{\mathrm{S}} < r_{\mathrm{S}}$, therefore, E_U always exists.

Proof of (II). $E_I = \left(0, 0, b_{\mathrm{S}}^{-1}(1 - \frac{a_{\mathrm{S}}}{l_{\mathrm{S}}}), \frac{l_{\mathrm{D}}}{b_{\mathrm{S}} a_{\mathrm{D}}}(1 - \frac{a_{\mathrm{S}}}{l_{\mathrm{S}}})\right)$. When $a_{\mathrm{S}} < l_{\mathrm{S}}$, $l_{\mathrm{S,D}} \neq 0$ both nonzero components of E_I are positive.

Proof of (III). Suppose $a_{\mathrm{S}} < l_{\mathrm{S}}$, $1 < \frac{r_{\mathrm{D}}}{a_{\mathrm{D}} + l_{\mathrm{D}}} < \frac{r_{\mathrm{S}}}{l_{\mathrm{S}}}$, and

$$\left(\frac{a_{\mathrm{S}} r_{\mathrm{S}} - d_{\mathrm{S}} l_{\mathrm{S}}}{a_{\mathrm{D}} + l_{\mathrm{D}}}\right) \frac{b_{\mathrm{S}} d_{\mathrm{D}} a_{\mathrm{D}} r_{\mathrm{S}} - \beta_{\mathrm{D}} r_{\mathrm{D}}(r_{\mathrm{S}} - d_{\mathrm{S}})}{r_{\mathrm{S}} d_{\mathrm{D}}(r_{\mathrm{S}} - d_{\mathrm{S}})} < \beta_{\mathrm{S}} < \frac{b_{\mathrm{S}} a_{\mathrm{D}}(r_{\mathrm{S}} a_{\mathrm{S}} - l_{\mathrm{S}} d_{\mathrm{S}})}{(l_{\mathrm{S}} - a_{\mathrm{S}})(a_{\mathrm{D}} + l_{\mathrm{D}})}.$$

We show E_p is unique and strictly positive under these assumptions, where $E_p = (x_{\mathrm{S}}^*, x_{\mathrm{D}}^*, y_{\mathrm{S}}^*, y_{\mathrm{D}}^*)$.

For the interior steady state E_p to be positive x_{S}^*, x_{D}^*, y_{S}^* and y_{D}^*, the set of equations (4.18) must be positive while T is a positive root of quadratic $Q(T)$.

In Eq. (4.18c) denominator is always positive, because according to assumption (C6) $l_{\mathrm{S}} < r_{\mathrm{S}}$ and $d_{\mathrm{S}} < a_{\mathrm{S}}$, therefore, $a_{\mathrm{S}} r_{\mathrm{S}} - d_{\mathrm{S}} l_{\mathrm{S}} > 0$ and $r_{\mathrm{S}} - l_{\mathrm{S}} > 0$. Since denominator

in Eq. (4.18c) is always positive, for y_S^* to be positive, it suffices that the numerator be positive. Therefore, $r_S - d_S - \beta_S T > 0$.

Similarly in Eq. (4.18a) denominator is positive. Hence, for x_S^* to be positive numerator should be positive. Meaning $(r_S - d_S - \beta_S T)(a_S r_S - l_S d_S - l_S \beta_S T) > 0$. As we mentioned above y_S^* is positive if and only if $r_S - d_S - \beta_S T > 0$, therefore, x_S^* and y_S^* are positive if and only if $r_S - d_S - \beta_S T > 0$ and $a_S r_S - l_S d_S - l_S \beta_S T > 0$. Therefore, x_S^* and y_S^* are positive if and only if

$$T < \min\{\frac{r_S - d_S}{\beta_S}, \frac{r_S a_S - l_S d_S}{l_S \beta_S}\}$$

According to our assumption, $a_S < l_S$, therefore $\frac{a_S}{l_S} < 1$. Hence, $\frac{a_S}{l_S} r_S < r_S$.
Thus, $\frac{r_S \frac{a_S}{l_S} - d_S}{\beta_S} < \frac{r_S - d_S}{\beta_S}$. Therefore, $\min\{\frac{r_S - d_S}{\beta_S}, \frac{r_S a_S - l_S d_S}{l_S \beta_S}\} = \frac{r_S a_S - l_S d_S}{l_S \beta_S}$.
From set of equations (4.18), if x_S^* is positive, then x_D^* is also positive.
For y_D^* to be positive $\frac{(r_S - d_S)\beta_S - b_S(a_S r_S - l_S d_S)}{\beta_S + b_S(r_S - l_S)} < T$.
Therefore, x_S^*, x_D^*, y_S^*, and y_D^* are all positive if and only if quadratic Q has a positive root T^* such that

$$\frac{(r_S - d_S)\beta_S - b_S(a_S r_S - l_S d_S)}{\beta_S + b_S(r_S - l_S)} < T^* < \frac{r_S a_S - l_S d_S}{l_S \beta_S}. \tag{4.20}$$

According to our assumption, $\frac{r_D}{a_D + l_D} < \frac{r_S}{l_S}$, therefore the leading coefficient A of quadratic Q is positive. In addition according to our assumptions $((a_S r_S - d_S l_S)\big(b_S d_D a_D r_S - \beta_D r_D (r_S - d_S)\big)/((a_D + l_D))(r_S d_D (r_S - d_S)) < \beta_S$, therefore $C = Q(0) < 0$. Hence, quadratic Q has a unique positive root $T^* = \frac{-B}{2A} + \sqrt{(\frac{-B}{2A})^2 - \frac{C}{A}}$.

Now we need to show T^* satisfies inequality (4.20).

$$
\begin{aligned}
Q\left(\frac{r_{\mathrm{S}}a_{\mathrm{S}} - l_{\mathrm{S}}d_{\mathrm{S}}}{l_{\mathrm{S}}\beta_{\mathrm{S}}}\right) =& \frac{r_{\mathrm{S}}^2}{\beta_{\mathrm{S}}l_{\mathrm{S}}^2}\big(b_{\mathrm{S}}a_D(r_{\mathrm{S}}a_{\mathrm{S}} - l_{\mathrm{S}}d_{\mathrm{S}}) - (l_{\mathrm{S}} - a_{\mathrm{S}})(l_D + a_D)\beta_{\mathrm{S}}\big) \\
& \cdot \big((r_{\mathrm{S}}a_{\mathrm{S}} - l_{\mathrm{S}}d_{\mathrm{S}})\beta_{\mathrm{D}} + l_{\mathrm{S}}d_{\mathrm{D}}\beta_{\mathrm{S}}\big) \\
Q\left(\frac{(r_{\mathrm{S}} - d_{\mathrm{S}})\beta_{\mathrm{S}} - b_{\mathrm{S}}(a_{\mathrm{S}}r_{\mathrm{S}} - l_{\mathrm{S}}d_{\mathrm{S}})}{\beta_{\mathrm{S}} + b_{\mathrm{S}}(r_{\mathrm{S}} - l_{\mathrm{S}})}\right) =& \beta_{\mathrm{D}}\big(r_{\mathrm{D}}\beta_{\mathrm{S}}(l_{\mathrm{S}} - a_{\mathrm{S}}) - b_{\mathrm{S}}(a_{\mathrm{S}}r_{\mathrm{S}} - l_{\mathrm{S}}d_{\mathrm{S}})(r_{\mathrm{D}} - l_{\mathrm{D}})\big) \\
& - l_{\mathrm{D}}\beta_{\mathrm{S}}\Big(\beta_{\mathrm{D}}(r_{\mathrm{S}} - d_{\mathrm{S}}) + d_{\mathrm{D}}\big(b_{\mathrm{S}}(r_{\mathrm{S}} - l_{\mathrm{S}}) + \beta_{\mathrm{S}}\big)\Big)
\end{aligned}
$$

According to our assumption $\beta_S < \frac{b_{\mathrm{S}}a_D(r_{\mathrm{S}}a_{\mathrm{S}} - l_{\mathrm{S}}d_{\mathrm{S}})}{(l_S - a_S)(l_D + a_D)}$. Therefore, $Q\big(\frac{r_{\mathrm{S}}a_{\mathrm{S}} - l_{\mathrm{S}}d_{\mathrm{S}}}{l_{\mathrm{S}}\beta_{\mathrm{S}}}\big) > 0$.

Based of our assumption $a_{\mathrm{D}} + l_{\mathrm{D}} < r_{\mathrm{D}}$, hence $\frac{b_{\mathrm{S}}(r_{\mathrm{S}}a_{\mathrm{S}} - l_{\mathrm{S}}d_{\mathrm{S}})a_{\mathrm{D}}}{(l_{\mathrm{S}} - a_{\mathrm{S}})(a_{\mathrm{D}} + l_{\mathrm{D}})} < \frac{b_{\mathrm{S}}(r_{\mathrm{S}}a_{\mathrm{S}} - l_{\mathrm{S}}d_{\mathrm{S}})(r_{\mathrm{D}} - l_{\mathrm{D}})}{(l_{\mathrm{S}} - a_{\mathrm{S}})r_{\mathrm{D}}}$.

So when $\beta_{\mathrm{S}} < \frac{b_{\mathrm{S}}(r_{\mathrm{S}}a_{\mathrm{S}} - l_{\mathrm{S}}d_{\mathrm{S}})a_{\mathrm{D}}}{(l_{\mathrm{S}} - a_{\mathrm{S}})(a_{\mathrm{D}} + l_{\mathrm{D}})}$, then $\beta_{\mathrm{S}} < \frac{b_{\mathrm{S}}(r_{\mathrm{S}}a_{\mathrm{S}} - l_{\mathrm{S}}d_{\mathrm{S}})(r_{\mathrm{D}} - l_{\mathrm{D}})}{(l_{\mathrm{S}} - a_{\mathrm{S}})r_{\mathrm{D}}}$.

Therefore, $Q(\frac{(r_{\mathrm{S}} - d_{\mathrm{S}})\beta_{\mathrm{S}} - b_{\mathrm{S}}(a_{\mathrm{S}}r_{\mathrm{S}} - l_{\mathrm{S}}d_{\mathrm{S}})}{\beta_{\mathrm{S}} + b_{\mathrm{S}}(r_{\mathrm{S}} - l_{\mathrm{S}})}) < 0$.

Since $Q(\frac{(r_{\mathrm{S}} - d_{\mathrm{S}})\beta_{\mathrm{S}} - b_{\mathrm{S}}(a_{\mathrm{S}}r_{\mathrm{S}} - l_{\mathrm{S}}d_{\mathrm{S}})}{\beta_{\mathrm{S}} + b_{\mathrm{S}}(r_{\mathrm{S}} - l_{\mathrm{S}})})Q(\frac{r_{\mathrm{S}}a_{\mathrm{S}} - l_{\mathrm{S}}d_{\mathrm{S}}}{l_{\mathrm{S}}\beta_{\mathrm{S}}}) < 0$ and Q is a continuous function, Q has a unique positive root that satisfies the inequality (4.20). Therefore, under the theorem's assumptions there exists a unique interior steady state.

Proof of (IV). Let $E_p = (x_{\mathrm{S}}^*, x_{\mathrm{D}}^*, y_{\mathrm{S}}^*, y_{\mathrm{D}}^*)$ be the interior steady state. When $l_{\mathrm{S}} = l_{\mathrm{D}} = 0$, set of equations (4.18) can be rewritten as

$$
x_{\mathrm{S}}^* = \frac{(r_{\mathrm{S}} - d_{\mathrm{S}} - \beta_{\mathrm{S}}T)a_{\mathrm{S}}}{b_{\mathrm{S}}r_{\mathrm{S}}(T\beta_{\mathrm{S}} + a_{\mathrm{S}})}, \tag{4.21a}
$$

$$
x_{\mathrm{D}}^* = \frac{r_{\mathrm{D}}}{\beta_{\mathrm{D}}T + d_{\mathrm{D}}}x_{\mathrm{S}}^*, \tag{4.21b}
$$

$$
y_{\mathrm{S}}^* = \frac{\beta_{\mathrm{S}}T}{a_{\mathrm{S}}}x_{\mathrm{S}}^*, \tag{4.21c}
$$

$$
y_{\mathrm{D}}^* = \frac{T\big(T\beta_{\mathrm{S}}^2 + (Tb_{\mathrm{S}}r_{\mathrm{S}} + d_{\mathrm{S}} - r_{\mathrm{S}})\beta_{\mathrm{S}} + b_{\mathrm{S}}a_{\mathrm{S}}r_{\mathrm{S}}\big)}{b_{\mathrm{S}}r_{\mathrm{S}}(T\beta_{\mathrm{S}} + a_{\mathrm{S}})}, \tag{4.21d}
$$

where T is a positive root of the following quadratic $Q_1(T) = A_1T^2 + B_1T + C_1$ where

$A_1 := a_{\mathrm{D}}\beta_{\mathrm{D}}\beta_{\mathrm{S}}(b_{\mathrm{S}}r_{\mathrm{S}} + \beta_{\mathrm{S}})$,

$B_1 := a_D d_D \beta_S^2 + \Big(\big(b_{\mathrm{S}}r_S d_D - (r_S - d_S)\beta_D\big)a_D + a_S r_D \beta_D\Big)\beta_S + a_D a_S b_{\mathrm{S}} r_S \beta_D$,

$C_1 := a_{\mathrm{S}}\big(a_{\mathrm{D}}d_{\mathrm{D}}b_{\mathrm{S}}r_{\mathrm{S}} - \beta_{\mathrm{D}}r_{\mathrm{D}}(r_{\mathrm{S}} - d_{\mathrm{S}})\big) - a_{\mathrm{D}}d_{\mathrm{D}}(r_{\mathrm{S}} - d_{\mathrm{S}})\beta_{\mathrm{S}}$.

When $\beta_{\mathrm{S}} > \dfrac{a_{\mathrm{S}}\big(a_{\mathrm{D}}d_{\mathrm{D}}b_{\mathrm{S}}r_{\mathrm{S}} - \beta_{\mathrm{D}}r_{\mathrm{D}}(r_{\mathrm{S}} - d_{\mathrm{S}})\big)}{a_{\mathrm{D}}d_{\mathrm{D}}(r_{\mathrm{S}} - d_{\mathrm{S}})}$, $C_1 < 0$. On the other hand A_1 is always positive, therefore the above quadratic always has a unique positive root $T_1^* = \dfrac{-B_1}{2A_1} + \sqrt{(\dfrac{-B_1}{2A_1})^2 - \dfrac{C_1}{A_1}}$. For interior steady state to exist, we should show that for $T = T_1^*$, x_{S}^*, x_{D}^*, y_{S}^*, and y_{D}^* are all positive.

From the set of equations (4.21), when x_{S}^* is positive, x_{D}^*, y_{S}^* are positive. Therefore, a positive steady state exists if and only if for $T = T_1^*$, x_{S}^* and y_{D}^* are both positive.

$x_{\mathrm{S}}^* > 0$ if and only if $T_1^* < \dfrac{r_{\mathrm{S}} - d_{\mathrm{S}}}{\beta_{\mathrm{S}}}$.

$y_{\mathrm{D}}^* > 0$ if and only if $\dfrac{(r_{\mathrm{S}} - d_{\mathrm{S}})\beta_S - a_{\mathrm{S}}b_{\mathrm{S}}r_{\mathrm{S}}}{\beta_{\mathrm{S}}(b_{\mathrm{S}}r_{\mathrm{S}} + \beta_{\mathrm{S}})} < T_1^*$.

Therefore, there exists an interior steady state if and only if there exists a positive root of quadratic $Q_1(T)$ such that $\dfrac{(r_{\mathrm{S}} - d_{\mathrm{S}})\beta_S - a_{\mathrm{S}}b_{\mathrm{S}}r_{\mathrm{S}}}{\beta_{\mathrm{S}}(b_{\mathrm{S}}r_{\mathrm{S}} + \beta_{\mathrm{S}})} < T_1^* < \dfrac{r_{\mathrm{S}} - d_{\mathrm{S}}}{\beta_{\mathrm{S}}}$.

$Q_1(\dfrac{(r_{\mathrm{S}} - d_{\mathrm{S}})\beta_S - a_{\mathrm{S}}b_{\mathrm{S}}r_{\mathrm{S}}}{\beta_{\mathrm{S}}(b_{\mathrm{S}}r_{\mathrm{S}} + \beta_{\mathrm{S}})}) = \dfrac{-a_{\mathrm{S}}r_{\mathrm{D}}\beta_{\mathrm{D}}b_{\mathrm{S}}r_{\mathrm{S}}(a_{\mathrm{S}} - d_{\mathrm{S}} + r_{\mathrm{S}})}{(b_{\mathrm{S}}r_{\mathrm{S}} + \beta_{\mathrm{S}})} < 0$

$Q_1(\dfrac{r_{\mathrm{S}} - d_{\mathrm{S}}}{\beta_{\mathrm{S}}}) = \dfrac{br_{\mathrm{S}}^2(a_{\mathrm{S}} + r_{\mathrm{S}} - d_{\mathrm{S}})\big(\beta_{\mathrm{D}}(r_{\mathrm{S}} - d_{\mathrm{S}}) + \beta_{\mathrm{S}}d_{\mathrm{D}}\big)a_{\mathrm{D}}}{\beta_{\mathrm{S}}} > 0.$

Since Q_1 is a continuous function and $Q_1\Big(\dfrac{(r_{\mathrm{S}} - d_{\mathrm{S}})\beta_S - a_{\mathrm{S}}b_{\mathrm{S}}r_{\mathrm{S}}}{\beta_{\mathrm{S}}(b_{\mathrm{S}}r_{\mathrm{S}} + \beta_{\mathrm{S}})}\Big)Q_1\Big(\dfrac{r_{\mathrm{S}} - d_{\mathrm{S}}}{\beta_{\mathrm{S}}}\Big) < 0$, Q_1 has a positive root in interval $\Big(\dfrac{(r_{\mathrm{S}} - d_{\mathrm{S}})\beta_S - a_{\mathrm{S}}b_{\mathrm{S}}r_{\mathrm{S}}}{\beta_{\mathrm{S}}(b_{\mathrm{S}}r_{\mathrm{S}} + \beta_{\mathrm{S}})}, \dfrac{r_{\mathrm{S}} - d_{\mathrm{S}}}{\beta_{\mathrm{S}}}\Big)$. Since $C_1 < 0$ and $A_1 > 0$, T_1^* is the only positive root of $Q_1(T)$. Therefore,

$$\frac{(r_{\mathrm{S}} - d_{\mathrm{S}})\beta_S - a_{\mathrm{S}}b_{\mathrm{S}}r_{\mathrm{S}}}{\beta_{\mathrm{S}}(b_{\mathrm{S}}r_{\mathrm{S}} + \beta_{\mathrm{S}})} < T_1^* < \frac{r_{\mathrm{S}} - d_{\mathrm{S}}}{\beta_{\mathrm{S}}}$$

. □

Chapter 5

Summary

Clinical trials show oncolytic viral therapy is less toxic than conventional therapies and quite promising, but tumour eradication has rarely been reported. Our proposed models, Model (2.1) in Chapter 2 and Model (4.2) in Chapter 4, suggest that tumour eradication is not possible with oncolytic viral therapy. However, tumour size is considerably reduced with oncolytic therapy. Not only this result is seen in therapy with an oncolytic virus that is not modified to target a specific phenotype (see Chapter 2), but tumour eradication is not also achieved when an oncolytic virus that preferentially targets cancer stem cells is administrated (see Chapter 4). Our results agrees with most in vitro and in vivo studies of oncolytic viral therapy in that there are two possible outcomes for therapy: failure or partial success. Either the tumour grows back after an initial shrinkage, or tumour size considerably is reduced over the course of the experiment.

Our analysis in Chapter 2 concludes that higher transmission rate does not always lead to more tumour shrinkage and a more successful outcome. Komarova and Wodarz [60] under quasi-steady state assumption showed that viruses with fast spread result in a better outcome, meaning more tumour shrinkage. In Chap-

ter 2 by relaxing quasi-steady state assumption we show that treatment outcomes strongly depend on the viral timescale and virulence level of the free virus (see Figures 2.3 and 2.9). When the viral timescale is fast, our result is the same as the result of Komarova and Wodarz [60] in that viruses with higher transmission rate result in a better outcome, i.e., a smaller tumour size post therapy. However, when viral timescale is slow, there are thresholds for virulence level of the virus and the horizontal transmission rate such that if a virus with higher transmission rate or a more virulent virus is administrated in the experiment, then that results in sustained oscillations. In fact this threshold is a codimension-one manifold in the parameter space along which tumour size is minimum. This one dimensional curve can be obtained by solving $H = 0$ (see Eq. (2.21) for H).

Chapter 3 suggests that antibodies or CTLs do not affect the control threshold of the therapy; however, they can affect the optimal threshold of the therapy. Effect of a virus-specific immune response on the optimal threshold of the therapy depends on virulence level of the free virus Y_I and the clearance rate of the immune response n. If $Y_I < n$, then a virus-specific immune response does not affect the optimal threshold of the therapy. However, when $Y_I > n$, the optimal threshold of the therapy when a CTL immune response or an antibody immune response is active is higher than when no immune response is active (see Theorem 3.5 and Lemma 3.6). In Chapter 4, the control threshold ($R_0 = 1$, see Eq. (4.10)) and the optimal threshold of therapy ($R_U = 1$, see Eq. (4.12)) is calculated by taking phenotypic heterogeneity of the tumour into account, meaning under the assumption that the infection transmission rate of stem cells β_{S} per encounter with an infected cell is different with the infection transmission rate of a fully differentiated cell β_{D}. The control threshold of the therapy is a linear relation between β_{S} and β_{D}. The interesting fact is that the optimal threshold of the therapy depends only on the transmission rate of cancer stem cells. Another significant common result between all the models of this thesis

is that the optimal threshold of the therapy can only be obtained when infected cells are mitotic, meaning that they divide into infected daughter cells. When infected cells are nonmitotic and timescale of viral dynamics is fast enough, then increasing the infection transmission rate leads to smaller tumour size and treatment optimal threshold is at infinity, hence, in this case we say there is no optimal threshold.

Our simulations in Chapter 2 suggest that when the virus clearance rate is slow relative to the growth rate of uninfected cancer cells, then sufficiently high level of virulence causes oscillatory behaviour with large amplitudes (see Figure 2.10). Another observation that could lead to further investigation is that when the virus is sufficiently virulent, and the proper initial dosage is applied, early tumour shrinkage occurs to less than 9% of the initial tumour size and the tumour remains in remission for almost a year before relapsing. This raises multiple questions: 1- What happens if the treatment switches to another therapy before tumour relapse? 2- What form of new therapy can prevent relapse?

Chapter 3 suggests that a virus-specific immune response is not always a burden on the success of oncolytic viral therapy: in fact, sometimes establishment of a virus-specific immune response can enhance the result of the therapy. The most important message of this chapter is that a virus-specific immune response may be activated to interfere with the infection, but it can be a short response, and it does not remain active in the steady state. In Chapter 3 the conditions for establishment of antibodies (see Theorem 3.1) and CTLs (see Theorem 3.2) are formulated. Our analysis suggests that establishment of antibodies are either detrimental or neutral (see Figures 3.2 and Figures 3.3); however, establishment of CTLs is either detrimental or beneficial (see Figures 3.4 and 3.5). When a post-therapy tumour is partially infected and a virus-specific immune response is established, tumour size is always larger than in the absence of a virus-specific immune response. If a tumour is fully infected and an antibody immune response has been established, then the optimal

tumour size is the same as the optimal tumour size when no virus-specific immune response is established. When a tumour is fully infected and a CTL response has been established, optimal tumour size is lower than when no virus-specific immune response is active. Hence, the treatment outcome is enhanced. The extent to which the establishment of an immune response is detrimental or beneficial strongly depends on the virulence level of the free virus, Y_I, and a rescaled clearance rate of the free virus, n. If a post-therapy tumour is partially infected and an immune response has been established there are two possibilities; 1- if $Y_I > n$ by an increase in the difference $|Y_I - n|$, the impact of establishing a virus-specific immune response is more significant. 2- if $Y_I < n$ by an increase in $|Y_I - n|$, the detrimental effect of establishment of an immune response decreases. If a post-therapy tumour is fully infected and a CTL immune response is established, an increase in $|Y_I - n|$ enhances the positive effect of establishing a CTL immune response.

Our simulations in Chapter 4 recommend that stem cell fraction increases during an oncolytic viral therapy in which a virus that is modified to selectively targets a specific phenotype (stem cell or differentiated cells) is administrated. We suggest, based on our analysis detailed in Chapter 4 that when infected cancer cells are mitotic, treatment outcome is optimal under perfect stem cell targeting, i.e. administrating a virus that only targets cancer stem cells results in a better outcome than random targeting. However, when infected cells are nonmitotic, random targeting gives the same result as perfect stem cell targeting. In this scenario, the mean infection transmission rate is more critical. As the mean infection transmission rate increases, the treatment outcome enhances. In Chapter 4, for simplicity, only self-renewal and symmetric differentiation are considered. Model (4.2) can be extended to a full hierarchical model such as the one discussed in Williams et al. [113] to consider all types of differentiation. Another assumption ((C2)) that Model (4.2) is derived under is that the rate of the production of virus per infected stem cell and per infected dif-

ferentiated cell is the same. However, in practice, it may be different. The result of Chapter 4 can also be derived if this assumption is relaxed; just the formulation will be more complicated.

Since the interaction between cancer cells, the free virus and the immune response is quite complicated during oncolytic viral therapy, mathematical approaches, both analytical and computational, could broaden our knowledge about oncolytic viral therapy. The approach of my research is quite different in that it focuses on what to expect from oncolytic viral therapy, cure or containment and then by focusing on viral parameters and factors I try to realize how to enhance the treatment outcome. Of course, no matter how complicated a mathematical model is written, still including all the interactions from cellular to non-cellular level during oncolytic therapy is not possible. The models proposed in my thesis are simple yet helpful in confirming some results seen in clinical trials of oncolytic viral therapy.

Bibliography

[1] *antibody | Definition, Structure, Function, & Types | Britannica*, 2020-10-14, `https://www.britannica.com/science/antibody`.

[2] Hans-W. Ackermann, Laurent Berthiaume, and Michel Tremblay, *VIRUS LIFE in DIAGRAMS*, 1st ed. ed., CRC Press., 1998, `doi`.

[3] Manju Agarwal and Archana Bhadauria, *Mathematical Modeling and Analysis of tumour Therapy with Oncolytic Virus*, Applied Mathematics **2** (2011), 131–140, `doi`.

[4] M. Aghi, T. Visted, R. A. DePinho, and E. A. Chiocca, *Oncolytic herpes virus with defective ICP6 specifically replicates in quiescent cells with homozygous genetic mutations in p16*, Oncogene **27** (2008), no. 30, 4249–4254, `doi`.

[5] Muhammad Al-Hajj, Max S. Wicha, Adalberto Benito-Hernandez, Sean J. Morrison, and Michael F. Clarke, *Prospective identification of tumourigenic breast cancer cells*, Proceedings of the National Academy of Sciences of the United States of America **100** (2003), no. 7, 3983–3988, `doi`.

[6] Patricia Bach, Tobias Abel, Christopher Hoffmann, Zoltan Gal, Gundula Braun, Iris Voelker, Claudia R. Ball, Ian C.D. Johnston, Ulrich M. Lauer, Christel Herold-Mende, Michael D. Mühlebach, Hanno Glimm, and Chris-

tian J. Buchholz, *Specific Elimination of CD133 $^{+}$ tumour Cells with Targeted Oncolytic Measles Virus*, Cancer Research **73** (2013), no. 2, 865–874, doi.

[7] Zeljko Bajzer, Thomas Carr, Krešimir Josić, Stephen J. Russell, and David Dingli, *Modeling of cancer virotherapy with recombinant measles viruses*, Journal of Theoretical Biology **252** (2008), no. 1, 109–122 (en), doi.

[8] Gerd J. Bauerschmitz, Tuuli Ranki, Lotta Kangasniemi, Camilla Ribacka, Minna Eriksson, Marius Porten, Isabell Herrmann, Ari Ristimäki, Pekka Virkkunen, Maija Tarkkanen, Tanja Hakkarainen, Anna Kanerva, Daniel Rein, Sari Pesonen, and Akseli Hemminki, *Tissue-Specific Promoters Active in CD44 $^{+}$ CD24 $^{-}$/low Breast Cancer Cells*, Cancer Research **68** (2008), no. 14, 5533–5539, doi.

[9] John C Bell, Brian Lichty, and David Stojdl, *Getting oncolytic virus therapies off the ground*, Cancer Cell **4** (2003), no. 1, 7–11, doi.

[10] Robert A. Berkeley, Lynette P. Steele, Aat A. Mulder, Diana J. M. van den Wollenberg, Timothy J. Kottke, Jill Thompson, Matthew Coffey, Rob C. Hoeben, Richard G. Vile, Alan Melcher, and Elizabeth J. Ilett, *Antibody-Neutralized Reovirus Is Effective in Oncolytic Virotherapy*, Cancer Immunology Research **6** (2018), no. 10, 1161–1173 (en), doi.

[11] Ivana Bozic and Martin A. Nowak, *Resisting Resistance*, Annual Review of Cancer Biology **1** (2017), no. 1, 203–221, doi.

[12] Byram W Bridle, Kyle B Stephenson, Jeanette E Boudreau, Sandeep Koshy, Natasha Kazdhan, Eleanor Pullenayegum, Jérôme Brunellière, Jonathan L Bramson, Brian D Lichty, and Yonghong Wan, *Potentiating Cancer Immunotherapy Using an Oncolytic Virus*, Molecular Therapy **18** (2010), no. 8, 1430–1439, doi.

[13] Shyambabu Chaurasiya, Nanhai Chen, and Susanne Warner, *Oncolytic Virotherapy versus Cancer Stem Cells: A Review of Approaches and Mechanisms*, Cancers **10** (2018), no. 4, 124, doi.

[14] Yumin Chen, Paiboon Jungsuwadee, Mary Vore, D. Allan Butterfield, and Daret K. St. Clair, *Collateral Damage in Cancer Chemotherapy: Oxidative Stress in Nontargeted Tissues*, Molecular Interventions **7** (2007), no. 3, 147 (en), Publisher: American Society for Pharmacology and Experimental Therapeutics, doi.

[15] Michael F. Clarke and Margaret Fuller, *Stem Cells and Cancer: Two Faces of Eve*, Cell **124** (2006), no. 6, 1111–1115, doi.

[16] Matthew C. Coffey, James E. Strong, Peter A. Forsyth, and Patrick W. K. Lee, *Reovirus Therapy of Tumors with Activated Ras Pathway*, Science **282** (1998), no. 5392, 1332–1334, doi.

[17] Pippa G. Corrie, *Cytotoxic chemotherapy: clinical aspects*, Medicine **39** (2011), no. 12, 717–722, doi.

[18] Timothy P Cripe, Pin-Yi Wang, Paola Marcato, Yonatan Y Mahller, and Patrick WK Lee, *Targeting Cancer-initiating Cells With Oncolytic Viruses*, Molecular Therapy **17** (2009), no. 10, 1677–1682, doi.

[19] Mathieu J. F. Crupi, John C. Bell, and Ragunath Singaravelu, *Concise Review: Targeting Cancer Stem Cells and Their Supporting Niche Using Oncolytic Viruses*, STEM CELLS **37** (2019), no. 6, 716–723, doi.

[20] R. J. De Boer and A. S. Perelson, *T cell repertoires and competitive exclusion*, Journal of Theoretical Biology **169** (1994), no. 4, 375–390, doi.

[21] J.F. de Graaf, L. de Vor, R.A.M. Fouchier, and B.G. van den Hoogen, *Armed oncolytic viruses: A kick-start for anti-tumor immunity*, Cytokine & Growth

Factor Reviews **41** (2018), 28–39, doi.

[22] Andrew Dhawan, Seyed Ali Madani Tonekaboni, Joseph H. Taube, Stephen Hu, Nathalie Sphyris, Sendurai A. Mani, and Mohammad Kohandel, *Mathematical modelling of phenotypic plasticity and conversion to a stem-cell state under hypoxia*, Scientific Reports **6** (2016), no. 1, 18074 (en), doi.

[23] Nigel J. Dimmock, Andrew J. Easton, and Keith N. Leppard, *Introduction to modern virology*, John Wiley & Sons Incorporated, New York, 2016.

[24] D Dingli, C Offord, R Myers, K-W Peng, T W Carr, K Josic, S J Russell, and Z Bajzer, *Dynamics of multiple myeloma tumour therapy with a recombinant measles virus*, Cancer Gene Therapy **16** (2009), no. 12, 873–882, doi.

[25] David Dingli, Matthew D. Cascino, Kresimir Josic, Stephen J. Russell, and Zeljko Bajzer, *Mathematical modeling of cancer radiovirotherapy*, Mathematical Biosciences **199** (2006), no. 1, 55–78 (en), doi.

[26] David Dingli, Arne Traulsen, and Franziska Michor, *(A)Symmetric Stem Cell Replication and Cancer*, PLOS Computational Biology **3** (2007), no. 3, e53, doi.

[27] Brydon Eastman, Dominik Wodarz, and Mohammad Kohandel, *The effects of phenotypic plasticity on the fixation probability of mutant cancer stem cells*, Journal of Theoretical Biology **503** (2020), 110384, doi.

[28] R. Eftimie, C.K. Macnamara, Jonathan Dushoff, J.L. Bramson, and D.J.D. Earn, *Bifurcations and Chaotic Dynamics in a Tumour-Immune-Virus System*, Mathematical Modelling of Natural Phenomena **11** (2016), no. 5, 65–85 (en), doi.

[29] Minna Eriksson, Kilian Guse, Gerd Bauerschmitz, Pekka Virkkunen, Maija Tarkkanen, Minna Tanner, Tanja Hakkarainen, Anna Kanerva, Renee A

Desmond, Sari Pesonen, and Akseli Hemminki, *Oncolytic Adenoviruses Kill Breast Cancer Initiating CD44+CD24−/Low Cells*, Molecular Therapy **15** (2007), no. 12, 2088–2093, doi.

[30] Sébastien A. Felt and Valery Z. Grdzelishvili, *Recent advances in vesicular stomatitis virus-based oncolytic virotherapy: a 5-year update*, The Journal of General Virology **98** (2017), no. 12, 2895–2911, doi.

[31] Christos Fountzilas, Sukeshi Patel, and Devalingam Mahalingam, *Review: Oncolytic virotherapy, updates and future directions*, Oncotarget **8** (2017), no. 60, doi.

[32] Xinping Fu, Armando Rivera, Lihua Tao, Bart De Geest, and Xiaoliu Zhang, *Construction of an Oncolytic Herpes Simplex Virus That Precisely Targets Hepatocellular Carcinoma Cells*, Molecular Therapy **20** (2012), no. 2, 339–346, doi.

[33] Aaron Goldman, Sachin Khiste, Elizaveta Freinkman, Andrew Dhawan, Biswanath Majumder, Jayanta Mondal, Anthony B. Pinkerton, Elliot Eton, Ragini Medhi, Vineethkrishna Chandrasekar, M. Mamunur Rahman, Takaharu Ichimura, Kodaganur S. Gopinath, Pradip Majumder, Mohammad Kohandel, and Shiladitya Sengupta, *Targeting tumour Phenotypic Plasticity and Metabolic Remodeling in Adaptive Cross-Drug Tolerance*, Science signaling **12** (2019), no. 595, eaas8779, doi.

[34] Statistics Canada Government of Canada, *Leading causes of death, total population, by age group*, November 2020, Last Modified: 2020-11-26, https://www150.statcan.gc.ca/t1/tbl1/en/tv.action?pid=1310039401.

[35] Shashi Gujar, John Bell, and Jean-Simon Diallo, *SnapShot: Cancer Immunotherapy with Oncolytic Viruses*, Cell **176** (2019), no. 5, 1240–1240.e1,

doi.

[36] Piyush B. Gupta, Ievgenia Pastushenko, Adam Skibinski, Cedric Blanpain, and Charlotte Kuperwasser, *Phenotypic plasticity: Driver of cancer initiation, progression, and therapy resistance*, Cell Stem Cell **24** (2019), no. 1, 65–78, doi.

[37] Douglas Hanahan, *Hallmarks of Cancer: New Dimensions*, Cancer Discovery **12** (2022), no. 1, 31–46, doi.

[38] Douglas Hanahan and Robert A Weinberg, *The Hallmarks of Cancer*, Cell **100** (2000), no. 1, 57–70, doi.

[39] Douglas Hanahan and Robert A. Weinberg, *Hallmarks of cancer: the next generation*, Cell **144** (2011), no. 5, 646–674 (eng), doi.

[40] D. Harrison, H. Sauthoff, S. Heitner, J. Jagirdar, W. N. Rom, and J. G. Hay, *Wild-type adenovirus decreases tumour xenograft growth, but despite viral persistence complete tumour responses are rarely achieved–deletion of the viral E1b-19-kD gene increases the viral oncolytic effect*, Human Gene Therapy **12** (2001), no. 10, 1323–1332 (eng), doi.

[41] Terry W Hermiston and Irene Kuhn, *Armed therapeutic viruses: Strategies and challenges to arming oncolytic viruses with therapeutic genes*, Cancer Gene Therapy **9** (2002), no. 12, 1022–1035 (en), doi.

[42] Huiya Huang, Yiqi Liu, Weixi Liao, Yubing Cao, Qiang Liu, Yakun Guo, Yinying Lu, and Zhen Xie, *Oncolytic adenovirus programmed by synthetic gene circuit for cancer immunotherapy*, Nature Communications **10** (2019), no. 1, 4801, doi.

[43] Ann-Charlotte Iversen, Paula S. Norris, Carl F. Ware, and Chris A. Benedict, *Human NK Cells Inhibit Cytomegalovirus Replication through a Noncy-*

tolytic Mechanism Involving Lymphotoxin-Dependent Induction of IFN-beta, The Journal of Immunology **175** (2005), no. 11, 7568–7574 (en), doi.

[44] Sana Jahedi, Lin Wang, and James Watmough, *Fighting cancer with oncolytic viral therapy: identifying threshold parameters for success*, bioRxiv (2021) (en), doi.

[45] Nadishka Jayawardena, John T Poirier, Laura N Burga, and Mihnea Bostina, *Virus-Receptor Interactions and Virus Neutralization: Insights for Oncolytic Virus Development*, Oncolytic virotherapy **9** (2020), 1–15 (eng), Publisher: Dove, doi.

[46] Adrianne Jenner, Adelle Coster, Peter Kim, and Federico Frascoli, *Treating cancerous cells with viruses: insights from a minimal model for oncolytic virotherapy*, Letters in Biomathematics **5** (2018), 1–20, doi.

[47] Adrianne L. Jenner, Chae-Ok Yun, Arum Yoon, Adelle C. F. Coster, and Peter S. Kim, *Modelling combined virotherapy and immunotherapy: strengthening the antitumour immune response mediated by IL-12 and GM-CSF expression*, Letters in Biomathematics **5** (2018), no. sup1, S99–S116, doi.

[48] Adrianne Jennera, Chae-Ok Yun, Arum Yoon, Adelle Coster, and Peter Kim, *Modelling Combined Virotherapy and Immunotherapy: Strengthening the Antitumour Immune Response Mediated by IL-12 and GM-CSF Expression*, Letters in Biomathematics **5** (2018), no. 2, doi.

[49] Matthew D. Johnston, Carina M. Edwards, Walter F. Bodmer, Philip K. Maini, and S. Jonathan Chapman, *Mathematical modeling of cell population dynamics in the colonic crypt and in colorectal cancer*, Proceedings of the National Academy of Sciences of the United States of America **104** (2007), no. 10, 4008–4013, doi.

[50] Matthew D Johnston, Carina M Edwards, Walter F Bodmer, Philip K Maini, and S Jonathan Chapman, *Mathematical modeling of cell population dynamics in the colonic crypt and in colorectal cancer*, Proceedings of the National Academy of Sciences **104** (2007), no. 10, 4008–4013.

[51] Matthew D Johnston, Philip K Maini, S Jonathan Chapman, Carina M Edwards, and Walter F Bodmer, *On the proportion of cancer stem cells in a tumour*, Journal of theoretical biology **266** (2010), no. 4, 708–711.

[52] Matthew D. Johnston, Philip K. Maini, S. Jonathan Chapman, Carina M. Edwards, and Walter F. Bodmer, *On the proportion of cancer stem cells in a tumour*, Journal of Theoretical Biology **266** (2010), no. 4, 708–711 (en), `doi`.

[53] V. Kaminskyy and B. Zhivotovsky, *To kill or be killed: how viruses interact with the cell death machinery*, Journal of Internal Medicine **267** (2010), no. 5, 473–482, `doi`.

[54] Mi K Kang, Beong I Hur, Mi H Ko, Cheul H Kim, Seung H Cha, and Soo K Kang, *Potential identity of multi-potential cancer stem-like subpopulation after radiation of cultured brain glioma*, BMC Neuroscience **9** (2008), 15, `doi`.

[55] Elizabeth Kelly and Stephen J Russell, *History of Oncolytic Viruses: Genesis to Genetic Engineering*, Molecular Therapy **15** (2007), no. 4, 651–659, `doi`.

[56] Robert S. Kerbel, *A cancer therapy resistant to resistance*, Nature **390** (1997), no. 6658, 335–336, `doi`.

[57] Yangjin Kim, Ji Young Yoo, Tae Jin Lee, Joseph Liu, Jianhua Yu, Michael A. Caligiuri, Balveen Kaur, and Avner Friedman, *Complex role of NK cells in regulation of oncolytic virus–bortezomib therapy*, Proceedings of the National Academy of Sciences **115** (2018), no. 19, 4927–4932 (en), `doi`.

[58] Hiroaki Kitano, *Cancer robustness: Tumour tactics*, Nature **426** (2003), no. 6963, 125–125, doi.

[59] Carolien A.E. Koks, Steven De Vleeschouwer, Norbert Graf, and Stefaan W. Van Gool, *Immune Suppression during Oncolytic Virotherapy for High-Grade Glioma; Yes or No?*, Journal of Cancer **6** (2015), no. 3, 203–217, doi.

[60] Natalia L. Komarova and Dominik Wodarz, *ODE models for oncolytic virus dynamics*, Journal of Theoretical Biology **263** (2010), no. 4, 530–543, doi.

[61] ———, *Targeted Cancer Treatment in Silico*, Springer New York, New York, NY, 2014.

[62] S Koscielny, M Tubiana, M G Lê, A J Valleron, H Mouriesse, G Contesso, and D Sarrazin, *Breast cancer: Relationship between the size of the primary tumour and the probability of metastatic dissemination*, British Journal of Cancer **49** (1984), no. 6, 709–715, doi.

[63] Yuri A Kuznetsov, *Elements of Applied Bifurcation Theory*, 2nd ed., Springer, New York, 1998.

[64] Caterina A. M. La Porta, Stefano Zapperi, and James P. Sethna, *Senescent Cells in Growing Tumors: Population Dynamics and Cancer Stem Cells*, PLoS Computational Biology **8** (2012), no. 1, e1002316 (en), doi.

[65] Tsvee Lapidot, Christian Sirard, Josef Vormoor, Barbara Murdoch, Trang Hoang, Julio Caceres-Cortes, Mark Minden, Bruce Paterson, Michael A. Caligiuri, and John E. Dick, *A cell initiating human acute myeloid leukaemia after transplantation into SCID mice*, Nature **367** (1994), no. 6464, 645–648, doi.

[66] Ana Lemos de Matos, Lina S. Franco, and Grant McFadden, *Oncolytic viruses and the immune system: The dynamic duo*, Molecular Therapy - Methods &

Clinical Development **17** (2020), 349–358, doi.

[67] Xiaoxin Liao, Liqiu Wang, and Pei Yu, *Stability of dynamical systems*, 1st ed., no. 5, Elsevier, Amsterdam ; Boston, 2007 (en).

[68] Ta-Chiang Liu and David Kirn, *Targeting the Untargetable: Oncolytic Virotherapy for the Cancer Stem Cell*, Molecular Therapy **15** (2007), no. 12, 2060–2061, doi.

[69] W. M. Liu, *Criterion of Hopf Bifurcations without Using Eigenvalues*, Journal of Mathematical Analysis and Applications **182** (1994), no. 1, 250–256, doi.

[70] Nicholas Macedo, David M Miller, Rizwan Haq, and Howard L Kaufman, *Clinical landscape of oncolytic virus research in 2020*, Journal for Immunotherapy of Cancer **8** (2020), no. 2, doi.

[71] N. James MacLachlan and Edward J. Dubovi, *Chapter 2 - virus replication*, Fenner's Veterinary Virology (Fifth Edition), Academic Press, Boston, fifth edition ed., 2017, pp. 17–45, doi.

[72] Khaphetsi Joseph Mahasa, Amina Eladdadi, Lisette de Pillis, and Rachid Ouifki, *Oncolytic potency and reduced virus tumour-specificity in oncolytic virotherapy. A mathematical modelling approach*, PLOS ONE **12** (2017), no. 9, e0184347, doi.

[73] Ali Mahdipour-Shirayeh, Kamran Kaveh, Mohammad Kohandel, and Sivabal Sivaloganathan, *Phenotypic heterogeneity in modeling cancer evolution*, PLOS ONE **12** (2017), no. 10, e0187000, doi.

[74] John Mallet-Paret and James A. Yorke, *Snakes: Oriented families of periodic orbits, their sources, sinks, and continuation*, Journal of Differential Equations **43** (1982), no. 3, 419–450 (en), doi.

[75] Andriy Marusyk, Vanessa Almendro, and Kornelia Polyak, *Intra-tumour heterogeneity: a looking glass for cancer?*, Nature Reviews Cancer **12** (2012), no. 5, 323–334, doi.

[76] Andriy Marusyk and Kornelia Polyak, *Tumor heterogeneity: Causes and consequences*, Biochimica et Biophysica Acta (BBA) - Reviews on Cancer **1805** (2010), no. 1, 105–117, doi.

[77] Nicholas McGranahan and Charles Swanton, *Biological and Therapeutic Impact of Intratumour Heterogeneity in Cancer Evolution*, Cancer Cell **27** (2015), no. 1, 15–26, doi.

[78] Corbin E. Meacham and Sean J. Morrison, *Tumour heterogeneity and cancer cell plasticity*, Nature **501** (2013), no. 7467, 328–337, doi.

[79] C. D. Meyer, *Matrix analysis and applied linear algebra*, Society for Industrial and Applied Mathematics, Philadelphia, 2000.

[80] Liang Min, *Oncorine, the World First Oncolytic Virus Medicine and its Update in China*, Current Cancer Drug Targets **18** (2018), no. 2, 171–176 (en).

[81] Scott N. Mueller and Barry T. Rouse, *Immune responses to viruses*, Clinical Immunology (2008), 421–431, doi.

[82] S A Narod, *Tumour size predicts long-term survival among women with lymph node-positive breast cancer*, Current oncology **19** (2012), no. 5, 249–253, doi.

[83] Julia Niemann, Norman Woller, Jennifer Brooks, Bettina Fleischmann-Mundt, Nikolas T. Martin, Arnold Kloos, Sarah Knocke, Amanda M. Ernst, Michael P. Manns, Stefan Kubicka, Thomas C. Wirth, Rita Gerardy-Schahn, and Florian Kühnel, *Molecular retargeting of antibodies converts immune defense against oncolytic viruses into cancer immunotherapy*, Nature Communications **10** (2019), no. 1, 3236 (en), doi.

[84] Martin A. Nowak, *The Mathematical Biology of Human Infections*, Conservation Ecology **3** (1999), no. 2.

[85] Martin A. Nowak and Charles R. M. Bangham, *Population Dynamics of Immune Responses to Persistent Viruses*, Science **272** (1996), no. 5258, 74–79.

[86] Martin A. Nowak and Robert M. May, *Virus dynamics: Mathematical principles of immunology and virology*, Oxford University Press, Oxford, New York, 2001.

[87] Kelley A. Parato, Donna Senger, Peter A. J. Forsyth, and John C. Bell, *Recent progress in the battle between oncolytic viruses and tumours*, Nature Reviews Cancer **5** (2005), no. 12, 965–976 (en), doi.

[88] Tuan Anh Phan and Jianjun Paul Tian, *The Role of the Innate Immune System in Oncolytic Virotherapy*, Computational and Mathematical Methods in Medicine **2017** (2017), e6587258, doi.

[89] Noemi Picco, Robert A. Gatenby, and Alexander R. A. Anderson, *Stem Cell Plasticity and Niche Dynamics in Cancer Progression*, IEEE transactions on bio-medical engineering **64** (2017), no. 3, 528–537, doi.

[90] Tannishtha Reya, Sean J. Morrison, Michael F. Clarke, and Irving L. Weissman, *Stem cells, cancer, and cancer stem cells*, Nature **414** (2001), no. 6859, 105–111, doi.

[91] Ramazan Rezaei, Hadi Esmaeili Gouvarchin Ghaleh, Mahdieh Farzanehpour, Ruhollah Dorostkar, Reza Ranjbar, Masoumeh Bolandian, Majid Mirzaei Nodooshan, and Akbar Ghorbani Alvanegh, *Combination therapy with car t cells and oncolytic viruses: a new era in cancer immunotherapy*, Cancer Gene Therapy (2021), 1–14, doi.

[92] Dayana B. Rivadeneira, Kristin DePeaux, Yiyang Wang, Aditi Kulkarni, Tracy Tabib, Ashley V. Menk, Padmavathi Sampath, Robert Lafyatis, Robert L. Ferris, Saumendra N. Sarkar, Stephen H. Thorne, and Greg M. Delgoffe, *Oncolytic viruses engineered to enforce leptin expression reprogram tumour-infiltrating t cell metabolism and promote tumour clearance*, Immunity **51** (2019), no. 3, 548–560.e4, doi.

[93] E. J. Routh, *On Laplace's Three Particles, with a Supplement on the Stability of Steady Motion*, Proceedings of the London Mathematical Society **s1-6** (1874), no. 1, 86–97 (en), doi.

[94] Wang-Shick Ryu, *Virus Life Cycle*, Molecular Virology of Human Pathogenic Viruses (2017), 31–45, doi.

[95] Miyako Sagara, Hiroyuki Inoue, Shohei Miyamoto, Chika Sakamoto, Yuki Nakano, Koichi Takayama, Hiroyuki Shimizu, Yoichi Nakanishi, and Kenzaburo Tani, *440. CVB3 Infection Elicits Potent Oncolytic Activity Against Lung Cancer Stem Cells*, Molecular Therapy **21** (2013), S170, doi.

[96] R. Schofield, *The relationship between the spleen colony-forming cell and the haemopoietic stem cell*, Blood Cells **4** (1978), no. 1-2, 7–25.

[97] Alexander Schulz, Felix Meyer, Anna Dubrovska, and Kerstin Borgmann, *Cancer Stem Cells and Radioresistance: DNA Repair and Beyond*, Cancers **11** (2019), no. 6, 862, doi.

[98] Tsukasa Shibue and Robert A. Weinberg, *EMT, CSCs, and drug resistance: the mechanistic link and clinical implications*, Nature Reviews Clinical Oncology **14** (2017), no. 10, 611–629 (en), doi.

[99] I. P. Tomlinson and W. F. Bodmer, *Failure of programmed cell death and differentiation as causes of tumors: some simple mathematical models.*, Proceedings

of the National Academy of Sciences **92** (1995), no. 24, 11130–11134, doi.

[100] Seyed Ali Madani Tonekaboni, Andrew Dhawan, and Mohammad Kohandel, *Mathematical modelling of plasticity and phenotype switching in cancer cell populations*, Mathematical Biosciences **283** (2017), 30–37, doi.

[101] Ivan Trus, Nathalie Berube, Peng Jiang, Janusz Rak, Volker Gerdts, and Uladzimir Karniychuk, *Zika Virus with Increased CpG Dinucleotide Frequencies Shows Oncolytic Activity in Glioblastoma Stem Cells*, Viruses **12** (2020), no. 5, 579 (en), doi.

[102] Samra Turajlic, Andrea Sottoriva, Trevor Graham, and Charles Swanton, *Resolving genetic heterogeneity in cancer*, Nature Reviews Genetics **20** (2019), no. 7, 404–416, doi.

[103] C. Turner and M. Kohandel, *Investigating the link between epithelial–mesenchymal transition and the cancer stem cell phenotype: A mathematical approach*, Journal of Theoretical Biology **265** (2010), no. 3, 329–335, doi.

[104] James R Tysome, Nick R Lemoine, and Yaohe Wang, *Update on oncolytic viral therapy – targeting angiogenesis*, OncoTargets and therapy **6** (2013), 1031–1040, doi.

[105] P. van den Driessche and James Watmough, *Reproduction numbers and subthreshold endemic equilibria for compartmental models of disease transmission*, Mathematical Biosciences **180** (2002), no. 1, 29–48, doi.

[106] Serguei Vinogradov and Xin Wei, *Cancer stem cells and drug resistance: the potential of nanomedicine*, Nanomedicine **7** (2012), no. 4, 597–615, doi.

[107] H. Wakimoto, G. Fulci, E. Tyminski, and E. Antonio Chiocca, *Altered expression of antiviral cytokine mRNAs associated with cyclophosphamide's enhance-*

ment of viral oncolysis, Gene Therapy **11** (2004), no. 2, 214–223, doi.

[108] Susanne G. Warner, Dana Haddad, Joyce Au, Joshua S. Carson, Michael P. O'Leary, Christina Lewis, Sebastien Monette, and Yuman Fong, *Oncolytic herpes simplex virus kills stem-like tumour-initiating colon cancer cells*, Molecular Therapy Oncolytics **3** (2016), 16013, doi.

[109] Benjamin Werner, David Dingli, Tom Lenaerts, Jorge M. Pacheco, and Arne Traulsen, *Dynamics of mutant cells in hierarchical organized tissues*, PLOS Computational Biology **7** (2011), no. 12, 1–9, doi.

[110] Benjamin Werner, Jacob G. Scott, Andrea Sottoriva, Alexander R.A. Anderson, Arne Traulsen, and Philipp M. Altrock, *The Cancer Stem Cell Fraction in Hierarchically Organized tumours Can Be Estimated Using Mathematical Modeling and Patient-Specific Treatment Trajectories*, Cancer Research **76** (2016), no. 7, 1705–1713 (en), doi.

[111] WHO, *Cancer*, 2021, https://www.who.int/news-room/fact-sheets/detail/cancer.

[112] S. Wiggins, *Introduction to applied nonlinear dynamical systems and chaos*, Springer, Berlin, 1990.

[113] Marc J Williams, Benjamin Werner, Chris P Barnes, Trevor A Graham, and Andrea Sottoriva, *Identification of neutral tumour evolution across cancer types*, Nature genetics **48** (2016), no. 3, 238–244, doi.

[114] Dominik Wodarz, *Viruses as Antitumour Weapons: Defining Conditions for tumour Remission*, Cancer Research **61** (2001), no. 8, 3501–3507 (en).

[115] ———, *Computational approaches to study oncolytic virus therapy: insights and challenges*, Gene Ther Mol Biol **8** (2004), 137–146.

[116] ———, *Killer cell dynamics*, vol. 32, Springer, 2007.

[117] ———, *Computational modeling approaches to the dynamics of oncolytic viruses*, Wiley Interdisciplinary Reviews: Systems Biology and Medicine **8** (2016), no. 3, 242–252.

[118] Dominik Wodarz and Natalia L. Komarova, *Computational biology of cancer: lecture notes and mathematical modeling*, World Scientific, Hackensack, NJ, 2008 (en), doi.

[119] Dominik Wodarz and Martin A. Nowak, *Immune Responses and Viral Phenotype: Do Replication Rate and Cytopathogenicity Influence Virus Load?*, Journal of Theoretical Medicine **2** (2000), no. 2, 113–127, doi.

[120] Yuki Yamamoto, Masaki Nagasato, Teruhiko Yoshida, and Kazunori Aoki, *Recent advances in genetic modification of adenovirus vectors for cancer treatment*, Cancer Science **108** (2017), no. 5, 831–837 (en), doi.

[121] Shuya Yano, Hiroshi Tazawa, Yuuri Hashimoto, Yasuhiro Shirakawa, Shinji Kuroda, Masahiko Nishizaki, Hiroyuki Kishimoto, Futoshi Uno, Takeshi Nagasaka, Yasuo Urata, Shunsuke Kagawa, Robert M. Hoffman, and Toshiyoshi Fujiwara, *A Genetically Engineered Oncolytic Adenovirus Decoys and Lethally Traps Quiescent Cancer Stem–like Cells in S/G2/M Phases*, Clinical Cancer Research **19** (2013), no. 23, 6495–6505 (en), Publisher: American Association for Cancer Research Section: Cancer Therapy: Preclinical, doi.

[122] So Young Yoo, Seo Young Bang, Su-Nam Jeong, Dae Hwan Kang, and Jeong Heo, *A cancer-favoring oncolytic vaccinia virus shows enhanced suppression of stem-cell like colon cancer*, Oncotarget **7** (2016), no. 13, 16479–16489, doi.

[123] Wai-Kin Yu, Zhigang Wang, Chi-Chun Fong, Dandan Liu, Tak-Chun Yip, Siu-Kie Au, Guangyu Zhu, and Mengsu Yang, *Chemoresistant lung cancer stem*

cells display high DNA repair capability to remove cisplatin-induced DNA damage: High DNA repair capability of LCSCs confers chemoresistance, British Journal of Pharmacology **174** (2017), no. 4, 302–313, doi.

[124] Qing Zhang and Fusheng Liu, *Advances and potential pitfalls of oncolytic viruses expressing immunomodulatory transgene therapy for malignant gliomas*, Cell Death & Disease **11** (2020), no. 6, 1–11, doi.

[125] Meijun Zheng, Jianhan Huang, Aiping Tong, and Hui Yang, *Oncolytic Viruses for Cancer Therapy: Barriers and Recent Advances*, Molecular Therapy - Oncolytics **15** (2019), 234–247, doi.

Curriculum vitae

Candidate's full name:

Sana Jahedi

University attended:

University of New Brunswick, 2015-present

Shahid Beheshti, Master of Pure Mathematics, 2009-2012

ALzahra University, Bachelor of Pure Mathematics, 2005-2009

Publications and preprints:

- Sana Jahedi*, James Yorke. *When the best pandemic models are the simplest*, Biology 2020, 9(11), 353; https://doi.org/10.3390/biology9110353
- Sana Jahedi*, Lin Wang, James Watmough, *Fighting cancer with oncolytic viral therapy: identifying threshold parameters for success*, (2021), preprint https://doi.org/10.1101/2021.07.19.452846
- Sana Jahedi*, Kamran Kaveh, James Watmough, *Targeting Cancer Stem Cells: A modelling approach*, (2022), preprint.
- Sana Jahedi*, Lin Wang, James Watmough, *Enhancer or Burden: Effect of virus-specific immune response on oncolytic viral therapy*, (2022), preprint.

- Sana Jahedi*, Timothy Sauer, James Yorke. *Structured system of nonlinear equations*, (2022), preprint.
- Sana Jahedi*, Timothy Sauer, James Yorke. *Robustness of solutions of almost every system of equations*, (2022), preprint. https://arxiv.org/abs/2202.00503

Awards:

Mathematics & Statistics Graduate Scholarship, University of New Brunswick. 2021

UNB Graduate Bursary, University of New Brunswick, Fredericton, Canada. 2021

UNB Travel Awards, University of New Brunswick, Fredericton, Canada. 2019

UNB Graduate Bursary, University of New Brunswick, Fredericton, Canada. 2018

NBIF STEM Scholarship, New Brunswick Innovation Foundation, Canada. 2015

Exceptional talent award, Shahid Beheshti University, Tehran, Iran. 2009

Exceptional talent award, Alzahra University, Tehran, Iran. 2009

Presentations in conferences, seminars and colloquiums:

The equations of nature reveal the nature of equations, CMS (Canadian Mathematical Society) summer meeting, June 2021.

Oncolytic viral therapy; a computational modelling approach, York university, CDM (Canadian center for disease modeling) Incubation Day, February 2021.

When the best pandemic models are the simplest, AARMS COVID-19 seminar series, July 2020.

Covid-19 Containment methods, Howard university, July 2020.

Intraguild Predation, University of New Brunswick, June 2019.

Bogdanov-Taken Bifurcations, University of New Brunswick, February 2019.

Asymptotics of Speed in Large Drift, University of New Brunswick, November 2018.

Asymptotics of Eigenvalue in Large Drift, University of New Brunswick, September 2018.

Participation in conferences, workshops, Advanced schools

Fields Academy graduate courses, Winter 2022.

SMB (Society for Mathematical biology) annual meeting, Summer 2021.

Stem Cells and Immunotherapy Virtual Symposium, Webinar, The university of Texas MD Anderson Cancer Center, January 2021.

SMB (Society for Mathematical biology) annual meeting, Summer 2020.

Virtual Workshop on Computational modelling to study cancer biology and treatments, University of Montreal, August 2020.

IPAM workshop on Mathematical Models in understanding Covid 19, August 2020.

CSEE (Canadian Society for Ecology and Evolution), August 2020.

SMB (Society for Mathematical biology) annual meeting, Summer 2019.

AARMS Industrial Problem Solving Workshop, summer 2019.

AARMS summer school, Ordinary differential equations, University of Prince Edward Island, summer 2019.

CMS (Canadian Mathematical Society) summer meeting, Spring 2018.